Radar monitoring of heartbeats and respiration

Øyvind Aardal

Series of dissertations submitted to the
Faculty of Mathematics and Natural Sciences, University of Oslo
No. 1363

ISSN 1501-7710

Cover: Inger Sandved Anfinsen.
Printed in Norway: AIT Oslo AS.

Produced in co-operation with Akademika Publishing.
The thesis is produced by Akademika publishing merely in connection with the thesis defence. Kindly direct all inquiries regarding the thesis to the copyright holder or the unit which grants the doctorate.

Preface

This thesis has been submitted to the Faculty of Mathematics and Natural Sciences at the University of Oslo in partial fulfillment of the requirements for the degree *Philosophiae Doctor (Ph.D.)*. The work was carried out at Forsvarets forskningsinstitutt (FFI) and the Nanoelectronics group at the Department of Informatics, University of Oslo (UiO). The work has been supervised by Professor Svein-Erik Hamran, Dr. Tor Berger and Professor Tor Sverre Lande. The work is part of the MELODY project, funded by the Research Council of Norway under contract number 187857/S10.

Acknowledgements

First, I would like to express my thanks to my three supervisors, Professor Svein-Erik Hamran at FFI, Dr. Tor Berger at FFI and Professor Tor Sverre "Bassen" Lande at the Department of Informatics, UiO. My main supervisor, Svein-Erik, has been a source of inspiration and motivation. His constant stream of new ideas, enthusiasm and radar knowledge has played an important role in forming this thesis. I would also like to thank Tor for all his help. Whenever I was stuck at a signal processing problem or didn't know what approach to take, he gave me the tips and literature needed. Bassen's input has also been of great help, especially in the writing process where he always seems to know what will make a paper better.

I would like to thank my colleagues Yoann Paichard, Sverre Brovoll and Mats Jørgen Øyan. Yoann joining the project provided a great new boost and source of knowledge. Sverre and Mats Jørgen have always been available for discussions and help during experiments, as well as making the workdays more joyful. My other colleagues at FFI also deserve an expression of gratitude for providing a pleasant working environment. Jan Hammerstad in particular, for also helping me during several of the earlier measurement campaigns.

For making my days as a student wonderful, which in turn was an important factor in me pursuing a Ph.D., I give my thanks to His Royal Highness Ursus Major. Last, I would like to thank my family and friends for all their support, both in the work of this thesis and life in general.

Abstract

This thesis addresses the use of radar for heartbeat and respiration monitoring. Medical radar can be used for detecting vital signs at distances up to several meters. A medical radar works by transmitting electromagnetic waves towards a person, and receiving echoes reflected off the person. Vital signs appear as modulations in the radar data in period with the heartbeats and respiration. We have measured and analyzed these modulations.

The ability to detect human heartbeats from a distance can be used for monitoring patients' heartbeats without the need of attaching the measurement equipment to the patient. A radar system can be placed over a bed, integrated in a mattress or chair or used for non-intrusive home monitoring. It could also be used as an alternative to the diagnostic monitoring tools of today. In this thesis, the understanding of radar heartbeat detection is explored.

Although heartbeats and respiration monitoring using radar have been reported many times before, the optimal frequencies, waveforms and aspect angle of detection were not known. We

have described the vital signs modulations as functions of frequency and aspect angle, and found both narrowband and ultra wideband radar to be suited for the task. In addition to quantizing the modulations, an experimental approach to understanding why heartbeat and respiration detection with radar is possible was made. We found that small body surface movements are the cause of the observed heartbeat modulations in radar data, discarding the theory that reflections from internal body organs are seen. On-body radar have been used as well, and a closer connection between the actual movements of the heart and the radar recordings were found than what is achievable using remote radar. With on-body radar and the processing presented in this thesis, details of the heart mechanics can be identified using radar. It is also possible to see changes in the measured waveform when the pulse and blood pressure of the person changes.

List of publications

This thesis is based on the following six papers

I Ø. Aardal, S.-E. Hamran, T. Berger, J. Hammerstad, and T.S. Lande, "Radar cross section of the human heartbeat and respiration," in *Biomedical Circuits and Systems Conference, 2010 (BioCAS 2010).* IEEE, November 2010.

II Ø. Aardal, S.-E. Hamran, T. Berger, J. Hammerstad, and T.S. Lande, "Radar cross section of the human heartbeat and respiration in the 500MHz to 3GHz band," in *Radio and Wireless Symposium (RWS), 2011.* IEEE, January 2011.

III Ø. Aardal, S. Brovoll, Y. Paichard, T. Berger, T.S. Lande, and S.-E. Hamran, "Empirical model of modulation in radar heartbeat and respiration measurements"

IV Ø. Aardal, S.-E. Hamran, T. Berger, Y. Paichard, and T.S. Lande, "Chest movement estimation from radar modulation caused by heartbeats," in *Biomedical Circuits and Systems Conference, 2011 (BioCAS 2011).* IEEE, November 2011.

V Ø. Aardal, Y. Paichard, S. Brovoll, T. Berger, T.S. Lande, and S.-E. Hamran, "Physical Working Principles of Medical Radar," *IEEE Transactions on Biomedical Engineering,* vol. 60, no. 4, pp. 1142-1149, 2013.

VI Ø. Aardal, S. Brovoll, Y. Paichard T. Berger, T.S. Lande, and S.-E. Hamran, "Detecting changes in the human heartbeat with on-body radar," in *IEEE Radar Conference 2013, RadarCon 2013,* May 2013.

Related publications

VII Y. Paichard, T. Berger, Ø. Aardal, and S.-E. Hamran, "Close range microwave imaging of human chest," in *Applied Sciences in Biomedical and Communication Technologies (ISABEL), 2011 4th International Symposium on.* IEEE 2011.

VIII T. Berger, S.-E. Hamran, Y. Paichard, and Ø. Aardal, "Close Range Ultra Wideband Microwave Imaging in a Non-Homogeneous Background," in *Signal and Image Processing.* ACTA Press, 2011.

Contents

Chapter 1

Introduction

Cardiovascular diseases are the largest worldwide causes of death according to the World Health Organization (WHO) [7, 8]. An important factor in diagnosing and treating these diseases is to monitor the heart. To do this, there exist a wide range of instruments available to the medical personnel. The most commonly used tool in heartbeat monitoring is the electrocardiogram (ECG), which monitors the electrical activity of the heart. To monitor the actual movements of the heart, ultrasound can be used both for imaging and displaying various heartbeat parameters. Other methods span from the large and expensive Magnetic Resonance Imaging (MRI) and Computed Tomography (CT) machines which can provide detailed images of the entire human body, to simple pulse oxymeters which can monitor the pulse through a small device placed on the finger.

With the large number of people suffering from heart diseases, every improvement in diagnosis or monitoring is valuable. This is achievable through either improving the existing technologies, or through developing new ones. This thesis covers the use of radar for heartbeat and respiration monitoring. Even though this is an application first described several decades ago [9], the diagnostic possibilities are still largely unexplored. Medical radar is different from any existing heart or respiration monitoring techniques in that electromagnetic waves of small power in the gigahertz region are used to detect the physiological motions of the body. With radar technology, human heartbeats and respiration can be detected from a distance of several meters, or by placing the antennas on the body.

Radar is a broad field of study, and the topic of medical radar can span from radar system and chip design to a more medical study of body effects observable with the radar. The scope of this thesis is the study of heartbeats and respiration monitoring, focusing mainly on heartbeat monitoring. The aim has been both to understand the physical processes and the potential as a diagnostic and monitoring tool.

Going into the project, several questions were unanswered: Are the radar waves penetrating into the body so that reflections from the heart are seen? Is there an optimal waveform or frequency for heartbeat monitoring? Are there any medical diagnostic possibilities beyond detecting the heart rate? These were questions that demanded answers before delving deeply into system designs or signal processing. Vital signs detection using radar is a complex topic, involving electromagnetic waves and human anatomy changing from person to person. Theoretical and modelling work can thus never be more than an approximation to the real world, and a difficult approximation to make. Because of this, an experimental approach to answering the above questions was taken. The core of the work is based on measurements on humans, and the analysis and understanding of these.

The first topic discussed is the optimal detection of human vital signs using radar placed a short distance from the person, which is covered in papers I-III. We obtained results on which frequencies and from which aspect angles the detection is best achieved. From the results, an empirical model of the modulation as a function of frequency and aspect angle was made. This model can be used for finding optimal aspect angles and frequencies for detecting the vital signs. It was found that it is best to go up in frequency when detecting heartbeats and respiration. Surprisingly, it was also found that heartbeats are seen nearly equally good from the front and from the back of a seated person.

The second main topic, published in papers IV and V, is to understand why a radar is capable of detecting the vital signs from a distance and how this appears in the radar recordings. This way one can better create methods for extracting diagnostic information. The experimental results in these papers answer what earlier has only been theories, namely what are the physiological processes seen in the radar recordings. The measurements showed that when doing non-contact radar monitoring of heartbeats, it is the body surface movements that are seen and not the reflections from the actual heart itself. Signal processing methods were developed to robustly extract the chest wall motion. This last result made us shift focus toward placing the antennas on the body to see the heart movements. In paper VI results from the on-body heartbeat monitoring is presented. Among the results is a characteristic change in the heartbeat waveform with change in blood pressure and pulse. Radar can possibly be used for monitoring the blood pressure, and the observed change in heartbeat waveform opens the possibility of observing a similar change with different diseases as well.

Chapter 2 starts off with a short introduction to radar in general. In section 2.2 the Ultra wideband (UWB) and single frequency continuous wave (CW) waveforms used in the experimental parts of the thesis are described. The chapter ends with an introduction to the measurement equipment and detection of small movements using radar. In Chapter 3 an introduction to the human heart is given. Section 3.2 covers the dielectric properties of human tissues and the propagation of electromagnetic waves inside the human body. In the following section, a look is taken on the medical radar history. In Chapter 4 summaries of the papers are given, before the papers appear in full length in Chapter 6.

Chapter 2

Introduction to radar

2.1 General radar principles

The word radar originates from the term radio detection and ranging. A radar works by transmitting electromagnetic waves, and listening for echos reflected from objects within the antenna beam. Among the first applications for radar, were ship and airplane detection. These are still among the main applications, with both radars on board vehicles and used as traffic control systems or detection and tracking devices on the ground. Over the years, several other applications have emerged. Some examples include ground penetrating radar for geological applications, weather radar for meteorology, satellite-born radar, synthetic aperture radar (SAR), car radar, through the wall (TTW) radar and radar used for mines and improvised explosive devises (IEDs). Radar has been implemented where other sensor technologies such as optical devices are unable to work, for instance in fog, during night time, over long distances, through foliage and other obstacles.

For different applications, different radar systems are needed. For space radars and over the horizon radars, the systems are designed to see objects many kilometers away, with antennas several meters large and transmitted powers in the order of megawatts. Radars for medical applications rest on the other end of the scale, with the need to detect echos only a few meters away and a desire to have the systems as small as possible with a transmitted power only a fraction of a milliwatt.

One of the first things encountered in nearly all radar textbooks is the radar equation:

$$P_r = \frac{P_t G^2 \lambda^2 \sigma_{RCS}}{(4\pi)^3 R^4}. \tag{2.1}$$

It describes the received echo power P_r in terms of the transmitted power P_t, the antenna gain G in the direction of the target, the wavelength λ, the radar cross section σ_{RCS} of the reflecting target and the range R from the radar to the target. For human heartbeat and respiration monitoring, typical values are P_t around a milliwatt or less and R a couple of meters or shorter.

The radar equations tells a lot about the possibilities for detecting the reflection of a target. The received power P_r of (2.1) is dependent on both the target itself, the distance from the radar, and the radar system. To detect the target, the received power needs to be distinguished from the noise in the system receiver. Present in all radar recordings are phase noise and thermal noise. The phase noise consists of random fluctuations in a signal's phase, spreading the signal energy away form the carrier frequency. The thermal noise $N_0 f_B$ is uniformly distributed over the frequency spectrum.

N_0 is the noise spectral power density in watts per hertz, and f_B is the bandwidth of the receiver. The radar equation can be rewritten to the signal to noise ratio (SNR) radar equation, comparing P_r to the white noise $N_0 f_B$:

$$SNR = \frac{P_t G^2 \lambda^2 \sigma_{RCS}}{(4\pi)^3 R^4 N_0 f_B}. \tag{2.2}$$

Of course, in real life scenarios there will rarely be only one reflector in the scene. Other objects than the target, background and even weather will affect the radar recording. This changes the radar equation in that not a single object of RCS σ_{RCS} at a range R is seen, but a large number of different objects at different ranges from the radar. One of the main challenges in processing radar data is to separate the wanted information of the target of interest from everything else.

2.2 UWB and CW radar

By solving the wave equations derived from Maxwell's equations, see for instance Chapter 3 of [10], the time varying electric field of a propagating plane wave in the far field is given by:

$$E(x,t) = \Re\{E_0 e^{-\alpha x - ikx + i\omega t}\}. \tag{2.3}$$

E_0 is the initial value of the electric field, α is the attenuation in the medium of propagation, k is the wave number, $\omega = 2\pi f$ is the angular frequency, x is the spatial coordinate relative to the initial point (where $E = E_0$) and t is time. $\Re\{\cdot\}$ is the real operator. Any propagating wave in the real world cannot have imaginary components. Still, for readability, the $\Re\{\cdot\}$ operator will be omitted in the following equations.

By varying the parameters of (2.3), a variety of transmitted waveforms are possible: Pulsed, Continuous wave (CW), frequency modulated (FM) wave, noise, etc. In this work, two main waveforms have been used: Single frequency CW and linear FMCW waveforms. These are described in the following sections. A narrowband CW waveform is the simplest waveform, both in terms of hardware and in terms of processing the data. The other waveforms mentioned above are used to achieve a bandwidth, which in turn provides range resolution to the radar data. The reason for choosing FMCW over pulsed or noise radar systems in this thesis is based on the available hardware. FMCW UWB radars were already developed at FFI, and great flexibility in bandwidth was possible with lab equipment such as a network analyzer. FMCW, as opposed to impulse UWB radar, can be downconverted in frequency in the receiver, simplifying the sampling process.

2.2.1 CW waveform

A narrowband CW waveform is a propagating wave with an oscillating electric field described by (2.3) with a constant ω. A simple block diagram of a narrow-band CW radar is presented in Figure 2.1. In air, the conductivity is $\sigma = 0$ which means that the attenuation constant is $\alpha = 0$ and the wave number is $k = \omega/c$, with c being the speed of light. When the propagating wave encounters objects with different dielectric properties, parts of the wave will be reflected. The wave reflected

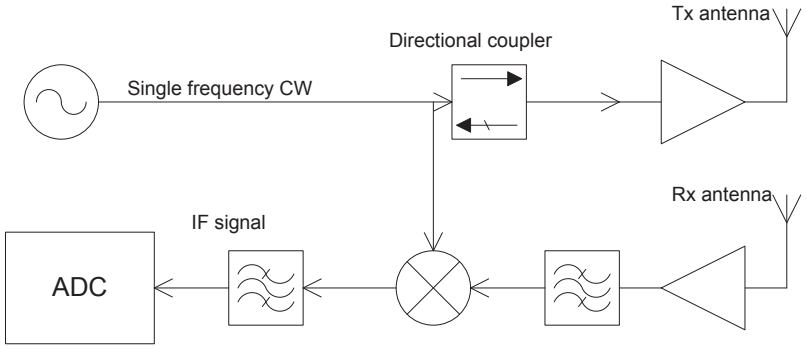

Figure 2.1: A simplified block diagram of a single frequency CW radar. An oscillator generates the signal waveform to be transmitted at the Tx antenna. The received signal is mixed with a copy of the transmitted signal, resulting in a low frequency intermediate frequency (IF) wave that can be sampled by an analog to digital converter (ADC).

off an object with RCS σ_{RCS} a distance R from radar received back at the radar antenna is:

$$E_r(R,t) = \frac{E_0\sqrt{\sigma_{RCS}}}{4\pi R^2} e^{\frac{-i2\omega R}{c}+i\omega t}. \tag{2.4}$$

For other media than air, c can be substituted with the appropriate propagation speed. The transmitted and received signal are rewritten using $k = \omega/c$ and the time delay $\tau = 2R/c$. With this substitution, the transmitted and received signals are

$$E_t(0,t) = E_0 e^{-i\omega t} \tag{2.5}$$

$$E_r(R,t-\tau) = \frac{E_0\sqrt{\sigma_{RCS}}}{4\pi R^2} e^{-i\omega(t-\tau)}. \tag{2.6}$$

To avoid the problem of sampling at GHz frequencies the received signal is mixed with the transmitted signal, a process known as homodyning. In the mixing, the received and transmitted signals are multiplied:

$$\begin{aligned} E_t E_r &= \frac{E_0}{2}(e^{-i\omega t} + e^{i\omega t}) \cdot \frac{E_0\sqrt{\sigma_{RCS}}}{2\cdot 4\pi R^2}(e^{-i\omega(t-\tau)} + e^{i\omega(t+\tau)}) \\ &= \frac{E_0}{2}\frac{E_0\sqrt{\sigma_{RCS}}}{2\cdot 4\pi R^2}\Big(e^{-i\omega(2t-\tau)} + e^{i\omega(2t-\tau)} + e^{-i\omega\tau} + e^{i\omega\tau}\Big). \end{aligned} \tag{2.7}$$

After mixing, the signal contains one part of twice the transmitted frequency and one part at zero frequency. A low pass filter placed after the mixer removes the high frequency components and the resulting signal is

$$\frac{E_0\sqrt{\sigma_{RCS}}}{4\pi R^2} e^{-i\omega\tau}. \tag{2.8}$$

In the last equation, the $E_0/2$ term from the transmitter to the mixer has been set to unity to simplify the following expressions. A moving target will not have a constant two-way travel time τ, but a time dependent $\tau(t) = 2R(t)/c$. The signal after low pass filtering will then have a Doppler frequency equal to the derivative of the signal phase:

$$\begin{aligned} f_D &= \frac{\partial}{\partial t}\Big(-f\frac{2R(t)}{c}\Big) \\ &= -\frac{2f}{c}\frac{\partial R(t)}{\partial t}, \end{aligned} \tag{2.9}$$

where $\frac{\partial R(t)}{\partial t}$ is the speed of movement.

In an I & Q receiver, the signal is summed with the same signal 90° out of phase, thus creating the complex bandpass signal

$$b(t) = H_{sys}\frac{E_0\sqrt{\sigma_{RCS}}}{4\pi R^2}e^{\frac{-i2\omega R}{c}}, \tag{2.10}$$

where H_{sys} includes the system related components such as antenna gain and transmission line delays.

In a real world scenario the received signal is not the echo from a single object, but the sum of the reflections from all the objects within the antenna beam:

$$b(t) = H_{sys}E_0\int_0^\infty \frac{\sqrt{\sigma_{RCS}(R,t)}}{4\pi R(t)^2}e^{\frac{-i2\omega R(t)}{c}}dR. \tag{2.11}$$

Such a CW radar recording is thus a vector b in the complex plane where each element is the response from the entire scene at a time instance.

2.2.2 FMCW waveform

When using a single frequency waveform, there is no resolution in range from the radar. In this context, resolution is defined as the distance needed to separate two point reflectors with equal strength. Range resolution can be achieved by using a waveform with a frequency bandwidth. When the frequency spectrum is flat, the range resolution of a wideband signal is

$$\Delta R = \frac{c}{2B}. \tag{2.12}$$

B is the bandwidth of the radar wave. This is because a rectangular window in the frequency domain is a $\sin(\tau)/\tau$ function in the time domain and vice versa, as seen in Figure 2.3. The width of the $\sin(\tau)/\tau$ function is $1/B$, which leads to the range resolution. There are several ways to achieve the bandwidth in the transmitted signal, such as pulsed waves, stepped frequency and noise radar. For the work in this thesis linear FMCW sweeps were used. A linear FMCW sweep is a sweep where the frequency is linearly increasing or decreasing during the pulse duration. A block diagram of a FMCW radar is shown in Figure 2.2.

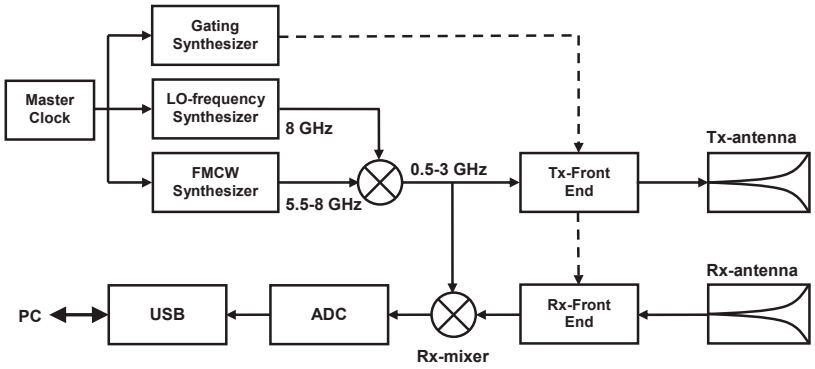

Figure 2.2: A block diagram of the HUBRA FMCW radar [11]. Two signals are mixed to form the transmitted linear FMCW signal. At the receiver, the transmitted and received signals are mixed to form a lower frequency IF signal that can be sampled by the ADC.

Linear FMCW can be described through (2.3), with a time varying frequency

$$\omega(t) = 2\pi(at + f_0) \tag{2.13}$$

$$a = \frac{B}{T}, \tag{2.14}$$

where a is the slope, T the pulse duration and f_0 is the start frequency of the sweep. The transmitted FMCW wave in air is

$$E(R,t) = E_0 e^{i2\pi(\frac{a}{2}t+f_0)t},\ t \in [0,T]. \tag{2.15}$$

In a radar recording, many sweeps are transmitted after each other, as illustrated in Figure 2.4. The rate at which the sweeps are transmitted is called the pulse repetition frequency (PRF), which is equal to $1/(T + t_r)$. For the measurements presented in this thesis, typical values are sweep time T and relaxation time t_r in the order of milliseconds, bandwidth in the order of GHz and PRF in the order of tens or hundreds of Hz.

Due to the the relation (2.13), the signal is said to be sampled in the frequency domain. Similar to the process described above for the narrow-band CW receiver, the received signal is mixed with the transmitted before sampling. The calculations of the mixing process can be found in [13]. After mixing in the receiver, the sampled signal reflected off a target $R = c\tau/2$ away from the radar is

$$b(\omega) = H_{sys}\frac{E_0\sqrt{\sigma_{RCS}}}{4\pi R^2}e^{i\omega\tau}. \tag{2.16}$$

τ is the two way travel time of the wave between the radar and the target. Each sweep is typically sampled with a fixed number of samples between f_0 and $f_0 + B$. Due to τ being in the size of nanoseconds it is also called fast time. This is to separate it from the other time variable t in the size of seconds or milliseconds, which is called slow time. In a real world scenario, the radar recording

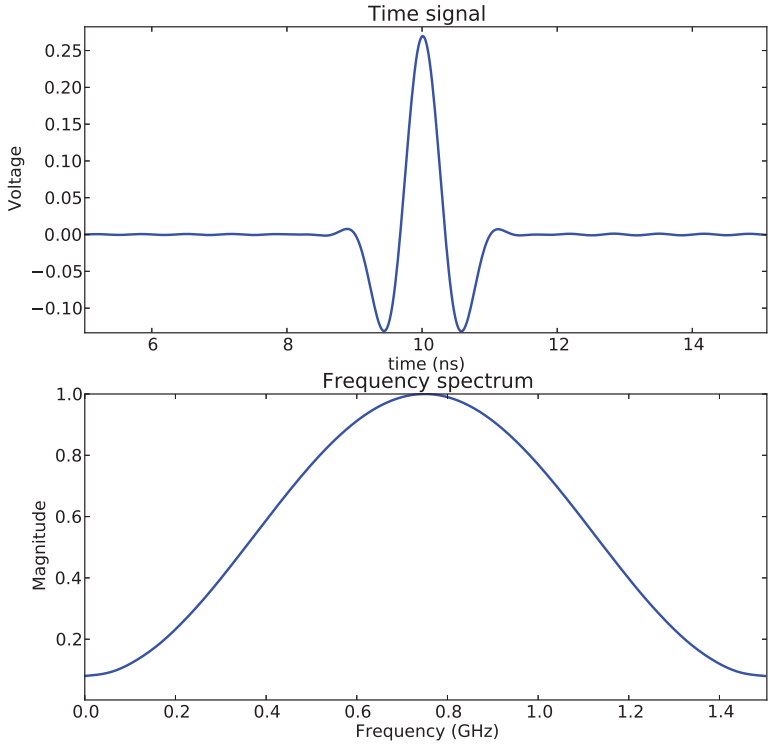

Figure 2.3: To the top is a pulse of short duration in the time domain. To the bottom is the frequency domain representation of the same pulse.

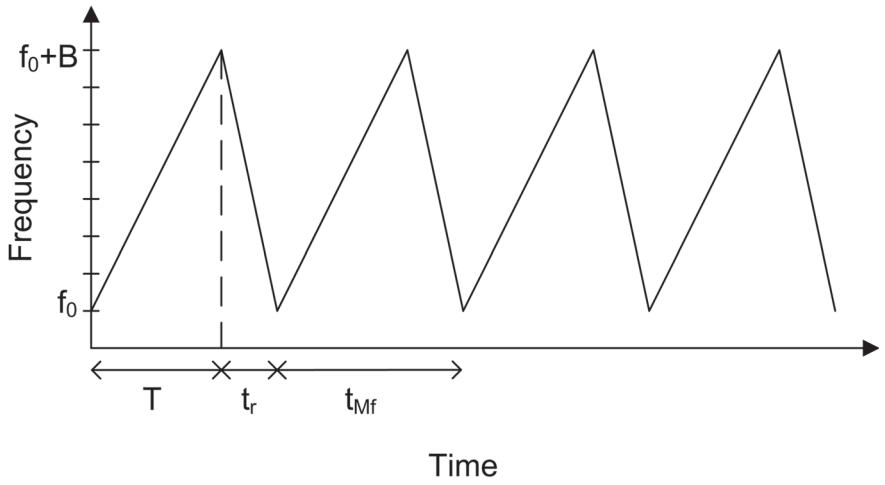

Figure 2.4: The sweeps in a FMCW radar. During the pulse duration T the frequency of the transmitted wave is increased from f_0 to $f_0 + B$. The radar then needs a reset time t_r before a new sweep is transmitted. Figure from [12].

is the recording of echos from all objects within the antenna beam:

$$b(\omega) = H_{sys} E_0 \int_0^\infty \frac{\sqrt{\sigma_{RCS}}}{4\pi R^2} e^{\frac{i2R\omega}{c}} dR \tag{2.17}$$

$$\omega = 2\pi(at + f_0), \quad t \in [0, T]. \tag{2.18}$$

See [13] for more details on FMCW.

In (2.17), it is seen that the range information is present in the signal phase. However, it is not immediately available in the frequency domain. To utilize the range resolution of the bandwidth in a FMCW wave, an inverse Fourier transform (IFT) of the pulse can be applied. The IFT transforms the radar signal from the frequency domain to the fast time domain. The fast time domain representation of a single target located at a two way travel time τ_1 from the radar is:

$$\begin{aligned} b(\tau) &= \int_{\omega_0}^{\omega_0 + 2\pi B} H_{sys} \frac{E_0 \sqrt{\sigma_{RCS}}}{4\pi R^2} \Re\{e^{i\omega\tau_1}\} e^{i\omega\tau} d\omega \\ &= H_{sys} \frac{E_0 \sqrt{\sigma_{RCS}}}{4\pi R^2} \left\{ e^{i(\omega_0 + \pi B)(\tau - \tau_1)} \frac{\sin(\pi B(\tau - \tau_1))}{\tau - \tau_1} \right. \\ &- \left. e^{-i(\omega_0 + \pi B)(\tau - \tau_1)} \frac{\sin(\pi B(\tau + \tau_1))}{\tau + \tau_1} \right\}. \end{aligned} \tag{2.19}$$

This is a sinc-function with main lobe width $\frac{2}{B}$ centered around $\tau = \tau_1$ in positive fast time. The inverse Fourier transform is performed on every sweep in a measurement series, which result in a series of pulses in the fast time domain as illustrated in Figure 2.5. The fast time domain τ is often also called the range domain due to the relation $R = c\tau/2$. The τ axis of Figure 2.5 can thus be seen both as the two way travel time from the antenna and the range in meters from the antenna. Similarly, the fast time representation of the data are also called range profiles.

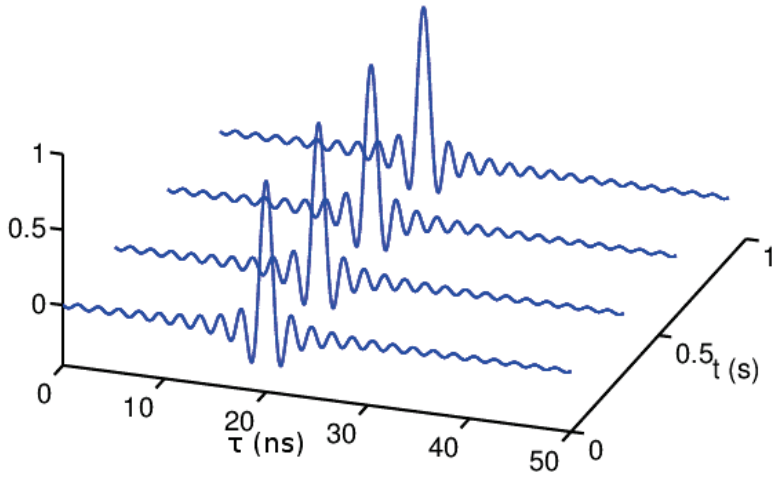

Figure 2.5: Four pulses in the fast time domain. The axis along each pulse is the fast time (τ) domain with units nanoseconds, while the axis from one pulse to the next is the slow time domain (t) with units seconds. The pulses are generally complex, in this figure the real part of the pulse has been plotted.

As with CW radar, in a real world scenario the radar does not record only a single scatterer, but the sum of all the scatterers in the scene. A radar recording is thus the integral of the contributions from all the two way travel times in (2.19). An example of a raw data recording using the HUBRA radar [11, 12, 14] is seen in Figure 2.6. The same data in the range domain is shown in Figure 2.7. One can however, focus on one point in the range domain by selecting a two way travel time $\tau = \tau_0$, and look at this point in (2.19). All targets less than one resolution cell away from τ_0 will then contribute directly to the total signal, while targets further away will contribute through side lobes. Applying a window function to the data before the inverse Fourier transform reduces the side lobes at the cost of an increased width of the main lobe.

2.2.3 Near and far field considerations

An electromagnetic wave radiated from a source will behave different depending on the distance from the source. To separate this behavior, the distances from an antenna are separated into the near field and far field regions. There is no abrupt change in the behavior, and sometimes an additional region between the near and far field called the transition zone is used. There exist several definitions on where the limit between near and far field is [15], depending on the acceptable level of errors in the application. In the following, two common limits are considered.

The electromagnetic fields radiated by an antenna contain terms attenuating by $1/R$, $1/R^2$ and $1/R^3$. In the near field, the square and cubic terms will dominate while they will rapidly attenuate with increasing distance in the far field. One definition of the far field boundary is thus the limit

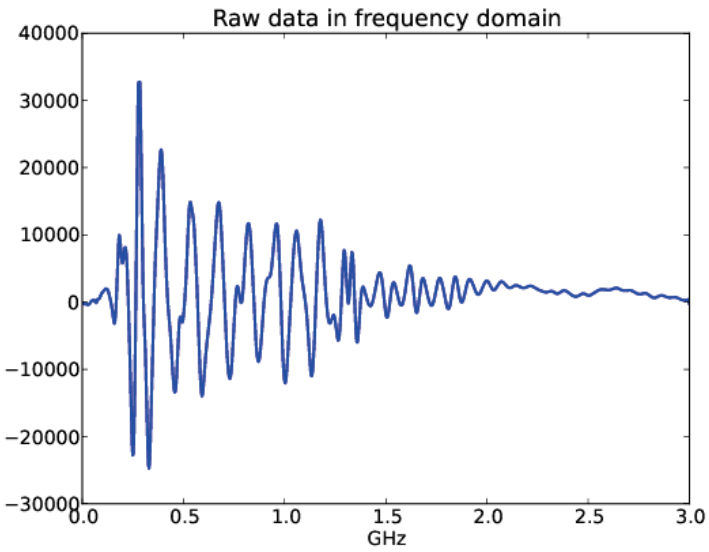

Figure 2.6: Example of the raw data recorded using the HUBRA radar with a sweep from 0 to 3 GHz.

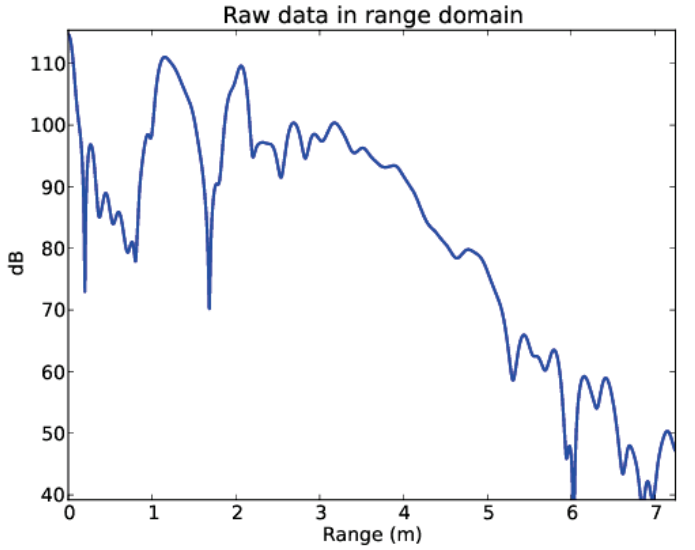

Figure 2.7: Example of the data of Figure 2.6 in the range domain. The peak at approximately 1 m is the direct coupling between the antennas, and the peak at a little more than 2 m is a person sitting in front of the radar.

where the $1/R$ term becomes dominating, which is defined in [15]:

$$R = \frac{\lambda}{2\pi}. \tag{2.20}$$

While this is the distance where the $1/R$ term becomes dominating, other limits such as $R > \lambda$ or $R > 2\lambda$ are also used depending on the acceptable error level from the $1/R$ approximation.

The above definition of the far field boundary was derived from the field strength. Another way to define the far field, is the distance from the antenna where the propagating wave can be approximated as a plane wave. A frequently used definition of when the wave can be considered a plane wave is the Rayleigh criterion. This is the region where the phase difference of a wave normally incident on a flat surface with largest dimension D is less than $\frac{\pi}{8}$. An equivalent definition is where the difference in distance,R_d, the wave has to travel from the source to any point on the surface is

$$R_d < \frac{\lambda}{16}. \tag{2.21}$$

This is illustrated in Figure 2.8 with a point source radiating a wave. In the figure it is shown that

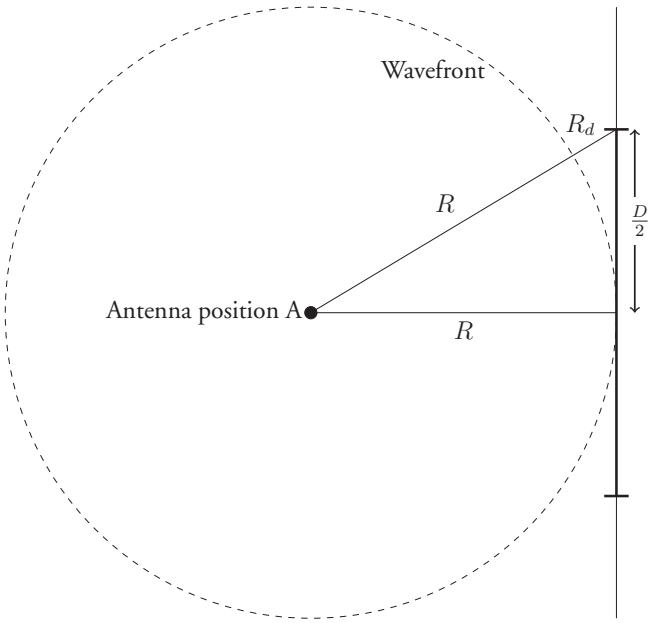

Figure 2.8: Defining the far field from the phase front of a propagating wave. The wave propagating from the antenna to an object of extension D has to travel a distance R to reach the closes part of the object, and a distance $R + R_d$ to reach the farthest part.

the wave has to travel different distances to reach the different parts of the object of extension D. The roles in Figure 2.8 can be reversed, instead considering an antenna of extension D radiating a wave towards point A. Using the Rayleigh criterion (2.21), the far field boundary is

$$R > \frac{2D^2}{\lambda}, \tag{2.22}$$

where D can be either the antenna dimension or the extent of the object in the antenna beam. As mentioned, the limits in (2.21) and (2.22) are just "rule of thumb" limits as the transition from near to far field is gradual and dependent on the needed accuracy of an application.

2.3 Radar equipment used in the work of this thesis

All the measurements presented in this thesis has been conducted using either an Agilent vector network analyzer (VNA) [16] or an UWB radar developed at FFI called the HUBRA radar [11, 12, 14].

2.3.1 Network analyzer

The VNA can transmit and receive signals from 10 MHz to 50 GHz in frequency at a variety of waveforms, both wideband and single frequency. A network analyzer is an instrument normally used to measure the amplitude and phase parameters of an electrical network. By connecting antennas to the ports of the network analyzer and recording the S parameters, the VNA operates as a radar. Parameter S_{nm} is the ratio between the transmitted voltage at port m and the received voltage at port n. Both the amplitude and phase are sampled as a real and imaginary pair in the I & Q receiver. A directional coupler in each port makes measurements of S_{11} and S_{22} parameters possible. The network analyzer is seen in Figure 2.9.

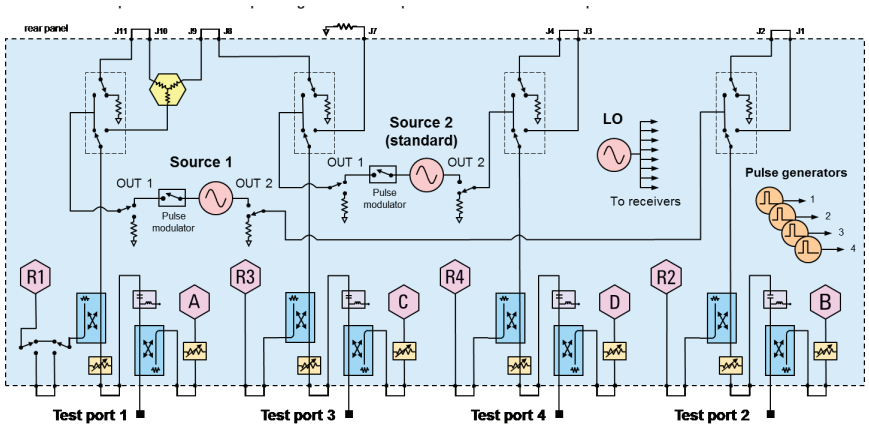

Figure 2.9: A block diagram of the network analyzer used in much of the experimental work of this thesis.

2.3.2 HUBRA radar

The HUBRA radar is an UWB radar operating in the 0-3 GHz range. For the work of this thesis, an FMCW waveform over either the entire band or sub-bands were used. Typical parameters for a HUBRA measurement are a sweep time of 1 ms, pulse repetition frequency of 100 Hz or more, sampling frequency of 1 MHz and an average transmitted power of 0 dBm. Figure 2.10 displays the HUBRA radar.

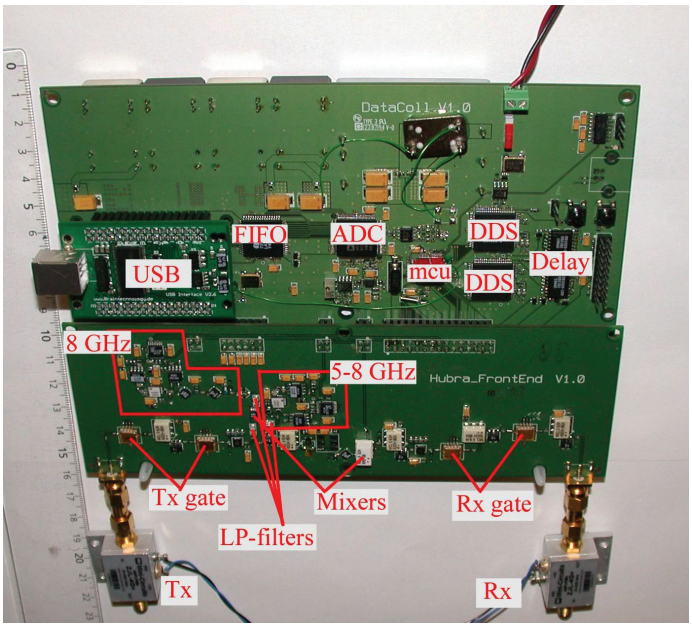

Figure 2.10: The HUBRA radar circuit boards. A more detailed description is given in [12].

2.3.3 Antennas

Depending on the frequency and applications, different antennas have been used. The performance of antennas are frequency dependent. Depending on the design, the gain and frequency range can vary greatly. For the ranged measurements in this thesis, three different antennas have been used. UWB Vivaldi antennas 28 cm in extent operating in the 0.5 - 4 GHz range [17] seen in Figure 2.11(a) were used for many of the measurements in this range. The antennas have little directivity, especially for the lower part of the frequency range. They are simple to fabricate, and can be made out of PCB. A pair of ridged horn antennas with an opening of 22.5 cm seen in Figure 2.11(b) were also used in the same frequency range, providing slightly more directivity in the transmitted field. For measurements in the 4 - 18 GHz range, a pair of smaller wideband Tecom horn antennas specified for this frequency range, and with dimensions 4 by 4 cm seen in Figure 2.11(c) were used.

When doing measurements with antennas placed in contact with the human body, the antennas mentioned above could not be used due their shape being a poor match with the body shape. A simple yet fitting antenna type are fat dipole antennas, such as the one seen in Figure 2.11(d). They can be made out of PCB, and a flat antenna of small size makes for good contact with the human chest. The design of antennas for good transmission inside the human body is a large topic in itself, and has not been further addressed in this thesis.

Due to lacking measurement equipment, no measurements of the antenna gains and beam patterns are available. The antennas shown in Figure 2.11(a) are described in [17], and the antennas shown in Figure 2.11(c) are specified by the manufacturer to work in the 4 - 18 GHz range. Other than this, only the S11 parameters measured by the network analyzer has been available. While this

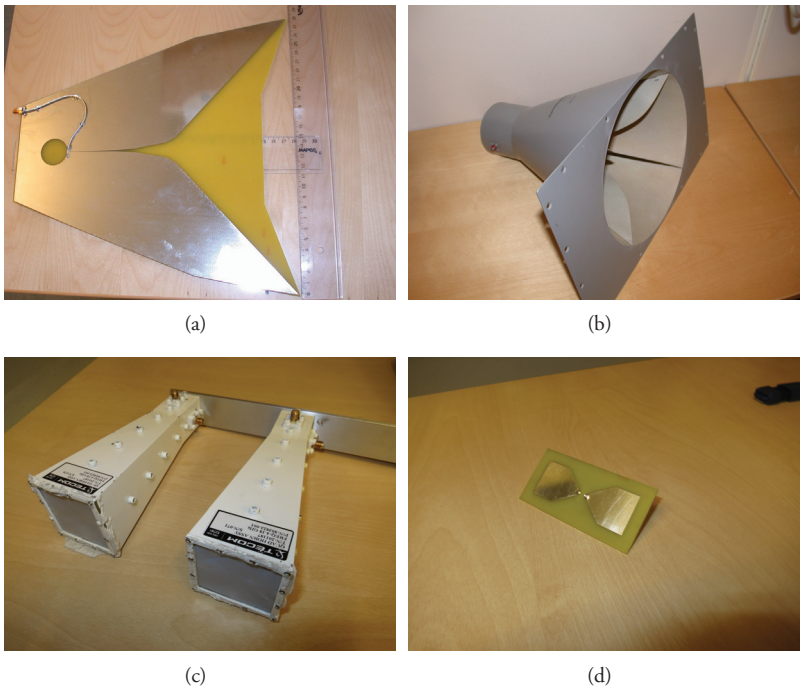

(a) (b)

(c) (d)

Figure 2.11: The antennas used. Displayed in (a) is a 0.5-4 GHz Vivaldi antenna, in (b) a 0.5-4 GHz horn antenna, in (c) the 4-18 GHz horn antennas and in (d) a fat dipole antenna.

may have resulted in us using sub-optimal antennas at times, it is not of great importance in the experiments performed in this thesis. In the RCS measurements the antenna gain is calibrated out, while in the other measurements it is the modulation that is of importance and not to maximize the signal power.

2.4 Considerations on the experimental work

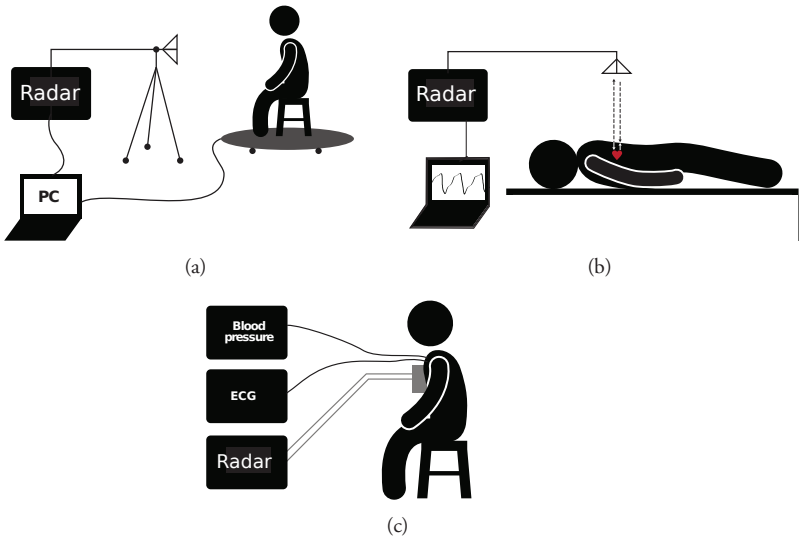

Figure 2.12: Three different heartbeat and respiration measurement scenarios. In (a), the person under test is seated on a chair, with the radar and antenna a distance away. In (b), the person is lying down, with the antenna placed above facing the torso of the person. Both these are illustrations of non-contact, or remote, monitoring of the vital signs. In (c), the radar antenna is placed in contact with the person's chest, an example of on-body, or contact, monitoring of the vital signs.

Monitoring of human heartbeats and respiration with radar can be performed in many ways. Figure 2.12 is an illustration of three examples of measurement setups. In Figure 2.12(a) and Figure 2.12(b), the vital signs are monitored from a distance without contact between the radar equipment and the person. In Figure 2.12(c), the antennas are placed in contact with the chest, transmitting the radar waves directly into the person instead of going through air first. These three setups, including variations of these, cover many of the intended applications mentioned in Chapter 1. Thus, our experimental work have mainly been based on these experimental setups. In the following are some considerations on carrying out such measurements.

2.4.1 General considerations

As seen in the radar equation (2.1), the power received at the antenna is inversely proportional to R^4, where R is the range between the antenna and the person. Additionally, as (2.2) shows,

the SNR is dependent on the ratio between the transmitted power and the noise floor. Both these arguments calls for a high transmitted power. On the other hand, radiation safety, system components and government regulations call for a low transmitted power. The HUBRA radar transmits a mean power of about 0 dBm over the frequency band, while the network analyzer is capable of transmitting up to 15 dBm. These values have been used for most of the experimental work. In comparison, mobile phones typically transmit a power of 20 - 30 dBm, and typical WLAN transmission power is around 15 dBm.

There exist regulations for the emission levels and frequencies of UWB medical devices. The European ETSI regulations allow unregulated use of the 6.0 - 8.5 GHz band with power spectral density emission levels below -41.3 dBm. This is a significantly smaller band than the US FCC regulations allowing emission in the 3.1 - 10.6 GHz band under the same power restrictions. In the experimental work of this thesis these regulations have not been obeyed, as the goal has not been to make a system working under the regulation. Indeed, the findings presented in this thesis show that as high frequencies as possible are best suited for remote vital signs monitoring, while low GHz or sub-GHz frequencies are best suited for on-body heartbeat monitoring. The frequency bands regulated for UWB medical radar are thus not the optimal bands to use.

For the ranged applications, the near/far field issues introduced in Section 2.2.3 need to be considered. The longest wavelength we used was 60 cm (at 500 MHz), which with the limit of $R > \lambda$ means that the distance from the antenna needs to be larger than 60 cm. If instead the limit (2.20) is used this limit reduces to less than 10 cm. At higher frequencies, the wavelength is shorter and the far field limit using the limit in (2.20) becomes closer to the radar. The Rayleigh limit (2.22) means that the person will need to be a few meters away from the antenna when approaching tens of gigahertz frequencies, depending on what size we define as the reflector of interest on the person. The limit is dependent on D, being either the size of the antenna or the target of interest, with a bigger D resulting in a longer distance between antenna and target needed for a far field scenario. The limit is also dependent on λ, with short wavelengths requiring a long distance between antenna and target, while long wavelengths can tolerate a shorter distance.

The human body is not a perfectly flat plate, and reflections from different parts of the body will sum up constructively or destructively depending on the phase difference between the parts. If the person is a shorter distance away from the antenna than the limit (2.22), this vector sum will become dependent on frequency and distance from the radar, possibly increasing or decreasing the reflection. This is important if characterization of the person's reflection is important, such as in RCS measurements. If, on the other hand one wants to characterize the vital signs waveforms or compare various recordings at the same frequency and range, the Rayleigh limit is not important to obey. This relates to the experiments of this thesis in the following way: The RCS (or modulation measure) measurements of papers I-III, need to obey both the limit (2.20) and (2.22). Other measurements aiming to describe the modulation, such as the ones in papers IV and V, should obey the limit (2.20), while the Rayleigh limit (2.22) is not that important.

The signal reflected off a moving target will have a Doppler shift of the frequency according to (2.9). When sampling this signal, care must be taken so that the frequency shifted signal is still within the bandwidth of the receiver. The HUBRA receiver has a wide bandwidth, while the network analyzer in CW mode can have an IF band-with set as low as 1 Hz. Setting the IF bandwidth low means an improvement in SNR, while the sampling frequency is decreased as well. The lowest IF bandwidth used for the measurements was $f_{IF} = 100$ Hz, with the network analyzer.

For the receiver to capture the movement, the limit

$$\frac{2fv}{c} < \frac{f_{IF}}{2}, \tag{2.23}$$

where v is the velocity of the moving target, must be obeyed. With an IF bandwidth of 100 Hz and a carrier frequency of $f = 20$ GHz, the velocity limit is $v < 0.375$ m/s. This should be well within the limit of the movements connected to the heartbeat.

A parameter dependent on the IF bandwidth for narrow-band signals is the sampling frequency f_s of the system. According to the Nyquist limit, the sampling frequency needs to be twice the bandwidth of the signal. With frequency components all the way down to DC, this means the largest frequency content of the signal. If the signal contains elements of frequency higher than $f_s/2$, they will be wrapped around to the start of the spectrum and lead to frequency ambiguities. For FMCW the equivalent to f_s in this case is the pulse repetition frequency f_{PRF}. In this context, the frequency is not the frequency of the EM wave, but rather the frequency of the vital signs activity in slow time. The sampling frequency f_s (or for FMCW the pulse repetition frequency f_{PRF}) should thus at least be in the order of tens or hundreds of hertz.

Additionally, for FMCW signals, range ambiguities can occur if the sweep is not sampled densely enough. The unambiguous two way travel time of an FMCW system is given by

$$\tau_{ua} = \frac{N_s}{2B}, \tag{2.24}$$

where N_s is the number of samples in one sweep and B is the bandwidth of the system. This gives an unambiguous range of

$$R_{ua} = \frac{v_p N_s}{4B}. \tag{2.25}$$

v_p is the phase velocity of the medium. In free space and air this is equal to the speed of light c. Any reflectors farther away than this will wrap into the range $[0, R_{ua}]$ and appear closer than they truly are. This distance includes the cable lengths and the electrical delay of the system, unless calibrated out. Filtering on the received signal can remove this effect.

When the antennas are placed on the body, much of the discussions above are not valid and the moving targets of interest may even be in the near field of the antennas. The experiments reported in this thesis used frequencies around 1 GHz for on-body measurements. With 1 GHz frequency and using the muscle permittivity of $\varepsilon_r = 54.8$ (see Figure 3.6), the wavelength inside the body is approximately $\lambda = c/(f \cdot \sqrt{\varepsilon_r}) = 0.04$ m. According to the Rayleigh limit (2.22), and using an antenna size of $D = 6.2$ cm, the plane wave far field criterion is $R > 2 \cdot 0.062^2/0.04 = 0.2$ m. This is clearly further away than the distance from the chest wall to the heart, and the waves incident on the heart wall can not be considered plane (there are additional dispersive and scattering effects due to the inhomogeneity of the human body). The limit (2.20) on the other hand, gives the criteria $R > 0.04/2 \cdot \pi \approx 6$ mm. With the distance from the chest surface to the heart wall around 2-3 cm, the $1/R$ term of the electromagnetic field is dominating.

The signal path between the antenna and chest surface is inhomogeneous and varies from person to person. But even with the complicated signal path, movements of the heart will lead to phase modulations in the received field. Because the waves incident on the heart wall can not be

considered plane and the spatial extent of the heart, backscattering from the different parts of the heart wall will sum with possible destructive and constructive interferences at the radar receiver. Because of this, different aspect angles should result in different recorded heartbeat waveforms.

2.4.2 The actual experiments

In a radar recording, energy will be backscattered toward the receiving antenna from every object within the antenna beam. The reflections from targets in the scene that are not of interest are often termed clutter. In the case of measuring heartbeats or respiration, this includes all other parts of the room, as well as the parts of the person that is not connected to the physiological motion, such as the arms and legs. In vital signs monitoring stationary clutter is not a big problem, as it may be filtered out. A more difficult problem is all other movement in proximity to the antenna, including body movements of the person, as this may distort or mask the modulations observed from the vital signs. The vital signs movements may also appear in the data at different phase shifts due to multi-path reflections of the signal, for example from floor reflections or ringing between the antennas. Other electromagnetic signals, such as wifi or mobile phones, in the same frequency range as the one used by the radar may also disturb the radar measurements.

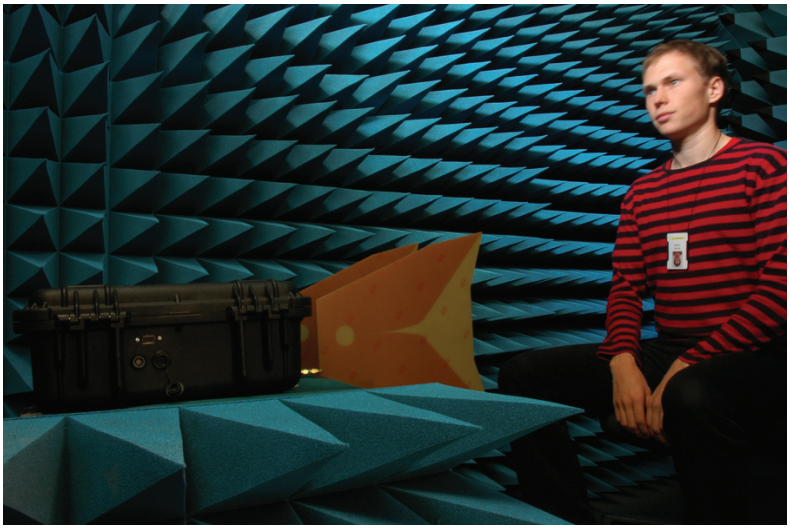

Figure 2.13: A measurement setup using the HUBRA radar with a pair of Vivaldi antennas directly connected to the radar. Measurements were performed in an anechoic chamber with a person seated in front of the antennas.

To minimize external disturbances of the radar recordings, an anechoic chamber was used for most of the measurements. The chamber walls and ceiling were covered in metal film and electromagnetic absorbers, as seen in Figure 2.13. Ideally, the room shields the antennas and measurement equipment from external EM sources. Additionally, any waves incident on the side walls should be attenuated by 25 dB, and the waves incident on the back walls should be attenuated by 35 dB according to the manufacturer. The actual chamber has an opening to allow people and equipment to enter, and parts of the floor needs to be left uncovered by absorbers to allow movement. Both

these factors degrade the attenuation properties. The chamber is also small in size, which means that the transmitted waves will not have a close to normal incidence on parts of the side wall. An effect of this is that the reflection will not be attenuated by as much as 25 dB. Still, the anechoic chamber provides a more controlled environment than a normal office or lab.

2.5 Micro Doppler and detection of small movements

Small movements of a reflector will be recorded as small phase changes in the radar echo. In the ideal case of only a single point reflector in the scene, this will in a single frequency CW radar be recorded as a change in the two way travel time τ in (2.10)

$$b(t) = H_{sys}\frac{E_0\sqrt{\sigma_{RCS}}}{\pi(c\tau(t))^2}e^{-i\omega\tau(t)}. \tag{2.26}$$

With movements $\tau(t)$ much smaller than the two way travel time to the target, the amplitude changes of the above equation can be ignored.

Looking at the same target with an FMCW system results in a very similar recording. Using only the positive two way travel times of (2.19), and choosing a two way travel time $\tau = \tau_0$, with τ_0 being the initial distance to the moving target, the recording is

$$b(t) = H_{sys}\frac{E_0\sqrt{\sigma_{RCS}}}{\pi(c\tau(t))^2}e^{i\omega_c\Delta\tau(t)}\frac{\sin(\pi B\Delta\tau(t))}{\Delta\tau(t)}. \tag{2.27}$$

Here, ω_c is the center frequency of the system and $\Delta\tau(t)$ is the time variating deviation in two way travel time from the initial τ_0. Since the movement $\Delta\tau(t)$ is small the deviations from zero in the argument of the sinc is small, and the sinc function can be approximated by 1:

$$b(t) = H_{sys}\frac{E_0\sqrt{\sigma_{RCS}}}{\pi(c\tau(t))^2}e^{i\omega_c\Delta\tau(t)}, \tag{2.28}$$

which is the same expression as the recorded single frequency CW recording. The difference between the two methods is seen when there are other scatterers in the scene, as a system with bandwidth can separate targets that are a distance apart. This comes with a tradeoff however, as the complexity of the system increases as well.

In (2.26) - (2.28) above, only the ideal case of a single point scatterer in the antenna beam was considered. In the real world this will never happen, as other objects within the antenna beam as well as coupling within the system itself will appear as reflections in the radar recording. All these static scatterers sum up to form the total DC in a recording. Separating small movements from larger targets in radar recordings have been covered earlier, for instance in [18, 19]. In Figure 2.14, a radar recording of a breathing person is shown. The data form what is close to an arc in the complex plane, corresponding to a phase modulation with a DC offset. Looking closely at the data trace, modulations on a smaller scale can be seen. These are a combination of heartbeat modulations and other factors such as involuntary movements of the person. The challenge in processing radar vital signs recordings lie in separating the details of the physiological motion from all the other factors present in the recording. This is discussed in more detail in Paper IV.

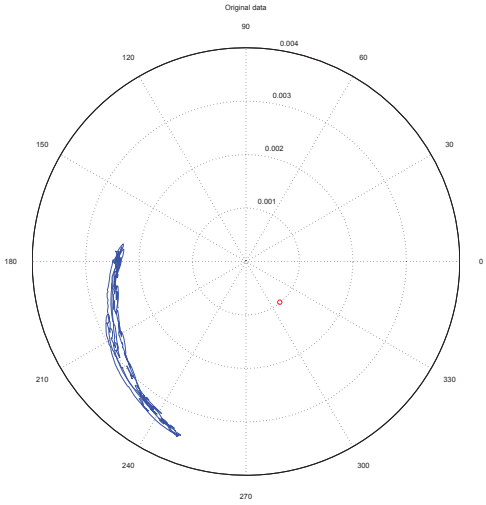

Figure 2.14: A recording of a breathing person using a narrow-band 18 GHz CW waveform. The data is plotted in the complex plane, with a red dot marking the estimated DC component.

Summary

In this chapter, an introduction to radar and the used radar waveforms were provided. All the experiments described in this thesis were performed using either narrowband continuous wave or ultra wideband FMCW waveforms. Both a vector network analyzer and an FFI developed radar were used. The experiments were carried out in an anechoic chamber, at distances according to the near/far field discussion in this chapter. By the equations outlined in this chapter, heartbeat and respiration monitoring is a matter of extracting small phase modulation from a complex set of data.

Chapter 3

Medical radar

3.1 Heart and thorax physiology, and heartbeat movement

The heart is located inside the chest slightly to the left of the sternum. Figure 3.1 displays an MRI image of a slice of the human chest, and shows the location of the heart inside the body. A

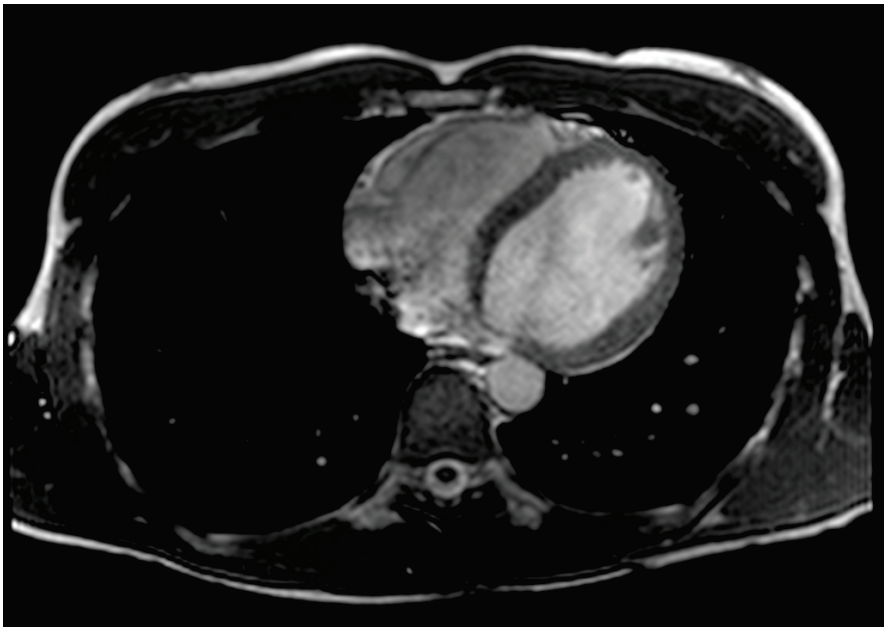

Figure 3.1: An MRI image of a male human chest. The image is a horizontal slice of the chest approximately at the middle of the heart, viewed from the bottom and up. The front of the person is facing up in the figure. The large grey area slightly to the left in the thorax (to the right in the picture) is the heart. The large dark areas are the lungs.

diagram of the heart is seen in Figure 3.2 [20]. The heart is a muscle consisting of four chambers; the right and left atria and the right and left ventricles. The ventricles are larger than the atria. The heart acts as a pump, transporting blood around the body. Deoxygenated blood is transported from the body into the heart through the vena cava, which is a large blood vein ending in the right

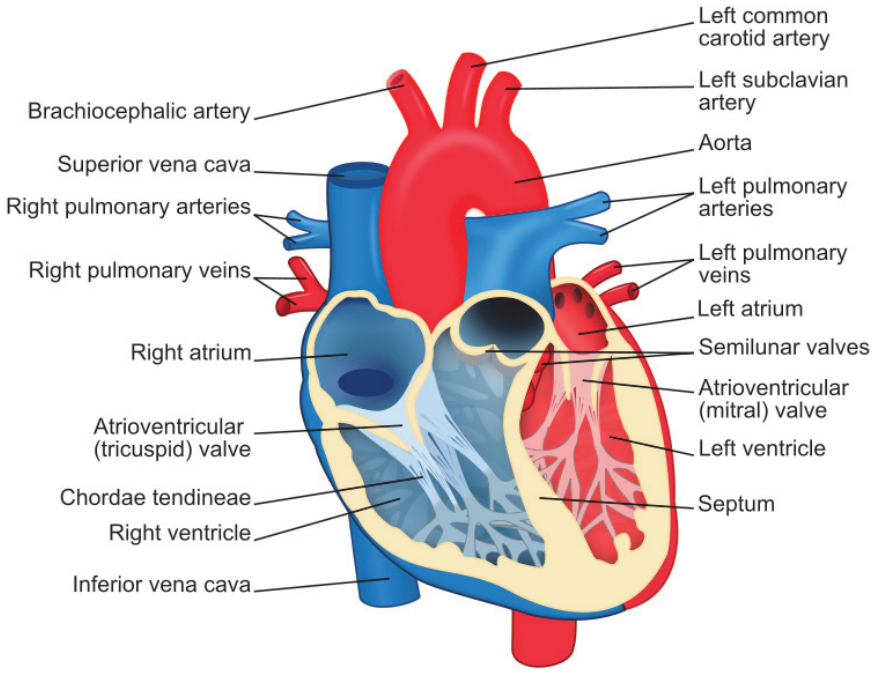

Figure 3.2: A diagram of the heart [20].

atrium. The blood is transported from the right atrium to the right ventricle, and pumped through the pulmonary artery to the lungs where carbon dioxide is deported and oxygen is taken up. The oxygenated blood from the lungs enter the heart in the left atrium and is transported further into the left ventricle. From the ventricle, the blood is pumped into the body through the aorta.

A heartbeat starts in the sinoatrial (SA) node, which contain autonomous oscillating cells. At the onset of each heartbeat it initiates an electrical action potential that propagates through the heart and triggers the contraction of the different heart muscles at different times. The cardiac cycle is shown in more detail in Figure 3.3, displaying the Wigger's diagram [21].

The heartbeat starts with the contraction of the atria, seen as the P-wave in the ECG. The weak fourth heart sound S_4 occurs right after the contraction of the atria. This is also the last part of the filling of the ventricles. The QRS complex in the ECG is the triggering of ventricle contraction. While the ventricles contract, pressure is built up until the pressure is higher in the ventricles than the arteries, and the Atrioventricular (AV) valve closes. The closing of the AV valve produces the first heart sound S_1. When the ventricular pressures exceed those in the aorta and pulmonary artery, the aortic and pulmonary valves open and blood flows from the ventricles into the aorta and pulmonary artery. At the end of the blood flow, the aortic and pulmonary valves close, producing the second heart sound S_2. With the opening of the AV valve and relaxation of the ventricles, ventricular filling starts. This event is associated with the third heart sound S_3. The next heartbeat starts with the atrial contraction.

During a heartbeat the heart contracts and expands, but this is not the only movement of the heart. In Figure 3.4 the longitudinal movements of the left ventricle wall is seen. Figure 3.5 shows

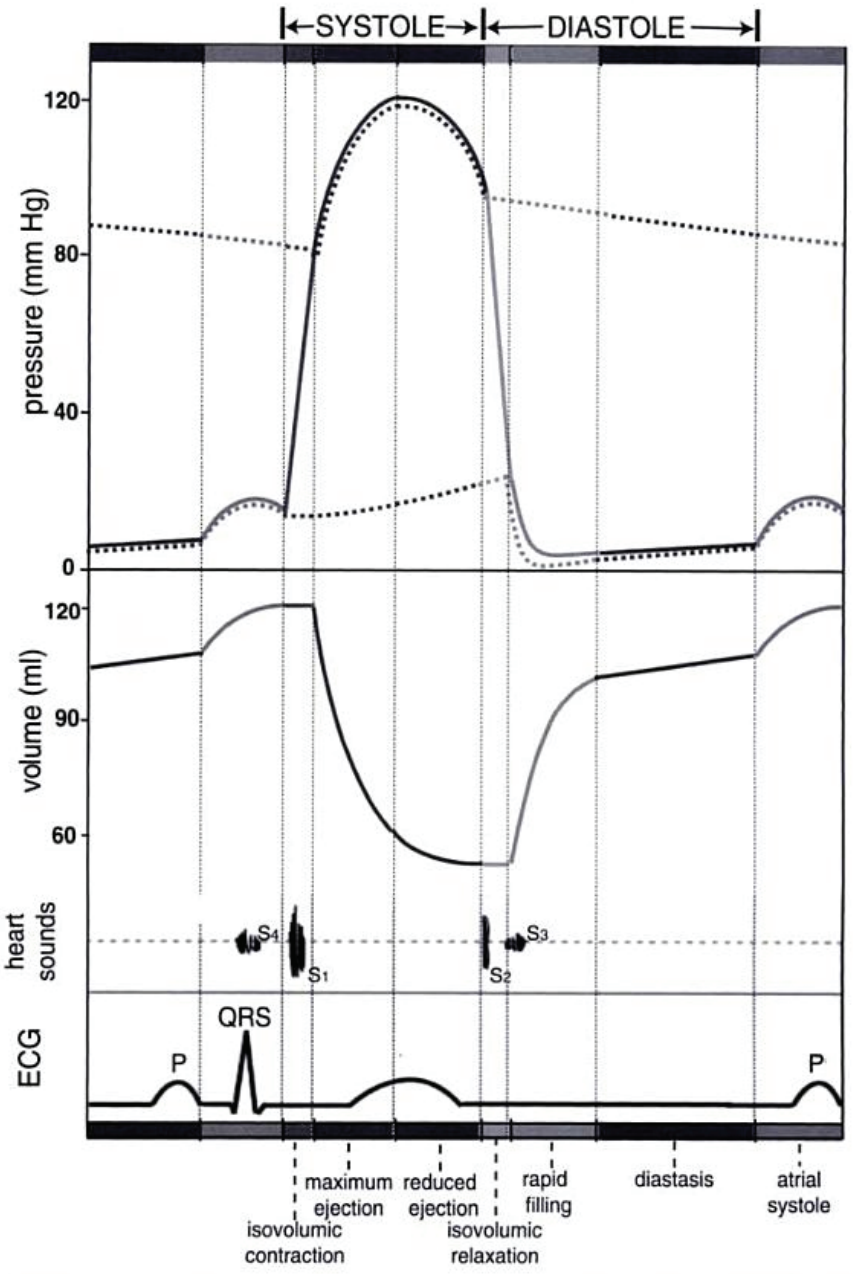

Figure 3.3: The heartbeat is divided into two main parts: Ventricular systole (ejection of blood from the ventricles) and ventricular diastole (the filling of the ventricles). Displayed from top to bottom: The ventricular pressure, the ventricular volume, the four heart sounds, and the ECG. The figure is found in [21]

the rotation of the heart during a heartbeat. Both figures are found in [22]. The apex of the heart is the lowest superficial part of the heart and is pointing forward and to the left. During a heartbeat the twist in the apex seen in Figure 3.5 results in the heart beating towards the chest. A radar

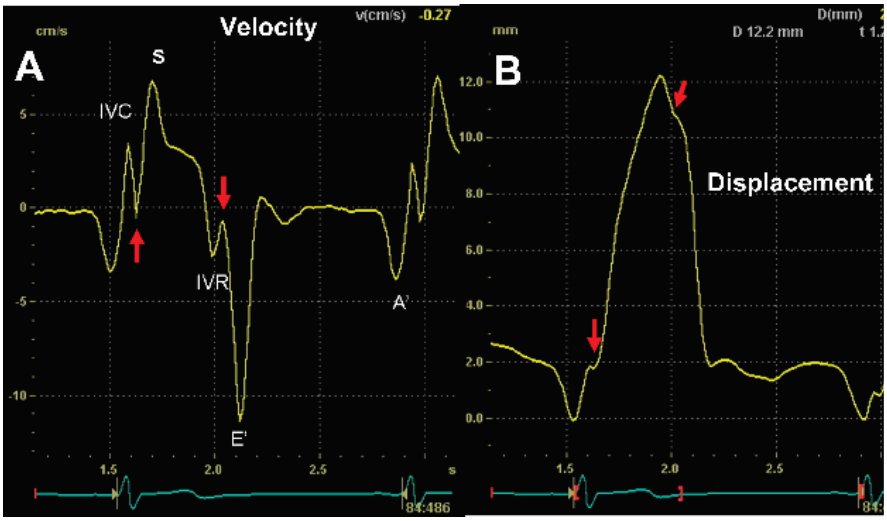

Figure 3.4: The longitudinal movement of ventricle walls during a heartbeat. To the left is the velocity, to the right the displacement. Figure from [22].

measuring the heart activity measures the sum of all these movements.

For further reading on the heart physiology and mechanics, the reader is referred to [21, 22, 23, 24, 25]

3.2 Electromagnetic wave propagation in the body

3.2.1 Dielectric properties of body tissues

The propagation of electromagnetic waves in a medium is dependent on the medium's dielectric constant ε and magnetic permeability μ. For non-magnetic materials, including all body tissues and air, the magnetic permeability is approximately equal to that of free space $\mu_0 \approx 1.257 \cdot 10^{-6}$ H/m. For most materials, the dielectric constant is complex, $\varepsilon = \varepsilon' - i\varepsilon''$, where ε' is the permittivity connected to the propagation and $i\varepsilon''$ is the imaginary part connected to the dissipation of energy in the material. Vacuum has dielectric constant $\varepsilon_0 \approx 8.854 \cdot 10^{-12}$ F/m. Other materials are often expressed relative to vacuum:

$$\varepsilon = \varepsilon_r \varepsilon_0 = (\varepsilon'_r - i\varepsilon''_r)\varepsilon_0. \tag{3.1}$$

Instead of ε'', the conductivity $\sigma = \omega\varepsilon''$, where ω is the angular frequency, is often used. Zero conductivity means no loss in the propagating electromagnetic wave, while a high conductivity means a high loss. For low conductivity materials, the permittivity affects the electromagnetic

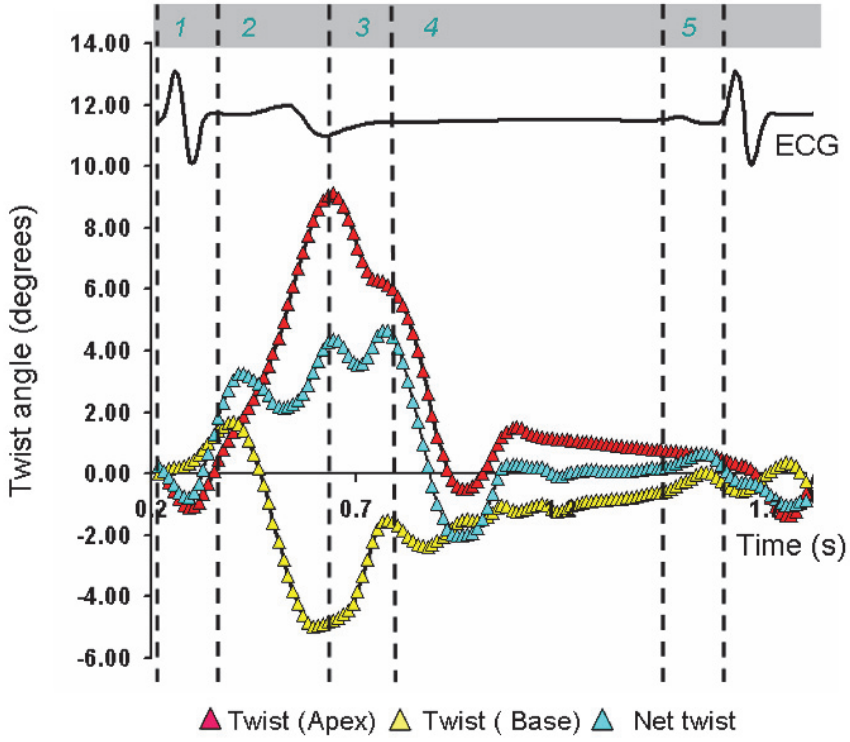

Figure 3.5: The rotation of the heart at the apex (bottom forward left part of the heart) and base (top right back of the heart) during a heartbeat. Figure from [22].

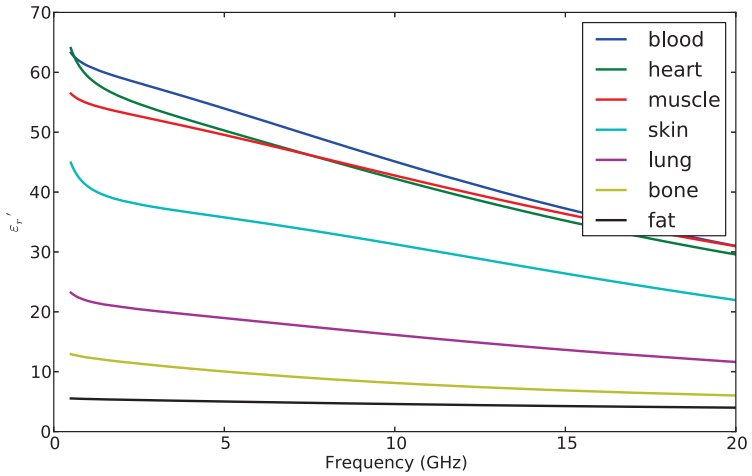

Figure 3.6: The relative permittivity ε_r' of some selected body tissues, calculated using the models of [26, 27, 28]. At sub-gigahertz frequencies the change in frequency is larger than in the gigahertz frequencies, making the body tissues more dispersive at low frequencies.

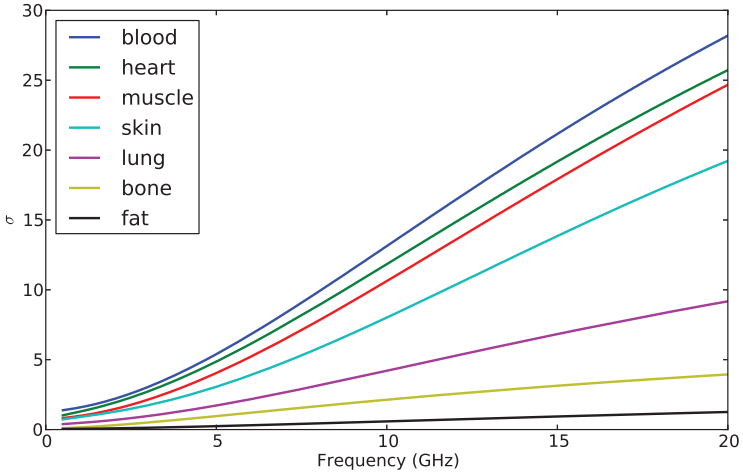

Figure 3.7: The conductivity of some selected body tissues, calculated using the models of [26, 27, 28]

propagation speed in the material through

$$v = \frac{c}{\sqrt{\varepsilon_r'}}. \tag{3.2}$$

The propagation of an electromagnetic wave is described in [5], and more general theory on electromagnetic propagation can be found in [10]. Some permittivities and conductivities of body tissues are shown in Figure 3.6 and Figure 3.7 as functions of frequency. These properties are found in the functions of human body dielectric properties by [26, 27, 28]. Using the permittivity values seen in Figure 3.6 and (3.2), it is clear that the propagation speeds in the body tissues are reduced relative to air. This increases the spatial resolution of UWB radars. With antennas placed in contact with the human chest, it also shifts the transmitting band into the body down in frequency. The conductivity plotted in Figure 3.7 is directly related to the attenuation of the wave in the medium. All the displayed body tissues have increasing conductivity with increasing frequency. Hence, the loss of a propagating wave is higher with higher frequency.

3.3 Medical radar history

Radar technology have existed for over a hundred years, with much of the early development focused around military applications in connection with World War II [29]. With radar systems becoming smaller due to the technology allowing higher frequency systems, new applications rose. According to [9], the first reports of using radar for detecting physiological volume changes dates back to 1958. In [30], radar was used for contact-less monitoring of breathing in infants, while the use of radar for detection of excess water in the lungs was proposed in [31]. Lin et. al. [32] were among the first to use radar for non-contact monitoring of heartbeats, through a 2.1-2.5 GHz

radar with the antenna placed 3 cm from the chest. They identified phases of the radar recording with phases of the heartbeat using simultaneous ECG and phonocardiogram.

Extensive literature reviews have been performed earlier, and will not be repeated here. Instead the reader is referred to the following publications for an overview of the literature. In 1992, the literature on heartbeat and respiration monitoring were reviewed [33]. In chapter 2 of [34], another literature review of the research per 2006 is provided. A list of selected publications on heartbeat and respiration monitoring using radar can be found in [35]. A large portion of the publications on medical radar have been focused on system design. The earliest systems cited above were single frequency Doppler radars working at a few gigahertz frequency. This continued until UWB radar popularity was increased following the micro power impulse radar [36, 37] further popularized through [38].

Since then a variety of systems have been demonstrated for heartbeat and respiration monitoring. Operating frequencies from a few hundred MHz [39] to over two hundred GHz [40] have been successful in monitoring the human heartbeats from a distance. A number of systems have used the open 2.4 GHz frequency with its cheap components. Some have focused on making the system as affordable and simple as possible, such as [41] using a baby monitor at 2.4 GHz and a passive sensor node. The small size of the heartbeat movements demand a high dynamic range of the radar system, making it challenging to achieve simplicity, low cost and good measurements at the same time.

3.3.1 Quantization of vital signs

The modulations in the radar data caused by the vital signs are small, regardless of measurement setup and radar system. Figure 3.8 shows an example heartbeat recording where the chest movement has been estimated. Especially for heartbeat detection performed from a range, the modulations may be lower than the noise floor for some ranges, frequencies and aspect angles. In the design of a system, it is important to know how sensitive the system needs to be with regards to parameters such as dynamic range and range to sufficiently detect the vital signs. Additionally, different applications require different radar systems.

One approach to quantizing the vital signs was taken by [42], where people's heartbeats are detected from a distance using Doppler radar. They knew the system parameters, and compared the observed heartbeat modulation with the system noise. This way, they could put a number on how reliable the vital signs could be detected from various ranges for this given radar system.

Another issue in non-contact patient monitoring is what aspect angle to use. A patient may move during the monitoring, and it is important to know how this change of aspect angle will affect the radar measurements. One way of approaching this problem is, again, to use the system at hand and measure what aspect angle is best. This approach was taken by [43], where a 27 GHz radar was tested for overnight monitoring of vital signs on human beings. They found that using this system, the heartbeats were best detected from the back and not from the front as one may expect.

The examples above are good for determining the performance of specific radar systems. But for systems that are different from the ones used it is not certain whether the results are the same or if they are system dependent. For example, in [42] it was found that the heartbeat detection reliability was falling for ranges over 1 m. Another system [40] using a higher frequency and a

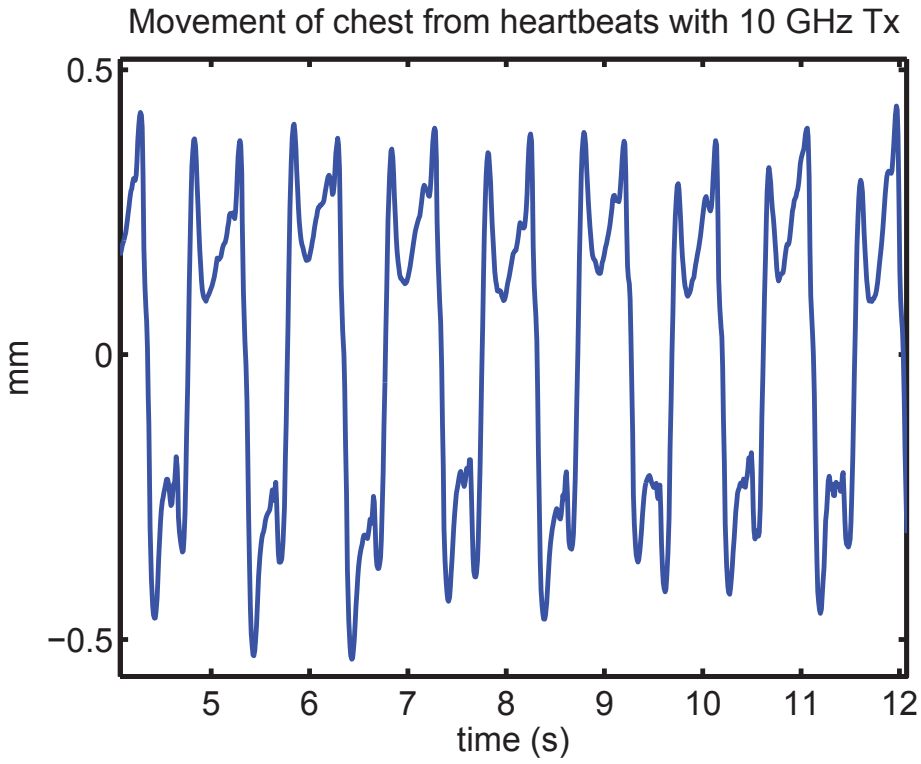

Figure 3.8: Estimated heartbeat movement using non-contact 10GHz radar.

different receiver, is able to detect vital signs at up to 50 m range. The best is to have a radar system independent measure of the human being vital signs modulation. Such a measure can be used for all systems and for a great variation of applications.

In [44], 2.4 GHz CW radar RCS measurements of a person lying down were performed. The amplitudes of the measured data were corrected using theoretical and data sheet values of the system. They measured the RCS of the person from the modulations originating from breathing. They found that the RCS of a breathing person was 0.326 m^2measured from the front of the person, and 2.9 m^2measured from the back of the person. The larger RCS seen from the back is attributed to the back being flatter than the front of the body. This however, was a RCS measurement of the moving parts of the person and does not directly quantize the breathing modulation itself. Such an experiment was performed by [45], using measurements of a person lying down using an UWB radar with 750 MHz center frequency. They calibrated the measurements using free space radiation between the antennas to remove the system influence on the measurements. Instead of measuring the RCS of the person, they estimated the size of the modulation itself, calling it the breathing cross section. It was found that the breathing modulation was largest when the person was lying on the side facing the antenna.

When breathing, harmonics and inter-modulation between the breathing and the heartbeats may hide or confuse the detections of the heartbeats. [46] provides a theoretical view on inter-modulation issues between the heartbeat and respiration movement. Through simulations it was found that there is an optimal frequency for detecting the heartbeat, depending on the size of the heartbeat and respiration movements. The optimal choice in real life scenarios is not necessarily to choose as high a frequency as possible as the findings in [3] suggest. This is due to the inter-modulation and harmonics with the respiration hiding the heartbeat response for both the higher and lower frequencies. In the simulation of [46] however, both the heartbeats and respiration were modeled as pure sine wave motions of a point scatterer. If the same effects occur with the real life waveforms is not certain and still needs to be investigated.

3.3.2 Vital signs signal characteristics

Even though what physical processes are the cause of heartbeat modulation in radar measurements have not been fully understood, some research has been put into characterizing the measurements and recorded waveforms. For some purposes, such as studying the harmonics and inter-modulations between respiration and heartbeats [46], the physiological modulation in the radar have been modelled by simple sine waves. It is clear from measurements that the actual recorded modulation does not follow such a simple waveform, but contains more information connected with the different parts of the heartbeat. Knowledge of the vital signs waveforms are also important in designing the optimal processing for a given application. A number of previous studies have been performed, mainly on characterizing the heartbeats. Some of these are mentioned below, separated into non-contact(Figure 3.9) and on-body (Figure3.10) analyses.

Non-contact analysis

Separating important physiological parameters in the radar waveform from clutter and noise is in many ways more difficult in the non-contact scenario than in the on-body scenario. Unless the frequency is very high or an array with substantial number of antennas is used, the radar recording

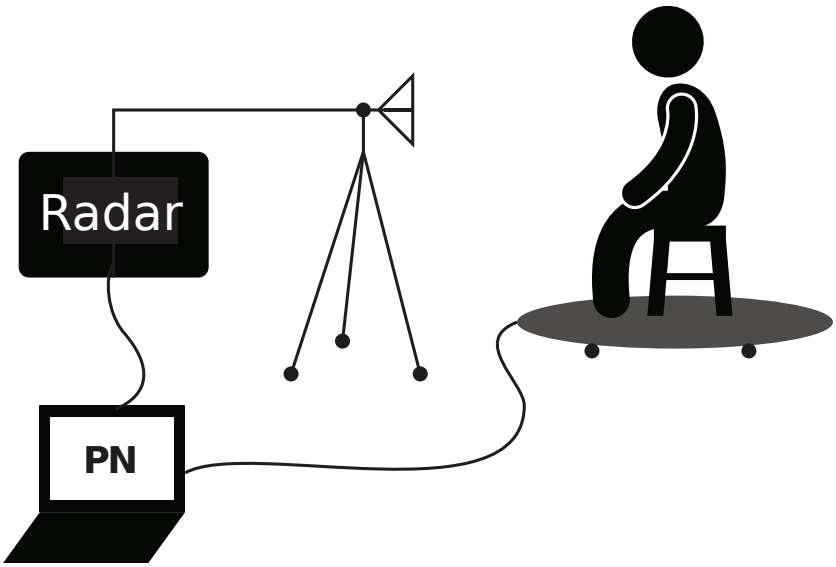

Figure 3.9: The setup of a non-contact heartbeat measurement.

will also contain echoes from other objects in the scene. Additionally, small body movements are visible in the measurements, and are often hard to totally separate from the wanted physiological signal [47]. Another problem is inter-modulation and harmonics from the respiration at the same frequencies as the heartbeats [48, 46].

A number of people have performed simultaneous ECG and radar recordings of the heartbeats. One such example is [49]. The ECG is a thoroughly studied measurement technique, and the characteristic parts of an ECG is connected to known phases of the heartbeat. In [32], antennas were placed 3 cm from the chest to monitor heartbeats using a 2.45 GHz radar. The radar measurements were compared with ECG and phonocardiogram. The known heartbeat monitoring techniques were used to connect features in the radar measurements with physiological phenomena. In [50], UWB measurements from four different angles of incidence at the chest were performed with simultaneous ECG data. They used the knowledge of the ECG to label parts of the radar recordings with physical happenings such as the contraction and relaxation of the atria and ventricles. The waveform of the radar recordings are different when different aspect angles are used.

On-body analysis

The characterization of heartbeats using on-body antennas started several decades ago with the findings reported in [9]. One antenna was placed on the chest while another was placed on the back of a person. The transmission loss between these antennas was measured, and the time development of this bore close resemblance to textbook ventricular volume changes. The authors of [51] used a similar setup, with 868 MHz, and compared the findings with photoplethysmograph recordings. A

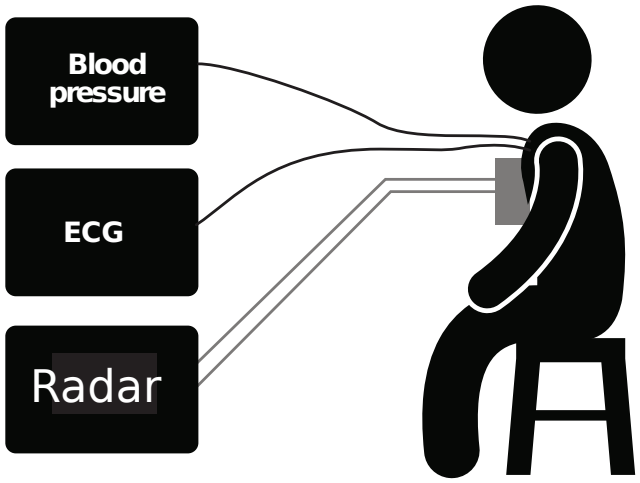

Figure 3.10: The setup of an on-body heartbeat measurement.

quite different waveform of the heartbeats is observed compared to the ones in [9]. Why this is the case is unclear. It could be differences between the persons under test, but more likely this difference is attributed to the different systems, frequencies and possibly separate antenna placements.

The work by [52, 53, 54] have described 2.45 GHz radar measurements in terms of ECG and ICG measurements. In [52], the antennas were placed on the sternum. Waveforms of both the received radar voltage and its derivative were displayed and ICG measurements were used to connect the radar measurements with parts of the heartbeats. In [53] the same exercise was performed with two radar channels and comparisons with ECG. Characteristic points of the heartbeats were found in the radar waveforms were there were none in the ECG, indicating that radar can be used to detect events in the heartbeat that the ECG cannot. In these papers, heartbeat events such as opening and closing of heart valves and ejection and filling phase of the heart chambers were found using the reference measurement technique. These events were marked in the radar recordings. In [54], contact radar measurements from different parts of the torso were performed. It was found that there is a significant difference in the signal when monitoring from different angles. This agrees well with the discussions in Section 3.1 of the heart movement, with the heart twisting and turning in different directions.

3.3.3 Processing

As outlined in Section 3.3.2, the heartbeat radar recording is a complex signal that can be hard to characterize. Additionally, especially for the non-contact case, the measurements are susceptible to degradation from other sources because the modulations are so small. Extracting the wanted information from the vital signs recordings are by and large a processing problem. What processing of the data is needed depends on the application. It is for example a totally different problem to estimate the heartbeat rate of a person and to look for defects in the heart of the person. In this section some basic processing methods are mentioned.

One simple yet useful parameter of the heartbeats is the heart rate variability (HRV) of a person

[55]. For such applications the details of the heartbeat is not of interest, while reliable detection of heartbeats is important. In [56] a processing scheme for estimation of human heartbeats using a Doppler radar is presented. They use a center clipping and autocorrelation approach which provide good results on heart rate estimation. If one is interested in the heartbeat rate alone, one can choose to look at the spectral contents of the signal only and disregard the heartbeat waveform altogether. However, for such an approach to work reliably, respiration harmonics need to be taken into account [46, 48].

For information beyond the heart rate, looking at the shape of the recorded waveforms is a good approach. As [4] showed, the heartbeat waveform can be seen as a complicated shape in the complex plane. In the papers [57, 58], the use of I & Q receivers to measure vital signs is discussed. In an I & Q receiver the output is a signal in the complex plane, as explained in Section 2.2, and seen in Figure 3.11. They use the assumption that the heartbeat modulation is caused by

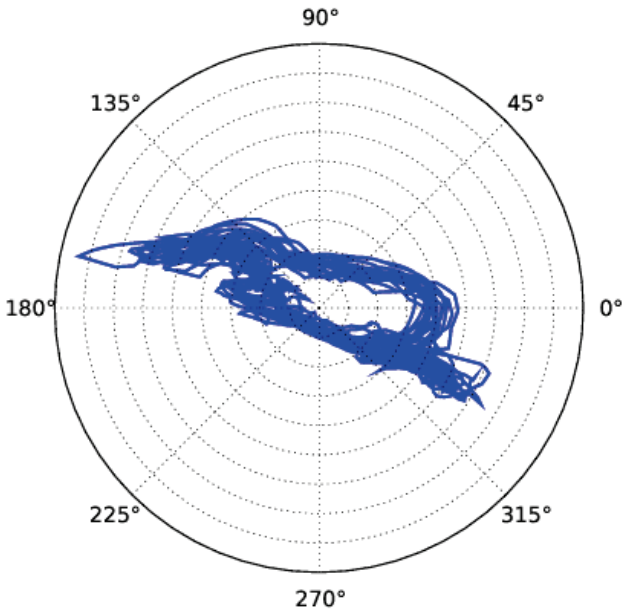

Figure 3.11: A 2 GHz recording of a series of human heartbeats plotted in the complex (I & Q) plane. The mean has been subtracted from the data, centering the modulation around origo.

a moving scatterer, which means that the modulation should appear as a phase modulation with a DC offset connected to the system DC and static scatterers. They explain the concept of estimating the DC offset and the phase modulation, a method they term arctangent demodulation. In [57] the respiration is used to provide an estimation of the DC offset and use this for the heartbeat phase estimation after filtering. However, as we show in [4], using the respiration as a basis for the heartbeat phase estimation is imprecise as different parts of the torso are connected with the heartbeat and the respiration.

While the phase estimation techniques of [4, 57, 58] provide the actual phase modulation which is directly connected to the movements of the body, they are susceptible to drift and random body

movements. Additionally, the complex shape makes the scaling of the phase estimations inaccurate and prone to variations that are not necessarily physical. For these methods to work properly, we believe that the measurements either need to be performed in controlled conditions, or very good body movement removal processing need to be implemented.

A more robust method, albeit less connected to the physical process, is to treat the modulations as variations along a straight line in the complex plane. When the movement is small compared to the wavelength, this simplification is quite accurate. In [48] linear regression is used to fit the cardiopulmonary movement along a straight line. The small movements of the chest caused by heartbeats or respiration causes a small phase deviation $\Delta\phi$ throughout the measurement. As long as the condition $\Delta\phi << 2\pi$ for the phase deviation $\Delta\phi$ of the physiological movement is met, the resulting waveform should be similar to that achieved by phase estimation. The possibility of estimating the movement is lost with this method of linear demodulation, as the relation $\Delta\phi = 2\omega\Delta R/c$ can not be used. For many applications though, this information may not be needed and the shape of the heartbeat waveform provided by the linear demodulation may be what is of interest. In Figure 3.12 the linear demodulation is compared to the movement estimation processing. While the two resulting waveforms are nearly identical in shape, the movement estimation contains information on the movements of the chest.

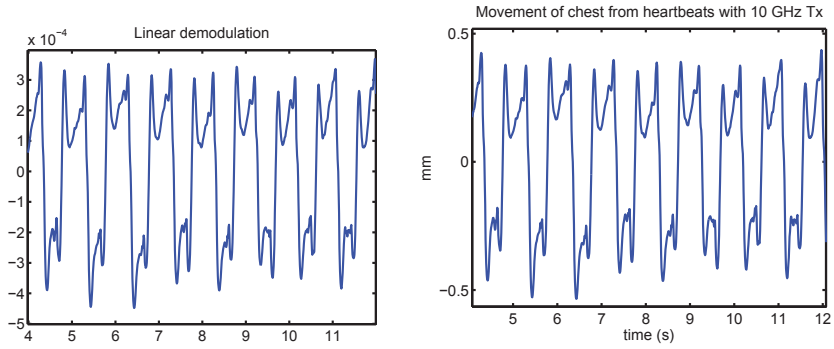

(a) (b)

Figure 3.12: Heartbeats recorded using a 10 GHz CW waveform and the antenna placed a distance away from the chest. In 3.12(a) a linear demodulator was used, and in 3.12(b) a center fitting function was used for phase and movement estimation. The two waveforms are visually nearly identical, but 3.12(b) is an estimation of the movement while 3.12(a) is of arbitrary units.

A practical consideration in processing cardiopulmonary radar data is the separation of heartbeats and respiration and the reduction of body movement modulations not connected to the vital signs. A simple approach both to separating the heartbeat and respiration and to remove unwanted movements and noise from the radar recordings is frequency selective filtering. In [1], we measured the slow time frequency distribution of respiration and heartbeat signals. This can be used for selecting cutoff frequencies when filtering the data. The paper does not analyze the importance of the filtered parts, and it is fully possible that important features of the heartbeat may be lost even though only a small portion of the energy is removed on filtering. Hence, this analysis is mainly

useful in applications where small details of the heartbeat waveform is not of interest.

Advanced filtering techniques may be required to properly extract the signal of interest. In [59] it is claimed that normal FIR filtering is not sufficient for heartbeat extraction. They achieved more success using Symmlet wavelets. The wavelet transform was also used by [60] to successfully separate heartbeats and respiration in non-contact measurements. In [47] antennas are placed both in front of and behind the torso to remove random body movements.

3.3.4 Understanding what is measured

As mentioned, radar have been successfully used for long term monitoring of patients' heartbeats and respiration. It is possible though, that information that may be used for diagnostic purposes may be available from radar heartbeat measurements. For radar to be used for something more than just keeping track of heartbeat and respiration rates, a deeper understanding of the connection between the observed measurements and the physiological processes are needed.

In [61] the common conception that the heartbeats observed in radar recordings are caused by small body movements stemming from the beating heart is challenged. They outlined a series of physical phenomena that could cause the heartbeat modulations in a radar recording. It was calculated that the most probable source of the modulation is the blood perfusion in the skin. The beating of the heart leads to cyclic changes in the concentrations of oxygenated blood in human tissues. This also changes the electromagnetic properties of the skin, which can cause changes in the reflected EM field. They state that body movements may also have an effect on the modulations. In [5], we investigate these theories experimentally and conclude that the body surface movements are the main causes of the observed modulations.

Summary

This chapter started with a quick overview of the physiology of the human heart, and the processes during a heartbeat. In the description of electromagnetic wave propagation in a human body, it was seen that there is a significant attenuation in body tissues. This attenuation is increasing with increasing frequency. An overview of the relevant medical radar literature was given. Topics relevant to the topics of this thesis were highlighted and discussed.

Chapter 4

Summary of papers

4.1 Radar cross section of the human heartbeat and respiration [1]

The papers [1, 2, 3] are on the topic of quantizing the human being vital signs. There existed no complete study of which frequencies and aspect angels which are optimal for the task. [1] and [2] was the road towards the final results in [3] which characterizes the vital signs modulation from aspect angles around the body. Frequencies in the range 0.5 - 18 GHz were used, and empirical models of the modulation were made that extend beyond these frequencies. In [1], a calibration procedure for such measurements are presented. The approach follows a classic approach to measuring the RCS of an object. In a radar measurement the received echo from an object is not only dependent on the object's RCS, but also on the system characteristics and range between antenna and object as seen in the radar equation (2.1). Additional influences on a measurement are reflections from other objects in the scene and multi-path components from the object.

The method presented in [1] is directed towards removing all these external influences leaving only the RCS of the person. In the processing of the data though, an important deviation from normal RCS measurements is made. Instead of returning the RCS of the person, the modulation is returned. This is achieved by high pass filtering the calibrated measurements and computing the modulation. In both [1] and [2] we call this the radar cross section of the heartbeat or respiration, because the measurement method follows that of an RCS measurement and the units of the measure is m^2. We have, however, realized that some may confuse this with the RCS of the person. In [3] the calibrated vital signs modulations are called the heartbeat or respiration modulation measure instead to more clearly separate it from the RCS of the person.

In [1], this procedure was used to analyze the main frequency content of vital signs using a 2 to 3 GHz UWB transceiver. Bandpass filters with varying pass-bands were applied to the calibrated measurements and the modulations were compared. From this analysis it was found that most of the energy in a heartbeat recording is contained in the 0.5 to 4 Hz band, and most of the energy in a respiration recording is in the respiration rate frequency. This knowledge can be useful for knowing which frequencies are most important to include in a measurement and filtering, but does not account for important but small features which may be excluded. For simple monitoring such as heartbeat detection and heart rate variability measurements, these results can be applied to secure a high signal to noise ratio. For more advanced methods involving analysis of the heartbeat

waveforms a larger frequency band is needed as some higher frequency components may contain important information even though they are small in amplitude.

4.2 Radar cross section of the human heartbeat and respiration in the 500MHz to 3GHz band [2]

In [2], we used a procedure similar to [1] to characterize the heartbeat and respiration modulation in the 500 MHz to 3 GHz frequency range. Again, the results were called the RCS of the vital signs. In this paper though, the focus was on determining which frequencies in the range were best suited for non-contact vital signs measurements. The frequency dependence of the RCS is useful for determining which transmitting frequencies to use. At the time, we only had the HUBRA radar available as a medical radar and wanted to know which parts of this band were best to use. The total frequency range was split into several sub-bandwidths to compute the heartbeat and respiration RCS. Ideally such an analysis would have been made on each frequency point in the sweep, but since this led to a low SNR integration of frequency sub-bands was necessary.

It was found that both the heartbeat and respiration RCS increases with increasing frequency. This was attributed to the increase in gain of the body surface with decreasing wavelength. At the time we were not sure whether we only recorded reflections off the body surface, or if waves penetrating into the chest and reflecting off the heart itself also contributed.

An additional benefit of the RCS measurements is that they provided a hint at answering the question of what is actually measured; surface reflections of the chest or reflections of the wave penetrating inside the body and being reflected from the heart. It is known that the attenuation in the body increases with increasing frequency [5, 62, 63]. The increase in heartbeat RCS found in [2] does not agree well with the increased attenuation of a wave travelling inside the body. A wave being reflected from the body surface on the other hand, should have this property, as the gain of the echo increases when the wavelength decreases compared to the body.

The increase in modulation with increasing frequency in the 0.5 to 3 GHz band led us to believe that this would increase further with higher frequencies.

4.3 Empirical model of modulation in radar heartbeat and respiration measurements [3]

[3] is the final paper on the quantization of vital signs included in this thesis. The approach to the problem is similar to the two papers mentioned above, but a much more thorough range of experiments were performed. In this paper, the computed system-independent modulation is called the physiological motion modulation measure and not the RCS as in the two former papers. The units (m^2) and method of computations are similar, but this term is used as the term RCS of the modulation is easily confused with the RCS of the person itself. A total frequency range of 0.5 to 18 GHz was used from aspect angles all around the body. The different aspect angles were achieved by seating the person on a computer controlled turntable, which was stepped in discrete angles between measurements. With these results, non-contact radar signatures of human vital signs have been mapped out in the frequency range, and this can be extrapolated to extend even above 18

GHz.

The methodology was similar to [1, 2], except that single frequency CW radar was used for the measurements. They were performed using a Network Analyzer, which provides high quality low noise measurements. As outlined in Chapter 2 the modulation appears similarly in single frequency and wideband measurements. The results agree with those of [2] with an increase in modulation with increasing frequency, and the modulation being of the same size in the frequency range used in [2].

It was found that the modulation of both respiration and heartbeats increase with frequency, but with different frequency dependencies. Additionally, both respiration and heartbeats are hard to detect from the side of the body. For many of the lower frequencies, the heartbeats disappeared below the noise floor when using aspect angles from the sides. To our surprise, the heartbeats create close to equal modulation whether the antennas are placed in front of or behind the person.

From the experimentally obtained data, models of the modulation as a function of frequency and aspect angles were made. Least squares fitting of suitable analytical functions to the data was used. Using these models, one can input the wanted frequency and aspect angle, and get a number describing the modulation of the respiration or heartbeats. In the paper this is illustrated with the through the wall application, but it is applicable to other analyses as well such as dynamic range considerations and antenna choices.

4.4 Chest movement estimation from radar modulation caused by heartbeats [4]

In [4] we analyzed the modulation in an I & Q receiver during non-contact heartbeat monitoring. A common conception is that heartbeats appear as phase modulations in the radar receiver. Through measurements, we showed that this is not the case. The heartbeats create modulation in amplitude as well as phase. We propose that the complex structure may be caused by the combination of several phase modulations at slightly different ranges or a combination of amplitude and phase modulations. A human chest is not flat, which means that parts of the chest at different distances from the antenna produces phase modulation in different direction in the complex plane.

Based on the approach of [57] we tested a phase estimator for extraction of the moving chest from DC and other static scatterers in the radar data. Because the phase is directly connected to the movement of the chest, it can be used to estimate the movement. [4] describes the process of estimating the chest heartbeat movement on both held breath and breathing person scenarios. The estimates of the chest movement were between 0.5 and 1 mm. These values are within earlier reported chest movements [34], but were varying from measurement to measurement.

Another result reported in [4] is that the respiration is not suited for estimating the heartbeat center DC. The movement estimations of the heartbeats based on this approach were different from the ones under held breath condition. This is attributed to different parts of the torso being connected to the heartbeats and the respiration. For example, the stomach is moving more during respiration, while the heartbeat vibrations are more centered around the chest area.

Even though the movement estimations varied in magnitude, we found that the estimated waveforms are stable in shape. Phase estimation of the data is thus not well suited for exact movement estimation, but can be very useful for a reliable waveform that can be used to extract medical

information from the data.

4.5 Physical Working Principles of Medical Radar [5]

In [61], the common conception that the heartbeats observed in radar recordings are caused by small body movements stemming from the beating heart was challenged. They outlined a series of physical phenomena that could cause the heartbeat modulations in a radar recording. It was calculated that the most probable source of the modulation is the blood perfusion in the skin. The beating of the heart leads to cyclic changes in the concentrations of oxygenated blood in human tissues. This change also changes the electromagnetic properties of the skin which can cause changes in the reflected EM field. They maintained that body movements also may have an effect on the modulations.

In [5], the theories of [61] were tested against each other experimentally. Leaning on the results in [61], the hypotheses were that the observable radar modulation connected to the heartbeats are caused by the skin perfusion, the movement of the chest surface or the movement of the heart inside the chest. To test the hypothesis against each other, three measurement setups were used. One normal recording of a person lying down and holding his breath, with the antenna placed at a distance above him pointing down on the chest. Next, the person's chest was pressed flat by a plexiglass plate while the rest of the setup was the same. The last setup also followed that of the first one, but with the person's chest covered in silver. Very thin silver leaves made for cooking were used, as they cling tightly to the skin and closely follows the contours of the body. Pictures taken of the three setups can be seen in Figure 4.1. In the plexiglass setup the movement was suppressed while the skin impedance changes remained the same. In the silver leaves setup the movement stayed the same, while there was a reduction in skin impedance changes observed by the radar as these were concealed by the conducting silver.

The modulation in measurements from the three setups were compared. It was found that covering the chest in silver leaves increased the modulation, while pressing the chest flat with the plexiglass plate decreased the modulation. This agrees well with the chest surface movement theory, and not with the other two theories. We found through the experiment that the heartbeat modulations are mainly caused by chest surface displacements. This means that non-contact radar does not measure the movements of the heart directly. It is the chest surface vibrations caused by the heart beating against the inside of the chest that is seen, possibly together with movements of other parts of the body. The surface reflections dominate over any reflections from inside the chest. In non-contact measurements any reflections from the actual heart wall are drowned in the much stronger response from the chest surface.

This does not immediately lead to the conclusion that non-contact radar can not be used for diagnostic purposes. ECG for instance, is used for information of the movement of the heart even though it is the electrical activity that is measured and not the actual heart movements. Likewise, it is possible that the non-contact waveforms indirectly provide information about the mechanical activity of the heart. However, since the heartbeat modulations are radar recordings of reflections of the moving chest, they are dependent on the chest morphology. This varies from person to person, which means that the heartbeat modulations will vary from person to person as well. We believe that it is hard to robustly characterize the heartbeat for all persons because of this.

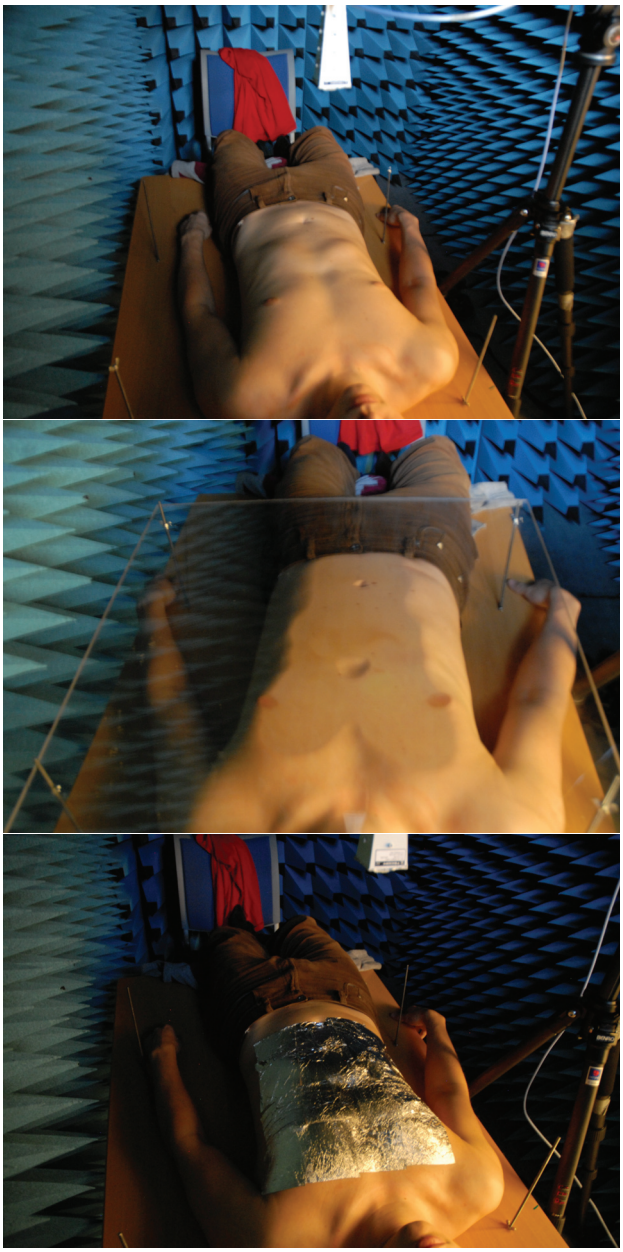

Figure 4.1: The three measurement setups of [5]. At the top is the bare chest measurement, followed by the plexiglass measurement and the silver leaf measurement.

4.6 Detecting changes in the human heartbeat with on-body radar [6]

By the results of [5], non-contact radar heartbeat monitoring records the chest surface movements. While this can be useful for several monitoring or detection applications, we believe that it limits the diagnostic potential. As outlined in Section 3.3.2 though, radar with antennas placed in contact with the body are also capable of recording human heartbeats. With this setup, the air-to-skin reflection is minimized, and the actual reflections from the heart becomes visible in the radar data. In addition to recording the actual movement of the heart, on-body monitoring does not suffer as much from involuntary movements of the person as non-contact monitoring does.

We performed single frequency CW measurements with antennas placed outside a T-shirt tight to the chest. ECG and radar were recording the heartbeats simultaneously, synchronized by a trigger pulse issued at the onset of the radar recordings. In addition to the results reported in [6], we performed synchronized measurements with a stethoscope seen in Figure 4.2. The stethoscope measurements can be matched in time with the heart sounds of the Wigger's diagram to locate the opening and closing of the heart valves as recorded by the radar. The identification of the opening and closing of the heart valves in [6] matches the one displayed in Figure 4.2.

Using the phase estimation techniques of [4], a heartbeat waveform was extracted from the measurements regardless of which channel received the most modulation. This reduces unwanted variations between measurements and makes for a stable extraction of a heartbeat waveform. While a lot of information is contained in this phase waveform, it is possible that it can be easier seen by displaying it in different ways. In [6] this is done by computing the instantaneous frequency of the signal.

In the phase waveform several parts of the heartbeat are connected to the radar recording, such as the filling and ejection of the ventricles. In the instantaneous frequency waveform other features are seen more clearly, such as the opening and closing of the heart valves. As important, these waveforms are stable over time making for a robust way to detect various details of the heartbeats.

The connection between the heart activity and the phase and instantaneous waveforms was further explored. Calibrated UWB measurements were performed to estimate the depth of the modulation in the chest. An exploration of the connection between the physiological state of the heart and the radar recordings was desired. In the limited way for us to alter the beating of the heart, some training exercises were performed to increase the heartbeat rate and blood pressure. Measurements during this state were compared to the resting heartbeats to explore the impact on the waveforms.

In this paper we found that the heartbeat modulations appear at a depth inside the chest that agrees well with the depth of the heart. The depth where the maximum modulation was found was at a two way travel time of 1.4 ns, which is approximately 2.8 cm into the body from the chest surface. In the paper, only the modulation depth with the antenna placed directly over the heart was measured. Heartbeats recorded from more positions than presented in [6] is shown in Figure 4.3.

A single or dual antenna setup like the one used here does not provide much spatial resolution (the only resolution is an eventual resolution in range connected to the bandwidth), and thus the radar records the sum of everything within the antenna beam. It is not possible to know a priori which parts of the heart is the main contributor to the recording.

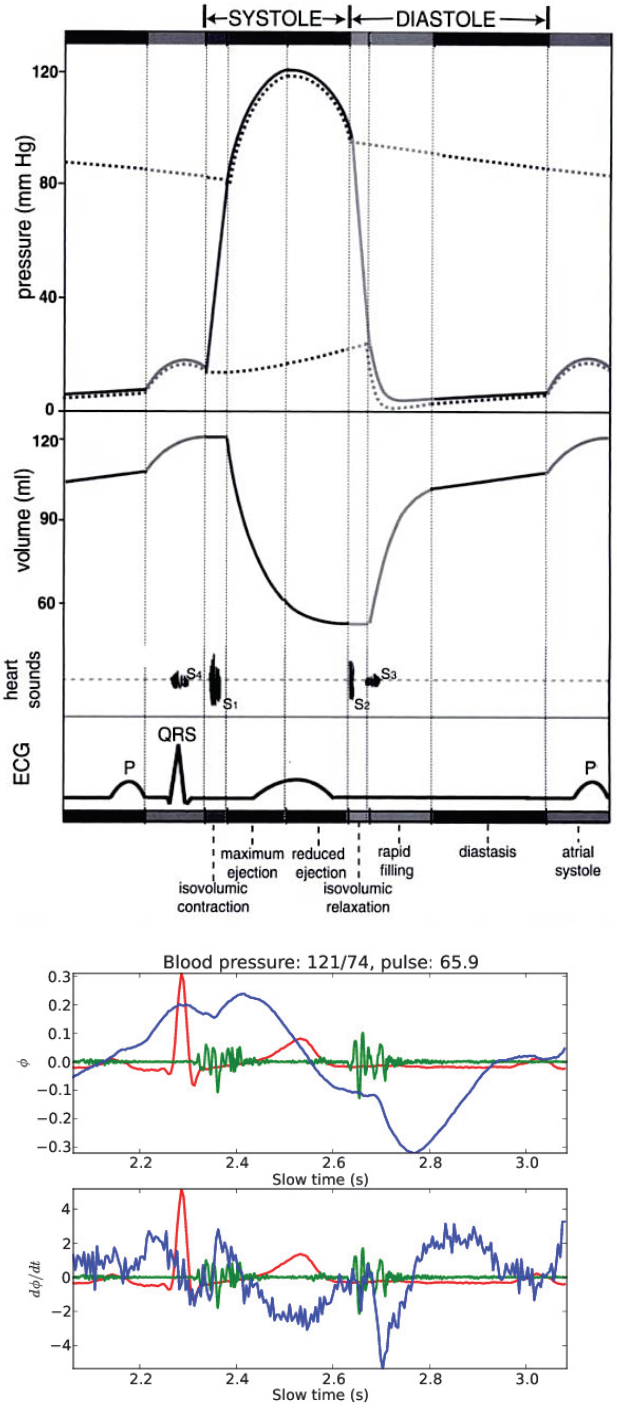

Figure 4.2: The top figure is the Wigger's diagram of the heart dynamics found in [21]. The bottom figure is the radar (blue), stethoscope (green) and ECG (red) recording of a heartbeat.

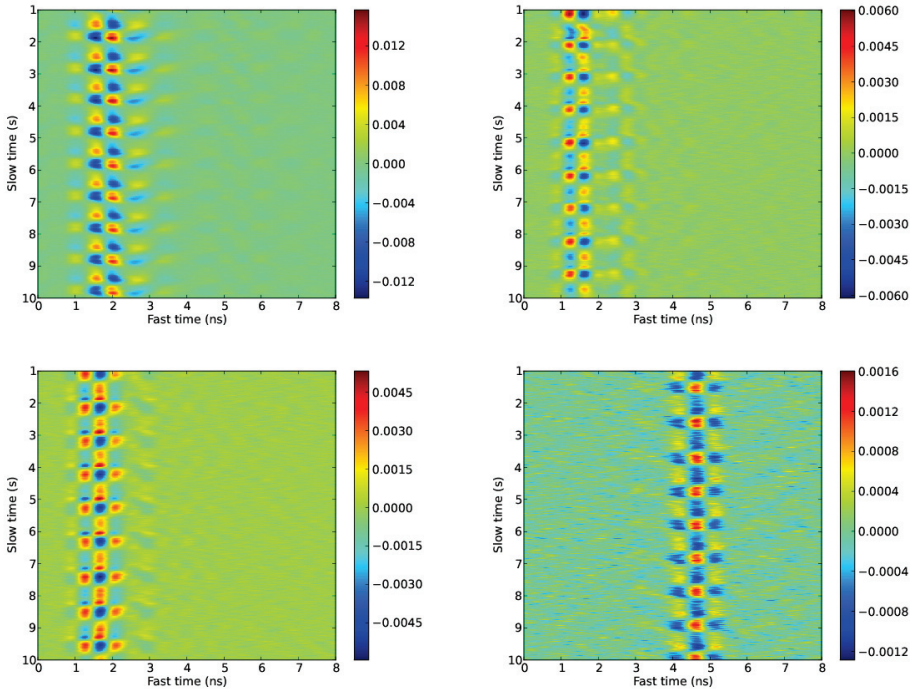

Figure 4.3: The real part of a heartbeat recording recorded from four different locations on the human chest. To the upper left, the antennas were placed at the middle of the chest. In the upper right figure the antennas were at the right side of the chest, while at the lower left figure the antennas were at the left part. In the last figure, one antenna was placed at the front of the chest and the other at the back, thus recording the wave propagating through the body.

[6] also shows recordings of a person right after exercising, meaning that the measurements were done on the person with higher pulse and blood pressure than at rest. These changes in the physiological state of the person results in characteristic changes in the heartbeat waveforms as well, which are stable over time. It is possible that these changes can be used to estimate the blood pressure of the person only by looking at the radar recordings of the heartbeat. In addition, it shows that changing the way the heart operates also changes the radar waveforms in a stable and reproducible way.

In this case only simple features such as the blood pressure and pulse were changed. Various heart diseases and heart failures also changes the way the heart operates. Since [6] demonstrated that we can robustly measure changes in the heartbeat with radar, it is possible that a number of heart diseases may be detected using radar. Only more research can unravel the unknown diagnostic possibilities of the medical radar.

4.7 Related papers on medical radar imaging: Paper VII and VIII

These papers are a bit on the side from the papers that make up this thesis, being on the topic of medical radar imaging. Radar imaging has been applied to medical applications earlier. One such approach is taken by [64, 65, 66] using a circular antenna array around the target to be imaged. They propose to use this system for brain imaging and stroke detection [67].

The most popular topic in medical radar imaging is breast cancer detection. The idea is to use antennas placed around the breast to form an image of what is inside. Cancerous tissues have slightly different dielectric properties from healthy tissues [68, 69] making it possible to detect tumors.

[70] is on the topic of imaging the human heartbeats and respiration. In contrast to the above mentioned imaging examples, imaging of the vital signs requires a frame rate in time in addition to the spatial resolution. To form the images, we use a velocity model of the human body to back propagate the received radar waves to form an image. This is done several times a second for the entire array of 8 receiver antennas. The back propagation and image formation algorithms are further explored in [71].

In [70] we are able to form a coarse radar image of a person seated in front of the antenna array. Contours of the chest and even the heart is identifiable in the image. This is mostly due to the velocity map model though, as the resolution in free space is not as good as in the image where the dielectric properties of the body is used. Movements of both the respiration and heartbeats are recognizable in the time development of the images.

Chapter 5

Conclusions

We ventured into this project with the aim of finding an optimal way of detecting heartbeats and respiration in terms of transmitting frequency, aspect angle and signal processing. Once this was figured out, we wanted to explore radar as a medical diagnostics tool. We found that both the heartbeat and respiration modulation increase with increasing transmitting frequency, and are best detected from the front and the back of a person. These studies culminated in an empirical model of the vital signs modulation in ranged radar recordings as a function of frequency and aspect angle. The ETSI and FCC frequency band allocations for medical radar are not the optimal frequencies for heartbeat detection, as remote monitoring is better with higher frequencies and on-body monitoring is better with lower frequencies.

One of the unanswered questions asked at the beginning of the work on this thesis was: What is actually measured in ranged radar vital signs monitoring? Is it body surface effects or the EM waves penetrating into the body reflected off the heart? Based on theoretical knowledge, we devised an experimental approach to these questions. The experiments showed that it is the chest surface motion that is seen when monitoring the human heartbeats from a distance using radar. Estimation techniques were used to estimate these movement, with a stable heartbeat waveform as the output. For such remote heartbeat monitoring purposes, UWB and narrowband radar are both equally suited for the motion estimation.

The knowledge on ranged heartbeat detection gained through the experimental work led us to believe that on-body heartbeat monitoring could have a larger diagnostic potential than non-contact. In a series of measurements we found that by placing the antennas in contact with the torso, one does indeed see heart movements directly. Several characteristic points in the radar recording are connected with specific parts of the heartbeat activity. We introduced two simple processing methods that provide a stable means for detecting these heartbeat instances. The last result found in the on-body heartbeat monitoring is a connection with the blood pressure and pulse and changes in the recorded radar waveform. This proves that changes in the beating of the heart is detectable using radar, which opens up the possibility of detecting heart diseases as well.

Remote monitoring of vital signs is still possible using radar. The result that heartbeats are observable both from the front and the back of the person, opens for several applications such as radar integrated in a chair or under a bed mattress. In light of the results in this thesis however, we believe that the greatest medical potential of radar vital signs monitoring lies in on-body radar. Exciting future work includes finding out if any heart diseases can be robustly detected using radar. Important aspects in this are the observation of the heart from various chest positions and development

of robust antenna systems that secure stable transmission into the body.

Bibliography

[1] Ø. Aardal, S.-E. Hamran, T. Berger, J. Hammerstad, and T. S. Lande, "Radar Cross Section of the Human Heartbeat and Respiration," in *Biomedical Circuits and Systems Conference, 2010. BioCAS 2010.* IEEE, November 2010, pp. 53–57.

[2] Ø. Aardal, S.-E. Hamran, T. Berger, J. Hammerstad, and T. S. Lande, "Radar cross section of the human heartbeat and respiration in the 500MHz to 3GHz band," in *Radio and Wireless Symposium (RWS), 2011 IEEE*. IEEE, January 2011, pp. 422–425.

[3] Ø. Aardal, S. Brovoll, Y. Paichard, T. Berger, T. S. Lande, and S.-E. Hamran, "Empirical model of modulation in radar heartbeat and respiration measurements," 2013.

[4] Ø. Aardal, S.-E. Hamran, T. Berger, Y. Paichard, and T. S. Lande, "Chest movement estimation from radar modulation caused by heartbeats," in *Biomedical circuits and systems conference (BIOCAS 2011), 2011 IEEE*. IEEE, November 2011, pp. 452–455.

[5] Ø. Aardal, Y. Paichard, S. Brovoll, T. Berger, T. S. Lande, and S.-E. Hamran, "Physical Working Principles of Medical Radar," *Biomedical Engineering, IEEE Transactions on*, vol. 60, no. 4, pp. 1142–1149, 2013.

[6] Ø. Aardal, S. Brovoll, Y. Paichard, T. Berger, T. S. Lande, and S.-E. Hamran, "Detecting changes in the human heartbeat with on-body radar," in *IEEE Radar Conference 2013*, May 2013.

[7] W. H. O. (WHO), "World health statistics 2012," http://www.who.int/gho/publications/world_health_statistics/EN_WHS2012_Full.pdf, 2012.

[8] ——, "The top 10 causes of death," http://www.who.int/mediacentre/factsheets/fs310/en/index.html, June 2011, accessed July 02, 2012.

[9] C. Johnson and A. Guy, "Nonionizing electromagnetic wave effects in biological materials and systems," *Proceedings of the IEEE*, vol. 60, no. 6, pp. 692–718, June 1972.

[10] C. Balanis, *Advanced engineering electromagnetics*. Wiley New York, 1989.

[11] T. Berger, S.-E. Hamran, L. Hanssen, and M. J. Øyan, "Ultra Wideband Radar Design for Detection of Vital Signs," in *NATO-RTO/SET-125 Symposium on Defence Against Terrorism*, April 2008.

[12] M. J. Øyan, S.-E. Hamran, T. Berger, and L. Hanssen, "Characterisation of ultra wideband frequency modulated and step frequency radar with range gating," in *Antennas, Radar, and Wave Propagation*. IASTED, ARP2009, July 2009.

[13] G. M. Brooker, "Understanding Millimetre Wave FMCW Radars," in *1st International Conference on Sensing Technology*, 2005.

[14] S.-E. Hamran, T. Berger, L. Hanssen, M. J. Øyan, V. Ciarletti, C. Corbel, and D. Plettemeier, "A prototype for the WISDOM GPR on the ExoMars mission," *Advanced Ground Penetrating Radar, 2007 4th International Workshop on*, pp. 252–255, June 2007.

[15] C. Capps, "Near field or far field?" *EDN-BOSTON THEN DENVER-*, vol. 46, no. 18, pp. 95–102, 2001.

[16] "Agilent Network Analyzer N5245A PNA-X, http://www.home.agilent.com/agilent/product.jspx?nid=-536902643.898624.00&cc=NO&lc=eng."

[17] D. Plettemeier, V. Ciarletti, S.-E. Hamran, C. Corbel, P. Cais, W.-S. Benedix, K. Wolf, S. Linke, and S. Roddecke, "Full polarimetric gpr antenna system aboard the exomars rover," in *Radar Conference, 2009 IEEE*, may 2009, pp. 1 –6.

[18] V. Chen, F. Li, S. Ho, and H. Wechsler, "Micro-Doppler effect in radar: phenomenon, model, and simulation study," *Aerospace and Electronic Systems, IEEE Transactions on*, vol. 42, no. 1, pp. 2–21, 2006.

[19] V. Chen, *The micro-Doppler effect in radar*. Artech House Publishers, 2011.

[20] http://en.wikipedia.org/wiki/File:Heart_diagram-en.svg, May 2012.

[21] A. Katz, *Physiology of the Heart*, 4th ed. Lippincott Williams & Wilkins, 2006.

[22] P. Sengupta, J. Korinek, M. Belohlavek, J. Narula, M. Vannan, A. Jahangir, and B. Khandheria, "Left ventricular structure and function: basic science for cardiac imaging," *Journal of the American College of Cardiology*, vol. 48, no. 10, pp. 1988–2001, 2006.

[23] R. M. Berne, M. N. Matthew, B. M. Koeppen, and B. A. Stanton, *Physiology*, 5th ed. Mosby, 1998.

[24] J. Sneyd and J. Keener, *Mathematical Physiology*. Springer, 2001.

[25] R. Acharya, J. Suri, and J. Spaan, *Advances in cardiac signal processing*. Springer Verlag, 2007.

[26] C. Gabriel, S. Gabriel, and E. Corthout, "The dielectric properties of biological tissues: I. Literature survey," *Physics in medicine and biology*, vol. 41, p. 2231, november 1996.

[27] S. Gabriel, R. Lau, and C. Gabriel, "The dielectric properties of biological tissues: II. Measurements in the frequency range 10 Hz to 20 GHz," *Physics in medicine and biology*, vol. 41, p. 2251, november 1996.

[28] ——, "The dielectric properties of biological tissues: III. Parametric models for the dielectric spectrum of tissues," *Physics in medicine and biology*, vol. 41, p. 2271, november 1996.

[29] M. Skolnik, "Radar in the twentieth century," *IEEE Aerospace and Electronic Systems Magazine*, vol. 15, no. 10, pp. 27–46, 2000.

[30] C. G. Caro and J. A. Bloice, "Contactless apnoea detector based on radar," *The Lancet*, vol. 2, pp. 959–961, October 1971.

[31] C. Susskind, "Possible use of microwaves in the management of lung disease," *Proceedings of the IEEE*, vol. 61, no. 5, pp. 673 – 674, May 1973.

[32] J. Lin, J. Kiernicki, M. Kiernicki, and P. Wollschlaeger, "Microwave apexcardiography," *Microwave Theory and Techniques, IEEE Transactions on*, vol. 27, no. 6, pp. 618–620, Jun 1979.

[33] J. Lin, "Microwave sensing of physiological movement and volume changes: A review," *Bioelectromagnetics*, vol. 13, no. 6, pp. 557–565, 1992.

[34] A. Droitcour, "Non-contact measurement of heart and respiration rates with a single-chip microwave Doppler Radar," Ph.D. dissertation, Stanford University, 2006.

[35] Ø. Aardal and J. Hammerstad, "Medical radar literature overview," 2010.

[36] T. McEwan and S. Azevedo, "Micropower Impulse Radar," *Science & Technology Review*, January/February 1996.

[37] T. McEwan, "Body monitoring and imaging apparatus and method," United States Patent 5,573,012, 1996.

[38] E. Staderini, "UWB radars in medicine," *Aerospace and Electronic Systems Magazine, IEEE*, vol. 17, no. 1, pp. 13–18, Jan 2002.

[39] M. Jelen and E. M. Biebl, "Multi-frequency sensor for remote measurement of breath and heartbeat," *Advances in Radio Science*, vol. 4, pp. 79–83, 2006. [Online]. Available: http://www.adv-radio-sci.net/4/79/2006/

[40] D. Petkie, C. Benton, and E. Bryan, "Millimeter wave radar for remote measurement of vital signs," in *Radar Conference, 2009 IEEE*, May 2009, pp. 1 –3.

[41] N. Hafner, I. Mostafanezhad, V. Lubecke, O. Boric-Lubecke, and A. Host-Madsen, "Non-contact cardiopulmonary sensing with a baby monitor," in *Engineering in Medicine and Biology Society, 2007. EMBS 2007. 29th Annual International Conference of the IEEE*, Aug. 2007, pp. 2300–2302.

[42] A. Droitcour, O. Boric-Lubecke, and G. Kovacs, "Signal-to-Noise Ratio in Doppler Radar System for Heart and Respiratory Rate Measurements," *IEEE transactions on microwave theory and techniques*, vol. 57, no. 10, 2009.

[43] C. Li, J. Lin, and Y. Xiao, "Robust overnight monitoring of human vital signs by a non-contact respiration and heartbeat detector," in *Engineering in Medicine and Biology Society, 2006. EMBS '06. 28th Annual International Conference of the IEEE*, 30 2006-Sept. 3 2006, pp. 2235–2238.

[44] J. Kiriazi, O. Boric-Lubecke, and V. Lubecke, "Radar cross section of human cardiopulmonary activity for recumbent subject," in *Engineering in Medicine and Biology Society, 2009. EMBC 2009. Annual International Conference of the IEEE*, sept. 2009, pp. 4808 –4811.

[45] A. Nezirovic, S. Tesfay, A. Valavan, and A. Yarovoy, "Experimental study on human breathing cross section using uwb impulse radar," in *Radar Conference, 2008. EuRAD 2008. European*, oct. 2008, pp. 1 –4.

[46] C. Li and J. Lin, "Optimal Carrier Frequency of Non-Contact Vital Sign Detectors," in *2007 IEEE Radio and Wireless Symposium*, 2007, pp. 281–284.

[47] ——, "Random Body Movement Cancellation in Doppler Radar Vital Sign Detection," *Microwave Theory and Techniques, IEEE Transactions on*, vol. 56, no. 12, pp. 3143 –3152, dec. 2008.

[48] D. R. Morgan and M. G. Zierdt, "Novel signal processing techniques for doppler radar cardiopulmonary sensing," *Signal Process.*, vol. 89, no. 1, pp. 45–66, 2009.

[49] I. Immoreev, "Practical application of ultra-wideband radars," in *Ultrawideband and Ultrashort Impulse Signals*, September 2006.

[50] F. Thiel, D. Kreiseler, and F. Seifert, "Non-contact detection of myocardium's mechanical activity by ultrawideband RF-radar and interpretation applying electrocardiography," *Review of Scientific Instruments*, vol. 80, p. 114302, 2009.

[51] G. Gentili, V. Tesi, M. Linari, and M. Marsili, "A versatile microwave plethysmograph for the monitoring of physiological parameters," *Biomedical Engineering, IEEE Transactions on*, vol. 49, no. 10, pp. 1204–1210, 2002.

[52] J. Thijs, J. Muehlsteff, O. Such, R. Pinter, R. Elfring, and C. Igney, "Comparison of continuous wave doppler radar to impedance cardiography for analysis of mechanical heart activity," *Proceedings of the 2005 IEEE Engineering in Medicine and Biology 27th Annual Conference*, pp. 3482–3485, 2005.

[53] J. Muehlsteff, J. Thijs, and R. Pinter, "The use of a two channel Doppler radar sensor for the characterization of heart motion phases," *Engineering in Medicine and Biology Society, 2006. EMBS '06. 28th Annual International Conference of the IEEE*, pp. 547–550, 30 2006-Sept. 3 2006.

[54] J. Muehlsteff, T. Pinter, G. Morren, and G. Muesch, "A handheld device for simultaneous detection of electrical and mechanical cardio-vascular activities with synchronized ECG and CW-Doppler Radar," *Proceedings of the 29th Annual International Conference of the IEEE EMBS*, pp. 5758–5761, August 2007.

[55] W. Massagram, N. Hafner, S. Yamada, V. Lubecke, and O. Boric-Lubecke, "Feasibility of hrv measurement from single-channel doppler radar," in *Antennas and Propagation Society International Symposium, 2007 IEEE*, June 2007, pp. 269–272.

[56] B. Lohman, O. Boric-Lubecke, V. Lubecke, P. Ong, and M. Sondhi, "A digital signal processor for Doppler radar sensing of vital signs," *Engineering in Medicine and Biology Magazine, IEEE*, vol. 21, no. 5, pp. 161–164, Sept.-Oct. 2002.

[57] B.-K. Park, O. Boric-Lubecke, and V. M. Lubecke, "Arctangent Demodulation With DC Offset Compensation in Quadrature Doppler Radar Receiver Systems," *Microwave Theory and Techniques, IEEE Transactions on*, vol. 55, no. 5, pp. 1073–1079, May 2007.

[58] A. Høst-Madsen, N. Petrochilos, O. Boric-Lubecke, V. Lubecke, B. Park, and Q. Zhou, "Signal processing methods for doppler radar heart rate monitoring," *Signal Processing Techniques for Knowledge Extraction and Information Fusion*, 2008.

[59] W. Jianqi, Z. Chongxun, L. Guohua, and J. Xijing, "A new method for identifying the life parameters via radar," *EURASIP Journal on Advances in Signal Processing*, vol. 2007, 2007.

[60] L. Guohua, W. Jianqi, Y. Yu, and J. Xijing, "Study of the ballistocardiogram signal in life detection system based on radar," in *Engineering in Medicine and Biology Society, 2007. EMBS 2007. 29th Annual International Conference of the IEEE*, Aug. 2007, pp. 2191–2194.

[61] G. Varotto and E. Staderini, "On the UWB medical radars working principles," *International Journal of Ultra Wideband Communications and Systems*, vol. 2, no. 2, pp. 83–93, 2011.

[62] D. Zito, D. Pepe, B. Neri, D. De Rossi, A. Lanata, A. Tognetti, and E. Scilingo, "Wearable System-on-a-Chip UWB Radar for Health Care and its Application to the Safety Improvement of Emergency Operators," in *Engineering in Medicine and Biology Society, 2007. EMBS 2007. 29th Annual International Conference of the IEEE*, Aug. 2007, pp. 2651 –2654.

[63] S. Pisa, P. Bernardi, M. Cavagnaro, E. Pittella, and E. Piuzzi, "Monitoring of cardiopulmonary activity with UWB radar: A circuital model," in *Electromagnetic Compatibility and 19th International Zurich Symposium on Electromagnetic Compatibility, 2008. APEMC 2008. Asia-Pacific Symposium on*, May 2008, pp. 224–227.

[64] S. Semenov, R. Svenson, A. Boulyshev, A. Souvorov, V. Borisov, Y. Sizov, A. Starostin, K. Dezern, G. Tatsis, and V. Baranov, "Microwave tomography: two-dimensional system for biological imaging," *IEEE Transactions on Biomedical Engineering*, vol. 43, no. 9, pp. 869–877, 1996.

[65] S. Semenov, R. Svenson, A. Bulyshev, A. Souvorov, A. Nazarov, Y. Sizov, A. Pavlovsky, V. Borisov, B. Voinov, G. Simonova *et al.*, "Three-dimensional microwave tomography: experimental prototype of the system and vector born reconstruction method," *Biomedical Engineering, IEEE Transactions on*, vol. 46, no. 8, pp. 937–946, 1999.

[66] S. Semenov, R. Svenson, A. Bulyshev, A. Souvorov, A. Nazarov, Y. Sizov, V. Posukh, A. Pavlovsky, P. Repin, A. Starostin *et al.*, "Three-dimensional microwave tomography: Initial experimental imaging of animals," *Biomedical Engineering, IEEE Transactions on*, vol. 49, no. 1, pp. 55–63, 2002.

[67] S. Semenov and D. Corfield, "Microwave tomography for brain imaging: Feasibility assessment for stroke detection," *International Journal of Antennas and Propagation*, vol. 2008, no. 2008, pp. 1–8, 2008.

[68] E. Bond, X. Li, S. Hagness, and B. Van Veen, "Microwave imaging via space-time beamforming for early detection of breast cancer," *Antennas and Propagation, IEEE Transactions on*, vol. 51, no. 8, pp. 1690 – 1705, aug. 2003.

[69] M. El-Shenawee, "Electromagnetic imaging for breast cancer research," in *Biomedical Wireless Technologies, Networks, and Sensing Systems (BioWireleSS), 2011 IEEE Topical Conference on*, jan. 2011, pp. 55 –58.

[70] Y. Paichard, T. Berger, Ø. Aardal, and S. Hamran, "Close range microwave imaging of human chest," in *Applied Sciences in Biomedical and Communication Technologies (ISABEL), 2011 4th International Symposium on*. IEEE, 2011.

[71] T. Berger, S. Hamran, Y. Paichard, and Ø. Aardal, "Close Range Ultra Wideband Microwave Imaging in a Non-Homogeneous Background," in *Signal and Image Processing*. ACTA Press, 2011.

Chapter 6

Papers

6.1 I Radar cross section of the human heartbeat and respiration [1]

Abstract

This paper describes an experimental approach for finding the radar cross section (RCS) of human heartbeats and respiratory movements. A measurement setup, a calibration routine and required processing steps are presented. Using a $2-3GHz$ Ultra Wideband (UWB) radar, heartbeats and respiration of a human subject were recorded from a distance of $1.14m$. Combining the recorded data to measurements with a calibration sphere, the calibrated human heartbeat and respiration RCS was detected.

I. Introduction

Conventional methods for measuring heartbeats in human beings, such as ECG, require contact between the sensor and the patient's skin. With radar, it is possible to sense heartbeats and respiration contactless and through clothing. UWB radar for medical applications is gaining interest due to its low power emissions, high range resolution and low cost. Although there are many reports using radar for respiration and heartbeat monitoring in the literature [1, 2, 3], there are still insufficient characteristics of what is actually measured.

The RCS in general is an important property in the field of radar, and is usually denoted σ. It is a measure of how well an object reflects incident radar power as a function of frequency and aspect angle. As part of the radar equation, σ is a necessary number for Signal to Noise Ratio (SNR) and detection computations and the understanding of radar signals in heartbeat and respiration monitoring. [4] and [5] measured the RCS of respiration. In [4], the human breathing cross section was investigated from various positions using an UWB impulse radar. The reflection was reported to be strongest when the person was facing the receiving antenna. In [5], the RCS of respiration was computed using the phase changes in a Continous Wave (CW) Doppler radar recording of a breathing person. From the recordings, the amplitude of the reflections off the person was estimated.

In this paper, we present the RCS of human heartbeats and respiration using calibrated UWB radar recordings. The results in this paper are not the RCS of the chest or person, but rather the RCS of the heartbeat or breathing motion itself. This is a subtle difference. In the radar recordings, the modulations are isolated from stationary reflections. By the RCS of the human heartbeat and respiration, we thus mean the magnitude of the modulations caused by the heart beating or the person breathing. This number is of major interest for detection purposes. Using calibrated measurements, we present the RCS of the human heartbeat and respiration recorded with a radar operating in the frequency range $2-3GHz$.

A Frequency Modulated Continous Wave (FMCW) UWB radar developed at FFI [6, 7, 3] was used for the measurements. A main challenge in quantifying the RCS of physiological motion is to isolate the contribution of the heartbeats or respiration to the recorded power from other contributing factors such as the radar itself, antennas, propagation through the air and other reflectors in the scene. For this purpose, an aluminum calibration sphere with known RCS was used. By doing radar recordings of a person and the calibration sphere using the same measurement setup, the only changes between the recordings are the two objects' RCS and some possible changes in the background scattering. External factors such as the generated signal, antennas, propagation and clutter may be isolated, and a calibrated RCS of the human physiological motion is computed.

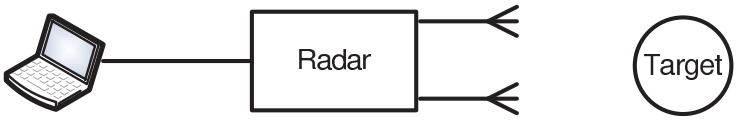

Figure 1: The measurement setup.

First, the measurement setup is described with the equipment used in obtaining the experimental data. Second, a model of the radar recordings is given before the calibration routine is outlined. The computation of the RCS is defined, and experimental results from recordings of a test person are presented.

II. Measurement setup

To obtain calibrated recordings of the human heartbeat and respiration, four separate radar recordings were conducted: Of the empty room for clutter subtraction, of a metallic sphere for calibration, of a person sitting still and holding his breath and of a person sitting still and breathing. All measurements were conducted in an anechoic chamber to avoid strong reflections off the walls and to reduce the multipath components. The distance from the antennas to the metallic sphere was the same as the distance from the antennas to the surface of the person's chest ($1.14m$). Between each recording, the only change was the target in the scene. In this way, the radar and antenna behavior and the clutter was constant for each of the four recordings. The measurement setup is sketched in Fig. 1.

All data were aquired using an UWB FMCW radar developed at FFI. The radar transmits a linear sweep in the frequency range $2-3GHz$. Operating after the homodyne principle, the echo from the reflectors in the scene received in the radar is mixed with the transmitted signal. This creates a signal with beat frequencies f_b proportional to the two way travel times τ between the radar and the reflectors. The beat signal after mixing is sampled in the frequency domain. After sampling, the data is stored in a computer for digital post processing. All of the calibration and processing described later in this paper is done digitally. An introduction to FMCW radar can be found in [8].

III. Calibration procedure

A Propagation channel model

A frequency domain scattering measurement model of the radar output is described in this section. The model is similar to those described by [9] and [10]. The radar generates a signal $V_t(\omega)$, where ω increases from the minimum to the maximum frequency within the bandwidth during the pulse transmission time T_s. This signal will be transmitted through an antenna, with transfer function $H_a(\omega)$. Next, the signal will propagate in the room, resulting in both coupling between the transmitting and receiving antennas, as well as scattering from the room. These factors are termed clutter, with response $H_C(\omega)$. If there is a target in the scene other than the clutter (i.e. either a person or a calibration sphere), the scattering of the target will be $H_T(\omega)$ and for the

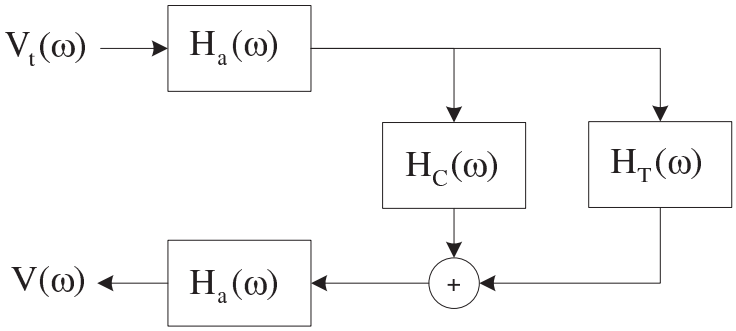

Figure 2: The channel model diagram.

sphere $H_S(\omega)$. The receiving antenna will impose the same changes $H_a(\omega)$ to the signal as the transmitting antenna, before the signal goes to the mixer. The output is a signal with an amplitude and phase that has been modulated by the above described steps, and beat frequencies proportional to the round-trip time of travel τ from the radar to the scatterers.

As the beat frequency and phase of the sampled signal are fully determined by the round-trip times of travel τ between the radar and the scatterers, the signal waveform is modelled into the scatterer transfer functions $H_C(\omega)$, $H_T(\omega)$ and $H_S(\omega)$ for simplicity. This is done since we ultimately only are interested in the amplitudes. Thus, in the scattering measurement model as shown in Fig. 2, $V_t(\omega)$ and $H_a(\omega)$ are purely amplitude modulations, while $H_C(\omega)$, $H_T(\omega)$ and $H_S(\omega)$ consist of both amplitude modulations and the signal shape.

Following are the signals received by the radar, described by the scattering measurement model. $H_C(\omega)$ is assumed to be approximately the same in (1)-(3). The empty room clutter measurement:

$$V_C(\omega) = V_t(\omega)H_a^2(\omega)H_C(\omega). \tag{1}$$

With the calibration sphere placed in the room, the scattering of the sphere is additive to that of the clutter:

$$V_S(\omega) = V_t(\omega)H_a^2(\omega)(H_C(\omega) + H_S(\omega)). \tag{2}$$

Replacing the sphere with a person at the same range from the radar, the measurement is:

$$V_T(\omega) = V_t(\omega)H_a^2(\omega)(H_C(\omega) + H_T(\omega)). \tag{3}$$

Equation (3) is used to describe both the case where the person is holding his breath and when the person is breathing.

The scattering function envelopes $|H_C(\omega)|$, $|H_S(\omega)|$ and $|H_T(\omega)|$ contains the attenuation from two way spherical spreading and the reflectivity of the scatterers. For a target a distance R from the radar, the magnitude $|H_S(\omega)|$ is

$$|H_S(\omega)| \quad = \quad \frac{1}{4\pi R^2}\frac{E_{r,S}(\omega)}{E_i(\omega)}, \tag{4}$$

and the magnitude $|H_T(\omega)|$ is

$$|H_T(\omega)| = \frac{1}{4\pi R^2}\frac{E_{r,T}(\omega)}{E_i(\omega)}. \quad (5)$$

Here, E_i is the incident radiated field, and E_r is the reflected electric field. The two equations (4) and (5) are only valid if the target and sphere reflects incoming waves from the range R only. For a sphere this is partially true, as the reflections received by the radar are from the front of the sphere. There are, however, also scatterings caused by waves travelling around the sphere. A person obviously has spatial extension and will reflect incoming waves at more than one range R. The complete chest surface will reflect incoming waves, and additionally some penetration into the body will occur. However, the span of ranges which contains reflections changing with a heartbeat is small relative to the distance from the radar. The approximation in (5) is considered to be adequate.

B The calibration

The calibration routine is based on [10], but changed to preserve the signal waveform while calibrating the amplitude. Also, the additional step of software gating in the fast time domain have been introduced. As seen in (1)–(3), the clutter appears additively in the calibration sphere and target measurements. The first step of the calibration is therefore to subtract the clutter measurement. In real measurements, the introduction of the sphere or a person in the scene will slightly change the clutter response $H_C(\omega)$ due to shadowing and changed multipath components. To reduce this effect, a software gating in the fast time domain around the range where the person and the sphere are located is introduced. Finally the measurement of the target is calibrated in the frequency domain using the calibration sphere measurement. Arranged as a three step routine, the calibration consists of:

1. First, the empty room clutter measurement (1) is subtracted from the sphere (2) and person (3) measurements:

$$\begin{aligned} \tilde{V}_S(\omega) &= V_S(\omega) - V_C(\omega) \\ &= V_t(\omega)H_a^2(\omega)H_S(\omega) \quad (6) \end{aligned}$$

and

$$\begin{aligned} \tilde{V}_T(\omega) &= V_T(\omega) - V_C(\omega) \\ &= V_t(\omega)H_a^2(\omega)H_T(\omega). \quad (7) \end{aligned}$$

2. Second, the software gating in the fast time domain is performed. To do this, $\tilde{V}_S(\omega)$ and $\tilde{V}_T(\omega)$ are zero padded and Fourier transformed to the fast time domain:

$$\begin{aligned} \tilde{V}_S(\omega) &\overset{FFT}{\rightarrow} \tilde{v}_S(\tau) \\ \tilde{V}_T(\omega) &\overset{FFT}{\rightarrow} \tilde{v}_T(\tau). \end{aligned}$$

Having measured the distance R from the radar to the sphere and chest surface of the person, we know the round-trip time of travel τ_T between the radar and the target through the relation $\tau = \frac{2R}{c}$. For the software gating, a Blackman window $w(\tau)$ is selected for its low

sidelobe levels. The window is centered at τ_T, and has width small enough to be zero at the back wall of the room and large enough to encompass the sphere and person. A width corresponding to $1m$ diameter was selected for this purpose. The windowing causes the modifications:

$$\begin{aligned} \hat{v}_S(\tau) &= \tilde{v}_S(\tau)w(\tau) \\ \hat{v}_T(\tau) &= \tilde{v}_T(\tau)w(\tau) \end{aligned}$$

The gated matrices are then inverse Fourier transformed to the frequency domain representations $\hat{V}_S(\omega)$ and $\hat{V}_T(\omega)$.

3. The last step uses $\hat{V}_S(\omega)$ to calibrate $\hat{V}_T(\omega)$:

$$V_{cal}(\omega) = \frac{\hat{V}_T(\omega)}{|\hat{V}_S(\omega)| + \left(\frac{1}{SNR(\omega)}\right)}. \tag{8}$$

$\frac{1}{SNR(\omega)}$ is a smoothing factor included to remove spikes in $V_{cal}(\omega)$, and will in most cases have little to no influence. The construction of $\frac{1}{SNR(\omega)}$ is described in [10].

With $R > 1m$, and the assumption that only the chest area around the heart and lungs is moving, the moving parts can be considered to be in the far field of the radar transmitting at $2-3GHz$. Under ideal conditions with the calibration sphere and target at the exact same distance R in the far field from the radar, $\frac{1}{SNR(\omega)} \to 0$ and all the clutter removed in $\hat{V}_T(\omega)$ and $\hat{V}_S(\omega)$, $|V_{cal}(\omega)|^2$ becomes the ratio $\frac{\sigma_T(\omega)}{\sigma_S(\omega)}$:

$$\begin{aligned} |V_{cal}(\omega)|^2 &= \frac{|\hat{V}_T(\omega)|^2}{|\hat{V}_S(\omega)|^2} \\ &= \frac{V_t^2(\omega)H_a^4(\omega)|\frac{1}{4\pi R^2}\frac{E_{r,T}(\omega)}{E_i(\omega)}|^2}{V_t^2(\omega)H_a^4(\omega)|\frac{1}{4\pi R^2}\frac{E_{r,S}(\omega)}{E_i(\omega)}|^2} \\ &= \frac{\sigma_T(\omega)}{\sigma_S(\omega)}. \end{aligned} \tag{9}$$

In (9) the RCS definition found in [11] is used:

$$\sigma = \lim_{R\to\infty} 4\pi R^2 \frac{|E_r|^2}{|E_i|^2}. \tag{10}$$

As is seen in (9), under ideal conditions the power of the calibrated measurement $V_{cal}(\omega)$ is the ratio of the unknown RCS $\sigma_T(\omega)$ to the calibration sphere's known RCS $\sigma_S(\omega)$. However, this RCS includes all stationary reflections off the person as well as those from the physiological movement. To isolate the RCS of the physiological movement, processing is done in the fast time-slow time domain.

C Processing

After the calibration steps, the calibrated recording $V_{cal}(\omega)$ can be transformed to the fast-time domain representation $v_{cal}(\tau)$ by FFT. The range resolution ΔR of a linear sweep signal has a well known relation to the bandwidth B:

$$\Delta R = \frac{c}{2B}.$$

With a bandwidth of $1GHz$, the range resolution is $\Delta R = 15cm$. Looking at data at one range from the radar means looking at contributions from a small radial window. Knowing that both the person chest surface and sphere are located a round-trip time of travel τ_T from the radar, we can now look at the calibrated recording in this range; $v_{cal}(\tau_T)$. This vector will change with slow time t. In $v_{cal}(\tau_T)$, much of the energy originates from stationary reflections. As the aim of this paper is to find the radar cross section of the human heartbeat and of human respiration, this information must be extracted from the stationary reflections off the body. During the radar recordings, the person was sitting still in a chair and assumed to be stationary. The only movement in the scene was then caused by the respiration and heartbeats of the person. When the person was holding his breath, only the heartbeats were a source of changes in the recordings.

All stationary reflections are manifested as a DC in slow time in the vector $v_{cal}(\tau_T)$. To remove this DC and any linear drift, a linear least squares estimation to the data is subtracted from $v_{cal}(\tau_T)$:

$$\tilde{v}_{cal}(\tau_T) = v_{cal}(\tau_T) - X(X^T X)^{-1} X^T v_{cal}(\tau_T). \tag{11}$$

In (11) $X = [k/K \quad 1]$ is a $K \times 2$ matrix where $k = [0, 1, \ldots, K-1]^T$, K is the length of $v_{cal}(\tau_T)$ in slow time and 1 is a vector of ones of length K.

To reduce unwanted high frequency noise from the respiration recording, $\tilde{v}_{cal}(\tau_T)$ is run through a low pass filter. Filters with cutoff frequency from $0.25Hz$ up to half the Pulse Repetition Frequency (PRF) has been tested, and the respiration RCS after each filter computed. In the held breath (heartbeat) recording, high frequency noise was also reduced. Because of the small amplitude of the heartbeat, these recordings are vulnerable to small movements by the person. To reduce this, frequency content lower than the heartbeat rate in addition to high frequencies are filtered out. Thus, for the heartbeat recording $\tilde{v}_{cal}(\tau_T)$ is run through a bandpass filter. Three different lower cutoff frequencies were tested, as well as upper cutoff frequencies from $1Hz$ up to half the PRF. All the filters are Chebyshev type 2 filters, with minimum $40dB$ stopband attenuation. The calibrated recording after processing is denoted $\check{v}_{cal}(\tau_T)$.

IV. Heartbeat and respiration RCS definition

After the processing steps, $\check{v}_{cal}(\tau_T)$ consists of the modulations in the calibrated data at the range where the person was sitting. As the only source of change is the heartbeat movement in the held breath-data, and respiration and heartbeat movement in the breathing-data, these modulations originate from physiological activity and noise. $|\check{v}_{cal}(\tau_T)|$ is then the magnitude of the physiological movement in the calibrated data. Using (9) the radar cross section of the human heartbeat, σ_H,

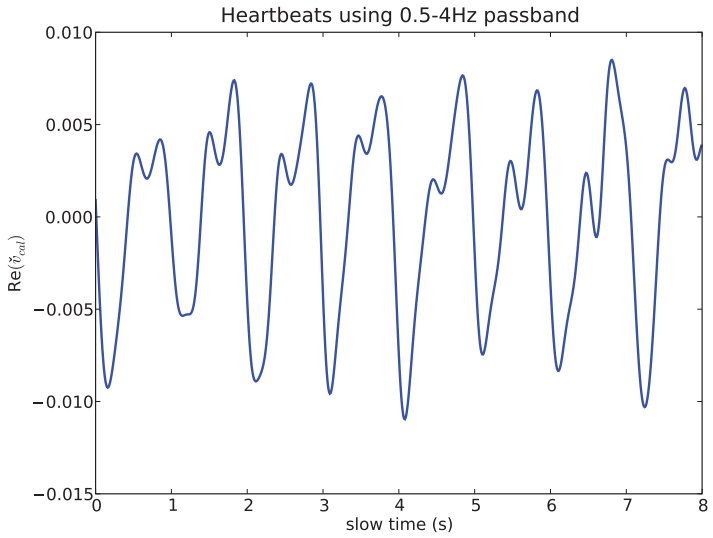

Figure 3: The slow time development of the real part of $\check{v}_{cal}(\tau_T)$ under held breath condition. The passband used in filtering is $0.5 - 4Hz$.

and the radar cross section of human respiration, σ_R, can be computed:

$$\sigma_H = |\check{v}_{cal}(\tau_T)|^2 \sigma_S, \quad \text{using held breath data.} \tag{12}$$

$$\sigma_R = |\check{v}_{cal}(\tau_T)|^2 \sigma_S, \quad \text{using respiration data.} \tag{13}$$

In the above equations, σ_S is the known RCS of the calibration sphere.

As $\check{v}_{cal}(\tau_T)$ is the vector of changes through slow time, it is clear that σ_H and σ_R also are vectors changing through slow time. $\bar{\sigma}_H$ and $\bar{\sigma}_R$ are the mean values taken through the slow time duration of the recordings. These are the mean RCS of the physiological movement through several periods of heartbeats or respiration.

V. Results

In this section, the computed heartbeat and respiration RCS of real measurements are shown. The presented results are computed from one recording of a person holding his breath, and one recording of the same person breathing while sitting still. Fig. 3 and Fig. 4 shows the real part of $\check{v}_{cal}(\tau_T)$ for heartbeats and respiration respectively. Fig. 5 shows the slow time development of the heartbeat RCS, σ_H, after the calibrated data has been passed through a $0.5 - 4Hz$ bandpass filter. Fig. 6 is a similar plot of the respiration RCS, σ_R, after a lowpass filter with cutoff frequency $5Hz$.

The calibrated data was filtered with several different passbands to remove high frequency noise, and to remove small movements appearing with a low frequency in the recordings. It is especially important to remove low frequency content in the heartbeat recording, as these may have a high amplitude relative to the heartbeat modulations. With a narrow passband in the filter, much of

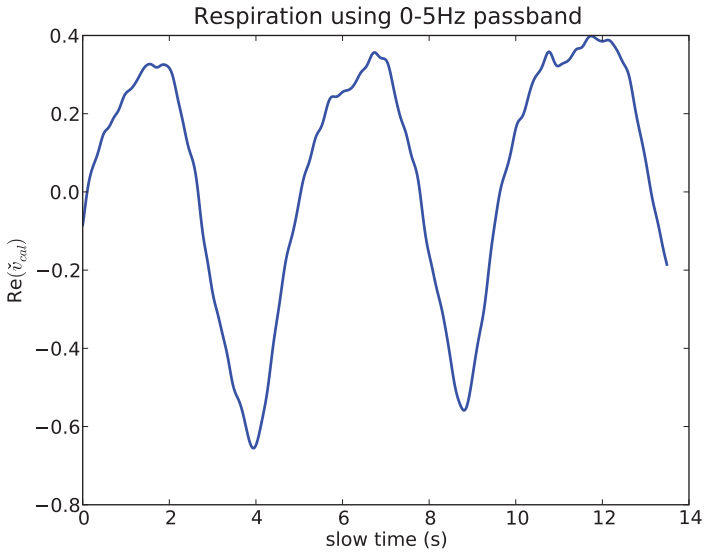

Figure 4: The slow time development of the real part of $\check{v}_{cal}(\tau_T)$ with the person breathing. A cutoff frequency of $5Hz$ was used in the processing.

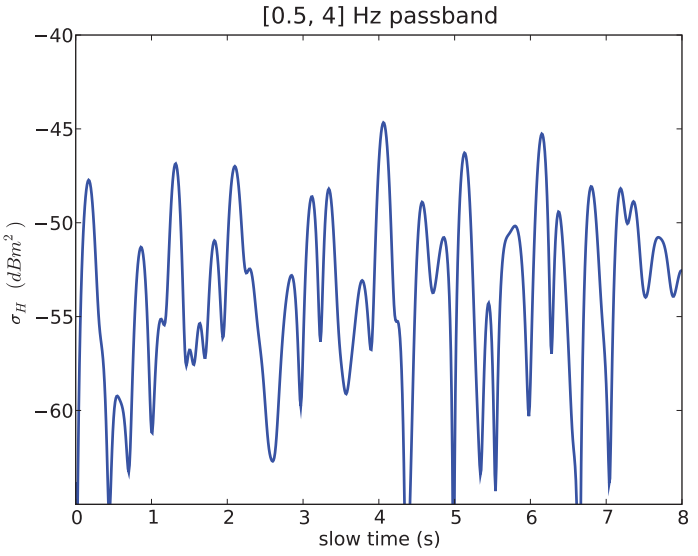

Figure 5: The slow time development of σ_H in dBm^2. The passband used in filtering is $0.5-4Hz$.

the noise and modulations caused by small movements are filtered out. However, more energy originating from the physiological motion is likely to be removed with a narrow passband. Presented in Fig. 7 is $\bar{\sigma}_H$ computed from $\check{v}_{cal}(\tau_T)$ filtered with different bandpass filters. From Fig. 7

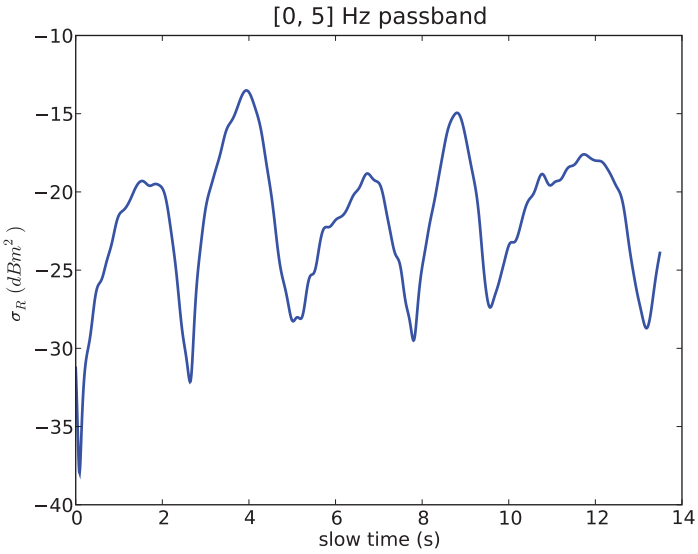

Figure 6: The slow time development of σ_R in dB.

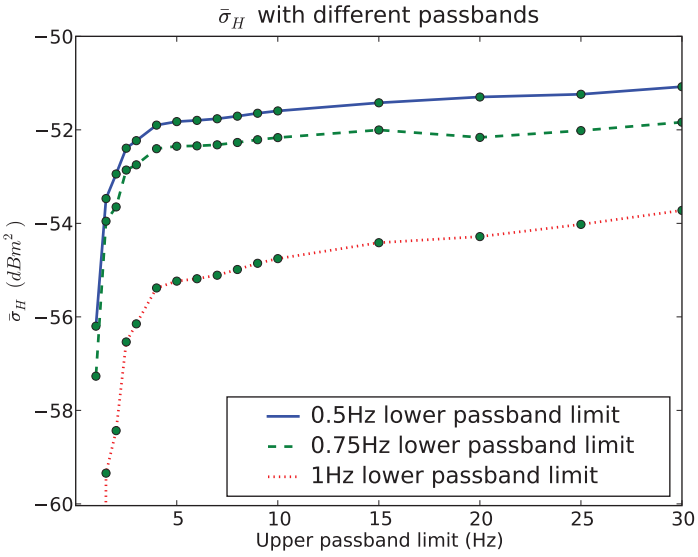

Figure 7: The mean heartbeat RCS $\bar{\sigma}_H$ computed using various passbands.

it is seen that a lowpass limit of $1Hz$ probably removes much of the heartbeat power. This is expected, as the heartbeat rate of the test person was just over 60 beats per minute. Also, filtering with an upper cutoff frequency below $4Hz$ significantly reduces the detected heartbeat RCS. From this single measurement it seems that most of $\bar{\sigma}_H$ is appearing in the $0.5 - 4Hz$ band. The

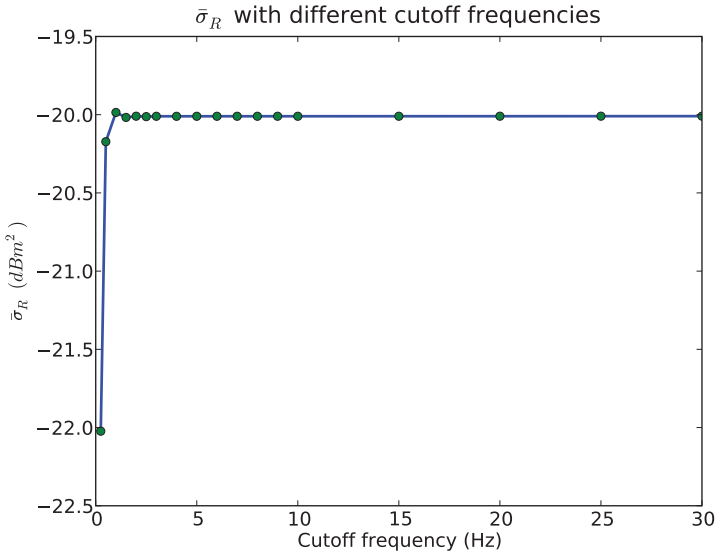

Figure 8: The mean respiration RCS $\bar{\sigma}_R$ computed using lowpass filters.

influence of the involuntary movement on the computed heartbeat RCS will be different between each measurement. It is also expected that $\bar{\sigma}_H$ will be different both between different people and between different heartbeat rates of the same person. The size of these variations though, is not studied in this paper. To compute the heartbeat RCS of human beings in general requires measurements on a larger number of different people.

In Fig. 8, $\bar{\sigma}_R$ computed from $\check{v}_{cal}(\tau_T)$ filtered with different lowpass filters is shown. As is seen from the figure, there is almost no variation in the respiration RCS when the cutoff frequency of the lowpass filter is higher than the respiration rate.

VI. Conclusion

A definition of the human heartbeat RCS and respiration RCS has been introduced. A mathematical model of UWB radar measurements was employed to describe the recording of a human being. This model was used to describe the calibration and processing steps necessary for computing the RCS of the human physiological movement. To demonstrate this approach, we used experimental results obtained by real recordings of a person and an aluminum calibration sphere. The computed RCS is dependent on the strictness of the processing and the person under test. This calls for using a larger number of measurements of different people. The results from the experimental data presented here shows that the human heartbeat RCS is around $6.5 \cdot 10^{-6} m^2$, while the human respiration RCS is around $1 \cdot 10^{-2} m^2$.

Acknowledgment

This work is part of the MELODY project funded by the Research Council of Norway under contract number 187857/S10. Thanks to Mats Jørgen Øyan and Leif Hanssen at FFI for hardware and help during the measurements.

References

[1] E. Staderini, "UWB radars in medicine," *Aerospace and Electronic Systems Magazine, IEEE*, vol. 17, no. 1, pp. 13–18, Jan 2002.

[2] I. Immoreev and T. Tao, "Uwb Radar for Patient Monitoring," *IEEE A & E Systems Magazine*, November 2008.

[3] T. Berger, S.-E. Hamran, L. Hanssen, and M. J. Øyan, "Ultra Wideband Radar Design for Detection of Vital Signs," in *NATO-RTO/SET-125 Symposium on Defence Against Terrorism*, April 2008.

[4] A. Nezirovic, S. Tesfay, A. Valavan, and A. Yarovoy, "Experimental study on human breathing cross section using uwb impulse radar," in *Radar Conference, 2008. EuRAD 2008. European*, oct. 2008, pp. 1 –4.

[5] J. Kiriazi, O. Boric-Lubecke, and V. Lubecke, "Radar cross section of human cardiopulmonary activity for recumbent subject," in *Engineering in Medicine and Biology Society, 2009. EMBC 2009. Annual International Conference of the IEEE*, sept. 2009, pp. 4808 –4811.

[6] M. J. Øyan, S.-E. Hamran, T. Berger, and L. Hanssen, "Characterisation of ultra wideband frequency modulated and step frequency radar with range gating," in *Antennas, Radar, and Wave Propagation*. IASTED, ARP2009, July 2009.

[7] S.-E. Hamran, T. Berger, L. Hanssen, M. J. Øyan, V. Ciarletti, C. Corbel, and D. Plettemeier, "A prototype for the WISDOM GPR on the ExoMars mission," *Advanced Ground Penetrating Radar, 2007 4th International Workshop on*, pp. 252–255, June 2007.

[8] G. M. Brooker, "Understanding Millimetre Wave FMCW Radars," in *1st International Conference on Sensing Technology*, 2005.

[9] A. Morgan, "Ultra-wideband impulse scattering measurements," *Antennas and Propagation, IEEE Transactions on*, vol. 42, no. 6, pp. 840–846, Jun 1994.

[10] S. Hantscher, B. Etzlinger, A. Reisenzahn, and C. Diskus, "UWB Radar Calibration Using Wiener Filters for Spike Reduction," in *Microwave Symposium Digest, 2006. IEEE MTT-S International*, June 2006, pp. 1995–1998.

[11] M. Skolnik, Ed., *Radar Handbook*, 2nd ed. McGraaw-Hill Book Company, 1990.

6.2 II Radar cross section of the human heartbeat and respiration in the 500MHz to 3GHz band [2]

Abstract

Cardiopulmonary motion can be detected from a distance using radar. Which frequencies that are best suited for detecting heartbeats or respiration is connected to the radar cross section (RCS) of the physiological motion. In this paper, we investigate the RCS of human heartbeats and respiration in the frequency range 500MHz to 3GHz through calibrated radar recordings of two persons.

I. Introduction

Where conventional systems for monitoring human vital signs are large and cumbersome, or requires contact between the sensor and the person, radar-based systems may be used from a distance and through clothing and various obstacles. It has been demonstrated that radar can be used for detecting human heartbeats and respiration using narrowband radar signals over a great span of frequencies, from 433MHz [1] up to 228GHz [2], as well as with ultra wideband (UWB) systems [3]. However, which frequencies and which bandwidths are best suited for radar-based vital signs detection are not studied systematically.

Finding the transmitting frequencies optimal for heartbeat and respiration detection is a question of finding the frequencies for which the heartbeat and respiration RCS is largest. RCS, usually denoted σ, is a measure of how well an object reflects incident radar power as a function of frequency and aspect angle. Thus, an analysis of the human heartbeat and respiration RCS is required to find the frequencies best suited for vital sign detection.

Presented in this paper is the human heartbeat and respiration RCS as a function of frequency in the range $500MHz$ to $3GHz$. The RCS values have been computed from one sub-band of the entire $0.5 - 3GHz$ band at a time, resulting in discrete RCS values for different frequency bands. By heartbeat and respiration RCS, we mean the radar cross section of the physiological motion, or in other words, the size of the slow time changes of the radar recordings measured in m^2 units.

To obtain the σ values, other factors than the physiological motion itself need to be isolated from the measurements of a person. An aluminum calibration sphere with known radar cross section was used in the exact same measurement setup as the person measurements. External factors such as the generated signal in the radar, antennas, clutter and propagation through the air could be removed, leaving calibrated measurements of the human being from which the RCS of the physiological motion could be computed.

II. Measurement setup

All results presented in this paper were obtained through measurements using an ultra wideband frequency modulated (FM) continous wave (CW) radar. The radar was developed at FFI [4, 5], and it has been demonstrated for human heartbeat and respiration detection [6, 7]. The radar transmits a linear sweep signal with frequency increasing from $500MHz$ to $3GHz$. At the receiver end the signal is homodyned with the FMCW signal and low pass filtered, creating a beat signal with frequency content proportional to the round-trip times of travel, τ, between the antennas and reflectors in the scene. The beat signal is sampled in the frequency domain at a 16 bit analogue to digital converter (ADC) and stored for digital postprocessing.

Measurements were conducted in an anechoic chamber. Two different measurement setups were used when conducting a radar recording of a person: One to compute the respiration RCS, and one to compute the heartbeat RCS. For the respiration measurements a person was sitting still in a chair about one meter away from the antennas facing the radar. The setup for the heartbeat measurements was the same, but with the person holding his/her breath. To calibrate the measurements, two additional setups were used: One measurement of the empty chamber for clutter subtraction, and one of an aluminum calibration sphere in the chamber at the exact same range from the radar as the person was sitting. With this recording scheme, the only change between the different recordings were the targets. Five sets of radar recordings were made, using two different persons under test.

III. Calibration and processing

In [7] a propagation channel model of the radar measurements and a calibration procedure were presented. In that paper, the calibration procedure was used on $2-3GHz$ FMCW radar measurements to compute the human heartbeat and respiration RCS. Essentially the same procedure is used in this paper to calibrate the respiration and heartbeat recordings. To analyze the RCS dependence on frequency, the calibration and processing are conducted on several sub-bands over the $0.5-3GHz$ range, as presented in the next section.

A Partition of the frequency range

Though the radar recordings were conducted using sweeps of the entire $0.5-3GHz$ range, the human heartbeat and respiration RCS were computed on sub-bands of this range. These sub-bands were selected digitally from the raw data recordings. A width of $\Delta f = 500MHz$ of data was selected for each sub-band using a Hamming window. A total of nine sub-bands, with center frequencies f_c ranging from $750MHz$ to $2.75GHz$ and with a step of $250MHz$ between the center frequencies of each band was used. Fig. 1 illustrates the selection of the frequency sub-bands from the raw data. This creates nine raw data matrices, consisting of zeros outside the selected band, and with the raw data weighted by the window function inside the band. Each raw data matrix is denoted $V(\omega),\ \omega \in B_{f_c}$,where B_{f_c} is the sub-band $[f_c - \Delta f, f_c + \Delta f]$ with center frequency f_c and width Δf. The exact same procedure was applied to the calibration sphere recordings, and empty room clutter recordings.

B Calibration and processing procedure

The procedure for calibrating the measurements is thoroughly explained in [7], and a short summary is provided here. A channel model for the radar recordings is shown in Fig. 2. In the empty room measurements, the signal received by the radar is

$$V_C(\omega) = V_t(\omega)H_a^2(\omega)H_C(\omega), \tag{1}$$

where $V_t(\omega)$ is the signal transmitted by the radar, $H_a(\omega)$ is the transfer function of the two identical antennas and $H_C(\omega)$ is the empty room clutter transfer function. For the calibration sphere measurements the aluminum sphere with transfer function $H_S(\omega)$ is placed some distance from the

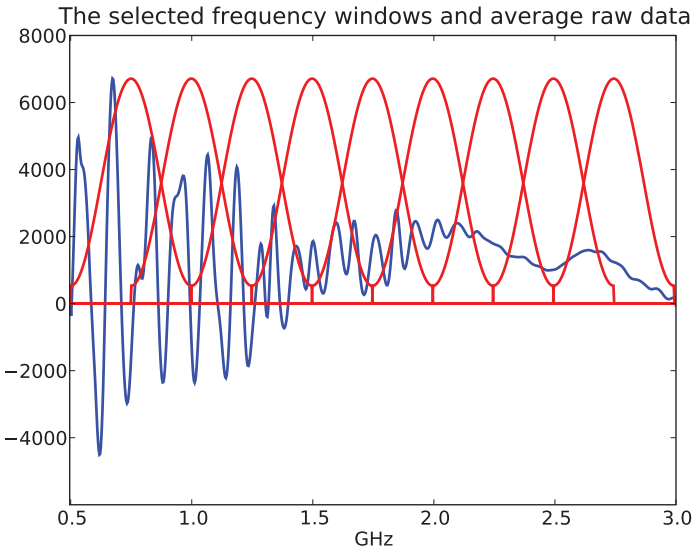

Figure 1: Selection of frequency subbands. The red lines are the Hamming windows applied to select a segment of the raw data.

antennas, making it appear additively in the measurements:

$$V_S(\omega) = V_t(\omega)H_a^2(\omega)(H_C(\omega) + H_S(\omega)). \tag{2}$$

For the measurements on a human being, the sphere is replaced with a person, either breathing or holding his breath, with transfer function $H_T(\omega)$ at the exact same distance from the antennas as the sphere was positioned:

$$V_T(\omega) = V_t(\omega)H_a^2(\omega)(H_C(\omega) + H_T(\omega)). \tag{3}$$

The calibration is then performed in a three step routine, on each sub-band at a time:

1. First, the empty room clutter measurement (1) is subtracted from the sphere (2) and person (3) measurements:

$$\begin{aligned} \tilde{V}_S(\omega) &= V_S(\omega) - V_C(\omega) \\ &= V_t(\omega)H_a^2(\omega)H_S(\omega),\ \omega \in B_{f_c} \end{aligned} \tag{4}$$

and

$$\begin{aligned} \tilde{V}_T(\omega) &= V_T(\omega) - V_C(\omega) \\ &= V_t(\omega)H_a^2(\omega)H_T(\omega),\ \omega \in B_{f_c}. \end{aligned} \tag{5}$$

2. Second, software gating in the fast time domain is performed. To do this, $\tilde{V}_S(\omega)$ and $\tilde{V}_T(\omega)$

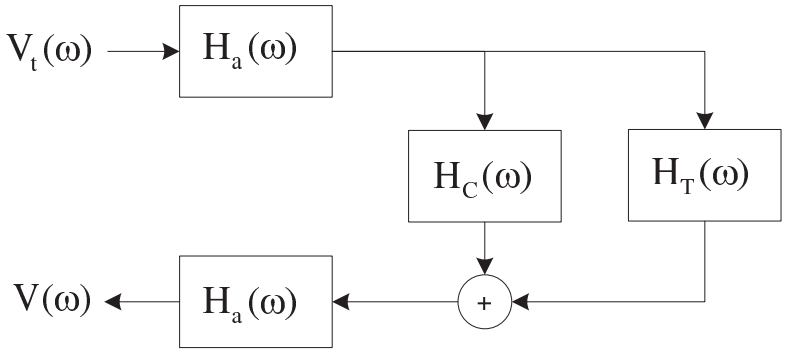

Figure 2: The channel model diagram.

are zero padded, and Fourier transformed to the fast time domain

$$\begin{aligned} \tilde{V}_S(\omega) &\overset{FFT}{\rightarrow} \tilde{v}_S(\tau) \\ \tilde{V}_T(\omega) &\overset{FFT}{\rightarrow} \tilde{v}_T(\tau). \end{aligned}$$

Knowing the round-trip time of travel τ_T between the radar and the target through the relation $\tau = \frac{2R}{c}$, τ_T is chosen as the center of the gating window. A Blackman window is chosen for its low sidelobe levels. A width of $10ns = 1.5m$ diameter is used, which removes reflections from the back wall of the chamber while keeping the reflections from the person or sphere. After the software gating, the matrices are inverse Fourier transformed to the frequency domain representations $\hat{V}_S(\omega)$ and $\hat{V}_T(\omega)$.

3. The last step uses $\hat{V}_S(\omega)$ to calibrate $\hat{V}_T(\omega)$:

$$V_{cal}(\omega) = \frac{\hat{V}_T(\omega)}{|\hat{V}_S(\omega)| + C}, \tag{6}$$

where C is a smoothing factor.

C RCS definition

After the calibration described above, one calibrated frequency domain measurement matrix $V_{cal}(\omega)$ has been computed for each freqency of the nine sub-bands B_{f_c}. These matrices were transformed to the fast time domain representation $v_{cal}(\tau)$ through FFT. Knowing that the person's chest was positioned at round-trip time of travel τ_T in the data, the vector $v_{cal}(\tau_T)$ is the vector of the slow time development at a distance $R = \frac{c\tau_T}{2}$ from the radar. As the topic of interest in this paper is the size of the physiological movements, the stationary content in $v_{cal}(\tau_T)$ was removed through linear least squares estimation:

$$\tilde{v}_{cal}(\tau_T) = v_{cal}(\tau_T) - X(X^T X)^{-1} X^T v_{cal}(\tau_T). \tag{7}$$

In (7) $X = [k/K \quad 1]$ is a $K \times 2$ matrix where $k = [0, 1, \ldots, K-1]^T$, K is the length of $v_{cal}(\tau_T)$ in slow time and 1 is a vector of ones of length K. This removes DC and linear trends in the data,

leaving only the slow time movement.

In [7] it was found that for a person with just over 60 heartbeats per minute, most of the slow time changes caused by heartbeats in the received signal was in the $0.5 - 4Hz$ band. As thermal noise is spread out over the entire spectrum, filtering the signal will improve the signal to noise ratio (SNR). For the heartbeat RCS computations, a $0.5 - 5Hz$ slow time bandpass filter was applied to the calibrated data vectors, ensuring that most of the heartbeat signal is intact while removing noise. For the respiration recordings, most of the signal is centered around the slow time frequency of breathing, and the SNRs are much larger than for the heartbeat recordings. A $5Hz$ lowpass filter was applied to the respiration data. The filtered vectors are termed $\check{v}_{cal}(\tau_T)$.

After the processing steps, $\check{v}_{cal}(\tau_T)$ consists of modulations in the calibrated data at the round-trip travel time where the person was sitting still. Apart from noise, these modulations are caused by the heart beating in the heartbeat data, and a combination of heartbeats and respiration in the respiration data. Using the formula for computing the human physiological motion RCS found in [7], the radar cross section of the heartbeats, σ_H, and the radar cross section of the respiration, σ_R, is:

$$\sigma_H = |\check{v}_{cal}(\tau_T)|^2 \sigma_S, \quad \text{using held breath data.} \tag{8}$$

$$\sigma_R = |\check{v}_{cal}(\tau_T)|^2 \sigma_S, \quad \text{using respiration data.} \tag{9}$$

In the above equations, σ_S is the known RCS of the calibration sphere. The mean values $\bar{\sigma}_H$ and $\bar{\sigma}_R$ are the mean RCS values through the recordings. These values were computed for each of the different bands B_{f_c} with center frequencies f_c.

IV. Results

In this section, RCS values found through experiments and using the calibration and processing procedure described above are presented. Multiple measurements were conducted on two persons, resulting in 5 sets of recorded data. To obtain a good signal to noise (SNR) ratio over the entire $0.5-3GHz$ range, separate measurements were done for the lower and upper part of the range. Fig. 3 shows the slow time development of a calibrated and processed heartbeat recording, $\mathbf{Re}[\check{v}_{cal}(\tau_T)]$, using the sub-band $B_{f_c} = [1,\ 1.5]GHz$. In Fig. 4 a similar respiration recording is shown. These examples show visually the recorded human physiological motion. It is also seen that the respiration is of a larger order of magnitude than the heartbeats.

For each frequency sub-band with center frequency f_c five $\bar{\sigma}_H(f_c)$ and $\bar{\sigma}_R(f_c)$ were computed from different measurements. The results can be seen in Fig. 5 and Fig. 6. Radar cross section in general is dependent on both frequency and the aspect angle on the target. All the data presented in this paper were recorded with the person directly facing the radar. However, as the measurements were conducted individually, there were some variations in the seating positions. This in addition to possible variations in heartbeat or respiration rate and intensity between the measurements leads to unknown variations in the perceived RCS values. Indeed, there are variations in the data as can be seen in Fig. 5 and Fig. 6. Especially the respiration RCS varies much due to the fact that two different persons were used and recordings were made at different times. Despite these variations, it seems that for both the respiration and heartbeat data, the RCS is increasing with increasing frequency. Throughout the increasing frequency band from $500MHz$ to $3GHz$, the

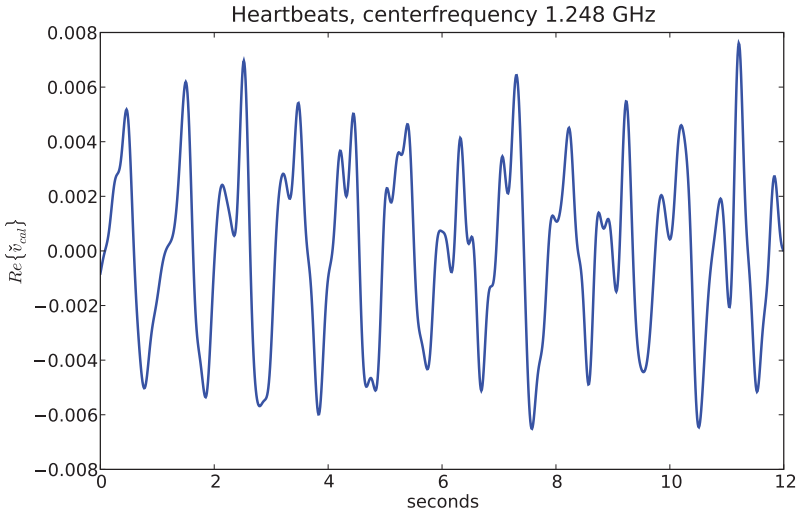

Figure 3: Slow time development of the real part of a heartbeat recording $\check{v}_{cal,1.25GHz}(\tau_T)$.

wavelength of the signal is decreasing from $60cm$ to $10cm$. For a signal reflected off the chest surface, an increasing gain in the direction of the radar is expected with decreasing wavelengths, as the wavelengths becomes small compared to the chest surface. This could explain the increase in RCS values for higher frequencies. If the motion detected in the heartbeat recordings are caused by reflections from the heart and not just the chest wall, wavelengths the size of the heart or smaller is expected to reflect better off the heart itself than larger wavelengths. However, a larger attenuation for the propagation through the chest is also expected with increased frequency [8].

A further analysis of the heartbeat RCS for a larger frequency band may shed some light to the question; what are we actually measuring? If the returned heartbeat signal has penetrated the body and been reflected off the heart itself, lower RCS values are expected with higher frequencies due to an increasing attenuation for the signal propagating through the body. An analysis of this however, is beyond the scope of this paper.

V. Conclusion

Presented in this paper is the radar cross section of the human heartbeat and respiration as a function of frequency in the range 500MHz to 3GHz. The results were found performing calibration and processing on real radar recordings on human beings. Although a sparse amount of data was available, the RCS values found in this paper indicates that both the respiration and heartbeat RCS is increasing with increasing frequency in the 0.5-3GHz frequency range.

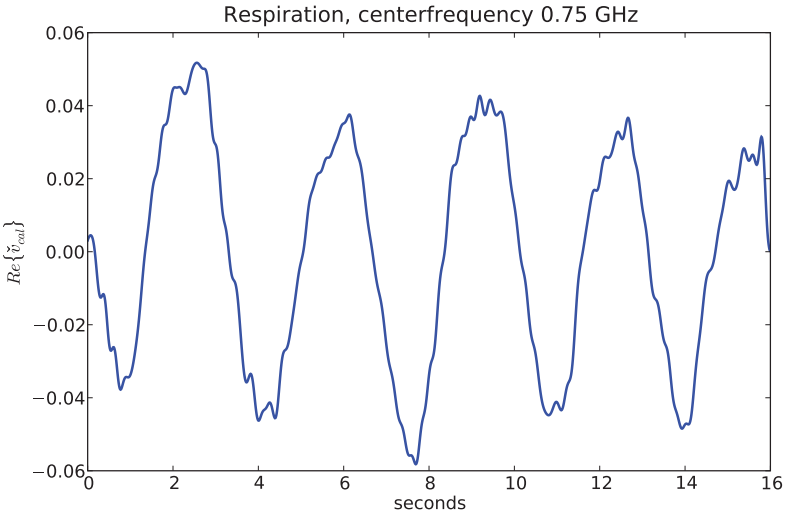

Figure 4: Slow time development of the real part of a respiration recording $\check{v}_{cal,0.75GHz}(\tau_T)$.

Acknowledgment

This work is part of the MELODY project funded by the Research Council of Norway under contract number 187857/S10. Thanks to Mats Jørgen Øyan and Leif Hanssen at FFI for hardware and measurement support.

References

[1] M. Jelen and E. M. Biebl, "Multi-frequency sensor for remote measurement of breath and heartbeat," *Advances in Radio Science*, vol. 4, pp. 79–83, 2006. [Online]. Available: http://www.adv-radio-sci.net/4/79/2006/

[2] D. Petkie, C. Benton, and E. Bryan, "Millimeter wave radar for remote measurement of vital signs," in *Radar Conference, 2009 IEEE*, May 2009, pp. 1 –3.

[3] M. Chia, S. Leong, C. Sim, and K. Chan, "Through-wall UWB radar operating within FCC's mask for sensing heart beat and breathing rate," in *Radar Conference, 2005. EURAD 2005. European*, Oct. 2005, pp. 267–270.

[4] M. J. Øyan, S.-E. Hamran, T. Berger, and L. Hanssen, "Characterisation of ultra wideband frequency modulated and step frequency radar with range gating," in *Antennas, Radar, and Wave Propagation*. IASTED, ARP2009, July 2009.

[5] S.-E. Hamran, T. Berger, L. Hanssen, M. J. Øyan, V. Ciarletti, C. Corbel, and D. Plettemeier, "A prototype for the WISDOM GPR on the ExoMars mission," *Advanced Ground Penetrating Radar, 2007 4th International Workshop on*, pp. 252–255, June 2007.

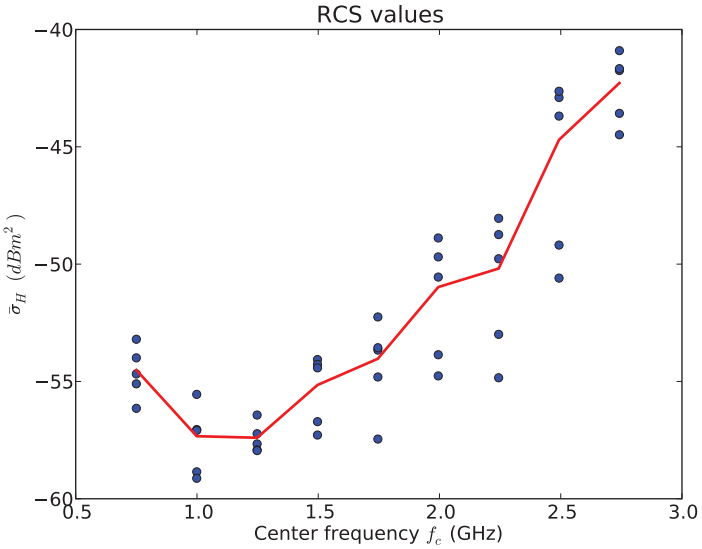

Figure 5: The RCS of human heartbeats as a function of frequency. The dots are measured values, and the line is the mean value.

[6] T. Berger, S.-E. Hamran, L. Hanssen, and M. J. Øyan, "Ultra Wideband Radar Design for Detection of Vital Signs," in *NATO-RTO/SET-125 Symposium on Defence Against Terrorism*, April 2008.

[7] Ø. Aardal, S.-E. Hamran, T. Berger, J. Hammerstad, and T. S. Lande, "Radar Cross Section of the Human Heartbeat and Respiration," in *Biomedical Circuits and Systems Conference, 2010. BioCAS 2010.* IEEE, November 2010, pp. 53–57.

[8] S. Pisa, P. Bernardi, M. Cavagnaro, E. Pittella, and E. Piuzzi, "Monitoring of cardio-pulmonary activity with UWB radar: A circuital model," in *Electromagnetic Compatibility and 19th International Zurich Symposium on Electromagnetic Compatibility, 2008. APEMC 2008. Asia-Pacific Symposium on*, May 2008, pp. 224–227.

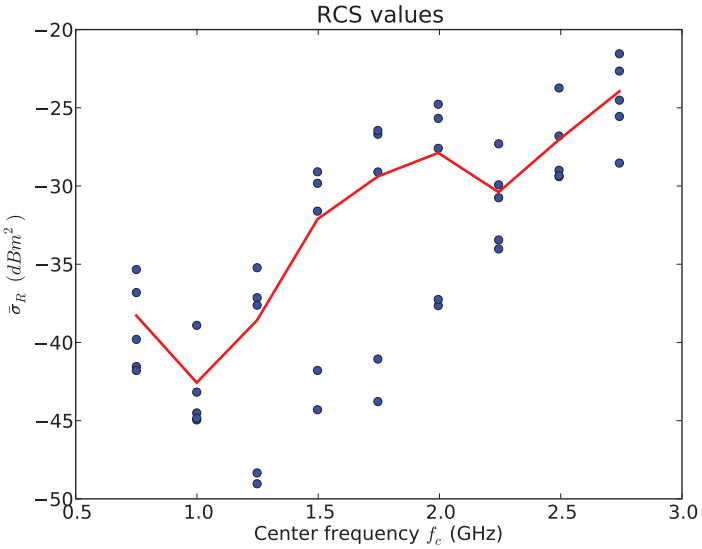

Figure 6: The RCS of human respiration as a function of frequency. The dots are measured values, and the line is the mean value.

6.3 III Empirical model of modulation in radar heartbeat and respiration measurements [3]

6.4 IV Chest movement estimation from radar modulation caused by heartbeats [4]

Abstract

Heartbeats can be measured at a distance using radar to record the chest movements. The physiological motion appear as modulations in both phase and amplitude in the radar recording. In this paper, a single reflector model of the heartbeat is used to estimate the chest motion and find the movement in millimeters. Experimental results from $10 - 18GHz$ measurements are presented, and the validity of the estimation discussed.

I. Introduction

Using radar technology, one can measure human heartbeats and respiration contact-less and through the air. A radar life sign monitor can be mounted above or in a patients bed, a heartbeat monitor integrated in a chair or in a doctor's office. Where conventional heartbeat monitoring techniques require contact between the patient and the equipment, wireless recordings of a patient's heartbeats can be made instantly and without contact between the patient and measurement equipment. In addition to vital signs detection, there are unexplored diagnostic possibilities in using radar for heartbeat measurements. Unlike today's most widely used heart disease diagnostic tool ECG, which records the electrical activity in the heart, radar records the actual chest motion caused by the heart beating.

Understanding the modulation caused by the heart beating in a radar recording is a non trivial task. A radar recording heartbeats from a distance does not only record the chest moving, but also all other objects within the antenna beam. In [1, 2], the problem of extracting the small heartbeat modulation from the stationary part of the signal caused by hardware and static scatterers in the scene is addressed. In this paper, we further investigate the heartbeat modulation through high frequency measurements. With higher frequency the movement becomes larger relative to the wavelength, resulting in an increased modulation in the received signal. Radar recordings on a person lying down were conducted using 10, 15 and $18GHz$ transmit frequencies. With these frequencies, the phase change caused by even sub-millimeter movements will be significant. Using the experimental data, the chest movement caused by the heart beating was estimated and found to be between 0.5 and $1mm$.

II. Physiological motion model

The heartbeat or respiration creates a periodic movement of the chest surface. An often used model for this movement is to model the chest as a reflector with an initial distance R_0 from the radar with a small range variation $R_h(t)$ [1, 2, 3]. Using this model, the time dependent distance between the antennas and the target is

$$R_m(t) = R_h(t) + R_0 \quad (1)$$

$$\Delta R = \frac{c\Delta\tau}{2} \quad (2)$$

$$R_0 = \frac{c\tau_0}{2}. \quad (3)$$

The simplest model for the movement is $R_h(t) = \Delta R \sin(\omega_h t)$, where ΔR is the maximum deviation in range from the initial position R_0, $\Delta\tau$ is the maximum deviation in two way travel time from the initial two way travel time τ_0 and ω_h the heartbeat angular frequency. [4] lists several studies reporting a typical movement of the chest caused by the heartbeat being in the range $0.035mm - 1mm$. An implicit assumption in this model, is that the electromagnetic wave does not penetrate into the body to be reflected back from interfaces at other initial distances R_0.

III. Modulation in signal from the motion model

The amplitude of a spherical wave traveling in air has decay proportional to $\frac{1}{R^2}$. The change in amplitude due to the change in range is negligible as the ΔR change in range makes a non-significant contribution to the amplitude when ΔR is in a millimeter order of magnitude. In a single channel receiver the modulation appear directly as phase modulation in the carrier translated to a modulation in received amplitude. A signal reflected off a point scatterer a varying distance $R_m(t)$ from the radar is:

$$v_R(t) = A_R \cos(\omega_c t - \frac{2\omega_c R_m(t)}{c}), \tag{4}$$

with ω_c being the angular carrier frequency and A_R the signal amplitude. In an I&Q receiver the received signal and the 90° phase shifted received signal are mixed with the transmitted signal and added together in a homodyning process. This creates a complex base-band signal with phase modulation corresponding to the moving target:

$$b(t) = A_s e^{i\phi_s} + A_m e^{i\phi_m(t)} + n(t), \tag{5}$$

$$A_s e^{i\phi_s} = \sum_n A_n e^{i\frac{2\omega_c R_n}{c}}, \tag{6}$$

$$\phi_m(t) = \frac{2\omega_c R_m(t)}{c} = \phi_h(t) + \phi_0. \tag{7}$$

$A_s e^{i\phi_s}$ is the sum of the stationary reflectors in the scene, while $A_m e^{i\phi_m(t)}$ is the response from the moving part of the body when assuming only one moving target and $n(t)$ is the receiver noise. $\phi_h(t)$ is a time varying phase proportional to the time varying distance $R_h(t)$, while ϕ_0 is a fixed phase stemming from the fixed distance R_0.

A Modulation in the signals

A single frequency recording model can be written

$$\begin{aligned} b(t) &= s + m(t) + n(t) = A_s e^{i\phi_s} + A_m e^{i\phi_m(t)} + n(t) \\ &= A_s e^{i\phi_s} + A_m e^{i\phi_h(t)} e^{i\phi_0} + n(t), \end{aligned} \tag{8}$$

which is illustrated in Figure 1. The total sampled signal is the sum of the stationary contributions and the moving target contribution. The total signal will thus have both a phase and amplitude modulation even though the isolated moving target only creates a phase modulation in the model. To further investigate these modulations, Equation (8) is rewritten as:

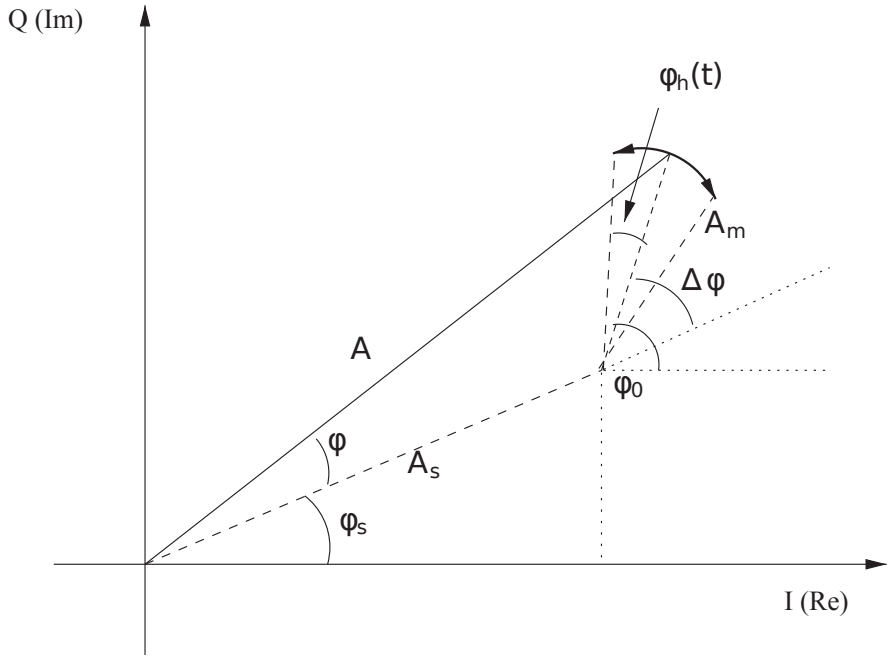

Figure 1: The signal in the complex plane with stationary and moving scatterers.

$$\begin{aligned} \Delta\phi &= \phi_0 - \phi_s, && (9)\\ b(t) &= e^{i\phi_s}\left[A_s + A_m e^{i\Delta\phi} e^{i\phi_h(t)}\right] + n(t), && (10)\\ &= e^{\phi_s} A(t) e^{i\phi(t)} + n(t) && (11) \end{aligned}$$

with $\Delta\phi$ being the phase difference between the stationary contributions and the mean phase of the moving scatterer, and $\phi_h(t)$ being the phase change caused by the movement. With (10), the stationary contribution A_s lies along the real axis, and the stationary phase component $e^{i\phi_s}$ acts as a rotation of the data. This is done to simplify the expressions for the modulation in the rest of this section, and is not something that is used in the processing and estimation described later in the paper. Using (9) and (10), the following identities for the real and imaginary parts of the signal are obtained:

$$\begin{aligned} \Re\{b(t)\} &= A_s + A_m \cos(\Delta\phi + \phi_h(t)) + \Re\{n(t)\} && (12)\\ \Im\{b(t)\} &= A_m \sin(\Delta\phi + \phi_h(t)) + \Im\{n(t)\}, && (13) \end{aligned}$$

which provides the expressions of the time varying amplitude and phase of the sampled signal:

$$\begin{aligned} A(t) &= \sqrt{A_m^2 + A_s^2 + 2A_sA_m\cos(\Delta\phi + \phi_h(t))} \\ &\quad +|n(t)|. \end{aligned} \tag{14}$$

$$\begin{aligned} \phi(t) &= \tan^{-1}\Big(\frac{A_m\sin(\Delta\phi + \phi_h(t))}{A_s + A_m\cos(\Delta\phi + \phi_h(t))}\Big) \\ &\quad +\angle n(t). \end{aligned} \tag{15}$$

Whether the modulation appears in the amplitude, phase, real or imaginary part in the total base-band signal model can be explained by the relative position and size of the stationary reflectors and the moving reflector. The complex problem of extracting the modulation from the stationary scatterers in the data is addressed in the following section.

IV. Stationary signal and modulation estimation

As we saw in the previous section the modulation can appear in various ways in the sampled signal. As stated in [2], estimating the movement $R_h(t)$ is a problem of estimating the stationary part $s = A_se^{\phi_s}$ of the base-band signal (8). The estimate $\hat{s}$ can be subtracted from the measurement leaving only the modulated signal and the estimation error e:

$$b(t) = m(t) + e. \tag{16}$$

A good estimate $\hat{s}$ of s leaves $b(t) \approx A_me^{i\phi_m(t)}$, and we can find both the amplitude A_m as well as the phase variation $\phi_m(t)$ of the moving target directly through arctangent demodulation [1]. From the phase, the range variation is found through

$$R_h(t) = \frac{\phi_h(t)c}{2\omega_c}. \tag{17}$$

However, a closed form expression for s does not exist [2]. Instead an estimator based on the moving part $m(t)$ can be used to find $\hat{s}$. From the model (8), the movement of the target forms an arc that is a fraction of a circle with radius A_m and center $s = A_se^{i\phi_s}$ in the complex plane as can be seen in Figure 1. The estimation problem is then a problem of estimating the center of this circle fraction. In [5] a comparison between three center estimation algorithms was made, and a recursive least squares fitting algorithm was deemed the best. In this paper, an iterative circle segment radius estimator found in [6] was used on our experimental data.

From (17) it can be seen that either a large angular carrier frequency ω_c or a large movement $R_h(t)$ results in a large phase variation $\phi_h(t)$. The performance of the stationary scatterer estimation depends on the maximum phase deviation ϕ_h [7]. To overcome the problem of small phase variation related to heartbeats using a $2.4GHz$ system, [7] uses the respiration base-band signal to estimate the stationary part s. Implicit in this approach is the assumption that the breathing and heartbeats create the same A_m in the base-band signal. As we will show through the experimental results presented in Section V., this is probably not an accurate assumption.

V. Experimental results

For the measurements an Agilent PNA-X network analyzer was used. Each measurement had a total acquisition time of 17.75 seconds using a sampling frequency of $113Hz$ and an IF bandwidth of $100Hz$. The person under test was lying down on his back with directive horn antennas positioned $\sim 0.5m$ above pointing down on the chest. Three different transmitting frequencies, 10, 15 and $18GHz$, were tested. For each transmitting frequency, both measurements where the target person was breathing and where he was holding his breath were conducted.

In the held breath data and the data where the respiration was filtered away, a center estimation was calculated for each individual heartbeat. The total center estimation $\hat{s}$ for a measurement was set to be the median of the estimates for all the heartbeats. High-pass filtering was used to separate heartbeats from respiration and other drift in the measurements. In [8] it was found that a cutoff frequency of $0.5Hz$ is suitable for heartbeat measurements.

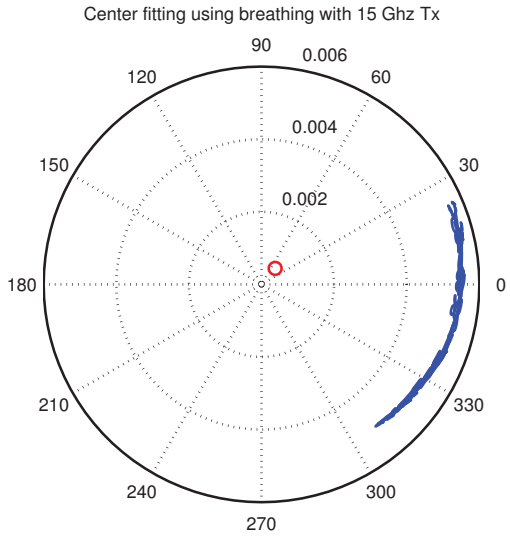

Figure 2: Breathing measurement in the complex plane with center estimation. The recorded respiration data is plotted in the blue line, while the estimated center is displayed as a red circle.

In the measurements where the person was breathing, a large arc can be seen in the polar plot. The respiration measurement using a $15GHz$ transmitting frequency is displayed in Figure 2. Next, the same data set was high-pass filtered to remove the respiration, leaving only the heartbeat modulation. This can be seen in Figure 3 with the DC added for better comparison with Figure 2. Figure 4 shows a recording at the same frequency, but this time with the person holding his breath. When the person was breathing the estimated stationary signal is small, while the estimated amplitude A_m of the moving scatterer is large. When there is no breath present in the data (Figure 3 and 4) on the other hand, the estimated amplitude A_m of the moving scatter is smaller. This is because when a person is breathing most of the torso is moving, which results in the moving

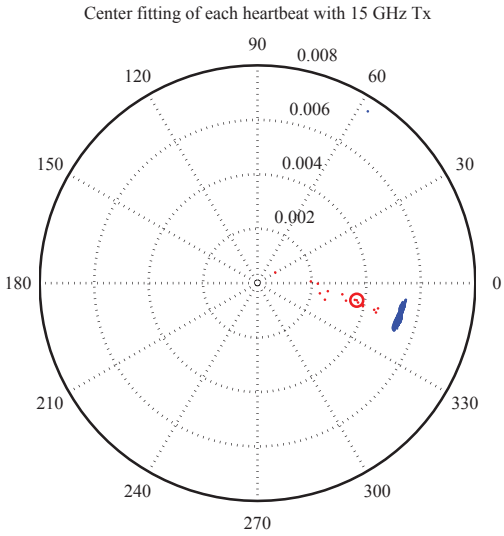

Figure 3: Heartbeat measurement in the complex plane with center estimation. The same data as displayed in Figure 2 was used, with the breathing filtered out. The dots are the center estimates for each individual heartbeat, while the circle is the median center estimate.

target being a big scatterer. When only heartbeats are the moving target, a smaller portion of the chest is moving while the rest of the upper body appear as a static scatterer. This leads us to believe that when estimating the static scatterer, separate estimations should be made when looking for respiration movement or heartbeat movements.

The center estimates on the heartbeat modulation displayed in Figure 3 and 4 have some spread, giving an uncertainty to the estimation. At these frequencies, even sub-millimeter motion will give a substantial phase shift in the measurement providing good conditions for the center estimation algorithm. This however, is under the assumption that the modulation in the base-band signal is caused by motion following the single reflector model (1) making the modulation appear as an arc in the complex plane. Figure 5 shows a zoom in on the measurement displayed in Figure 4. From the figure, it can be seen that the modulation is not a pure phase modulation following a circle segment arc but rather a combined phase and amplitude modulation. This warrants further research into the radar modulation from human heartbeats and a refinement of the simple single scatterer motion model.

From the estimation of s, A_m and ϕ_h, estimates of the chest motion $R_h(t)$ were made. These can be seen in Figure 6. As the same person was used for each recording, the motion should not differ too much between each measurement. In the $18GHz$ data a smaller motion amplitude R_h is seen. This can be caused by a change in positioning relative to the antennas or by error in the center estimation. The estimation of the chest motion assumes that the modulation appearing in phase only, which Figure 5 shows is not the case. This makes the estimation less accurate. [4] mentions several studies reporting $0.035mm - 1mm$ chest movement caused by the heartbeat, and the values

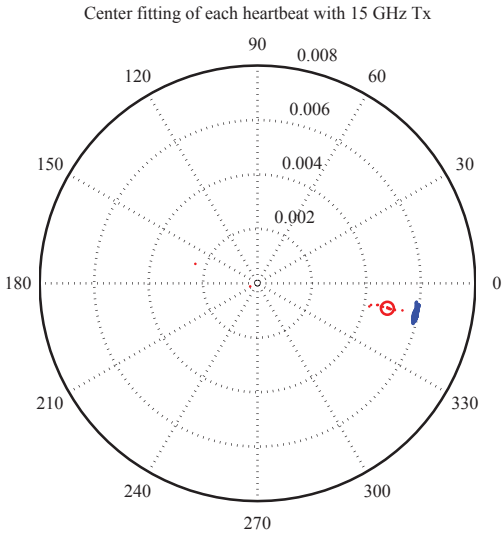

Figure 4: Heartbeat measurement where the person was holding his breath.

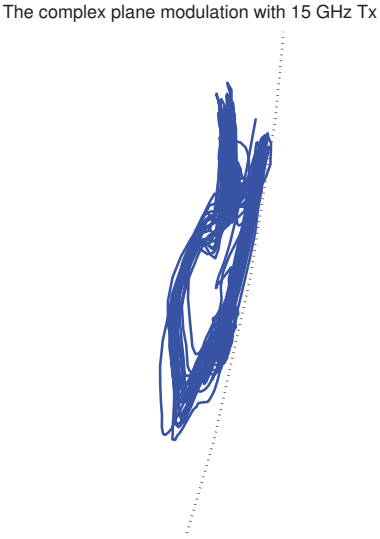

Figure 5: A close up view of the heartbeat modulation in the I & Q plane. About 17 seconds of heartbeat measurements is displayed.

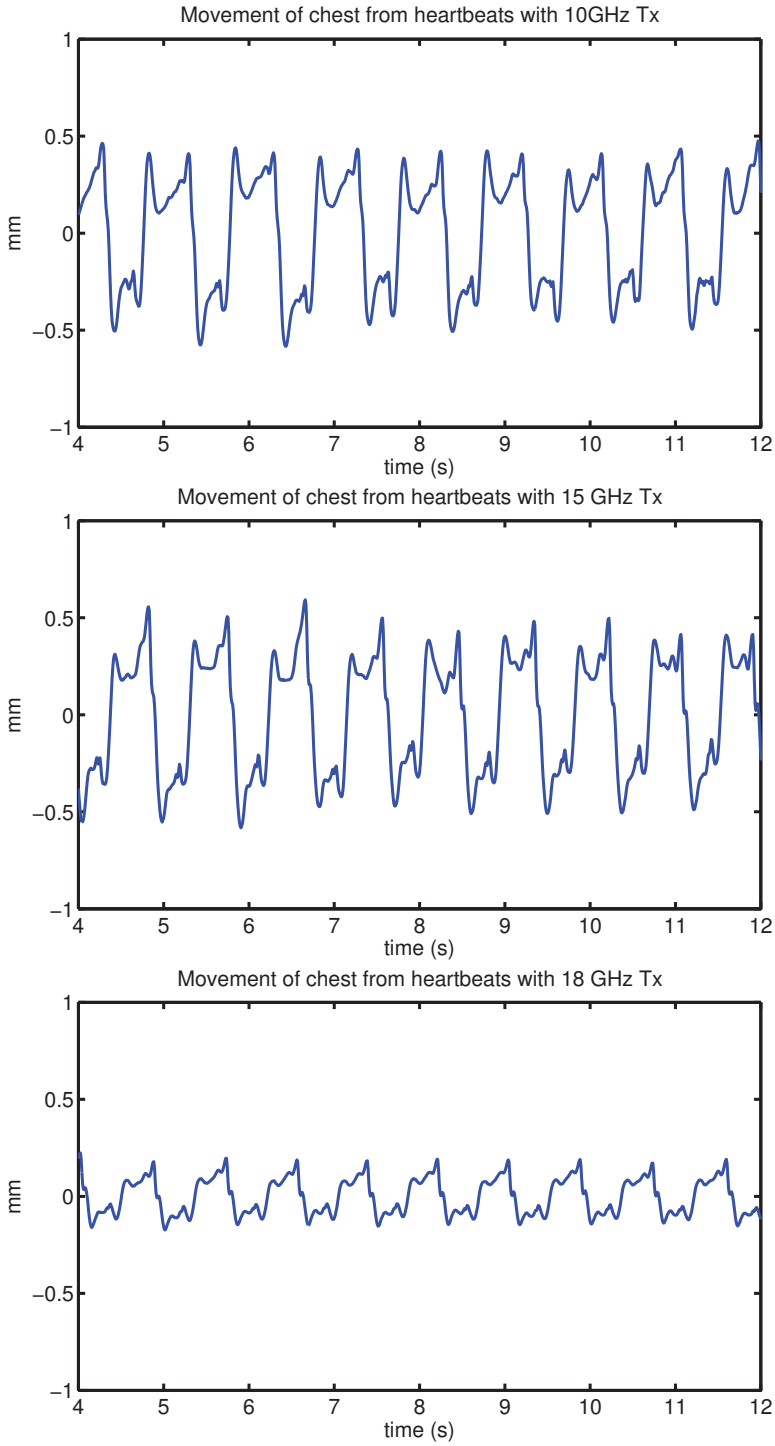

Figure 6: Estimated movement caused by heartbeat, using data obtained with from top to bottom 10, 15 and 18GHz Tx frequency.

in Figure 6 fit well within that region.

VI. Conclusion

In this paper the modulation in radar heartbeat recordings was investigated to estimate the heartbeat chest movement. A radar recording of human heartbeats contains both stationary parts, slowly moving breathing and heartbeats. Presented in this paper is a method for separating the heartbeat modulation and estimate the chest motion. Measurements results on a person using 10, 15 and $18GHz$ transmitting frequencies give estimates of the heartbeat chest movement being 0.5-1mm. It was also found that due to the complex geometry of the chest, the heartbeat modulation is not only a phase modulation but a combination of phase and amplitude modulation.

Acknowledgment

This work is part of the MELODY project funded by the Research Council of Norway under contract number 187857/S10.

References

[1] B.-K. Park, O. Boric-Lubecke, and V. M. Lubecke, "Arctangent Demodulation With DC Offset Compensation in Quadrature Doppler Radar Receiver Systems," *Microwave Theory and Techniques, IEEE Transactions on*, vol. 55, no. 5, pp. 1073–1079, May 2007.

[2] A. Høst-Madsen, N. Petrochilos, O. Boric-Lubecke, V. Lubecke, B. Park, and Q. Zhou, "Signal processing methods for doppler radar heart rate monitoring," *Signal Processing Techniques for Knowledge Extraction and Information Fusion*, 2008.

[3] C. Li and J. Lin, "Optimal Carrier Frequency of Non-Contact Vital Sign Detectors," in *2007 IEEE Radio and Wireless Symposium*, 2007, pp. 281–284.

[4] A. Droitcour, "Non-contact measurement of heart and respiration rates with a single-chip microwave Doppler Radar," Ph.D. dissertation, Stanford University, 2006.

[5] M. Zakrzewski, H. Raittinen, and J. Vanhala, "Comparison of center estimation algorithms for heart and respiration monitoring with microwave doppler radar," *Sensors Journal, IEEE*, vol. 12, no. 3, pp. 627–634, 2012.

[6] G. Taubin, "Estimation of planar curves, surfaces, and nonplanar space curves defined by implicit equations with applications to edge and range image segmentation," *IEEE Transactions on Pattern Analysis and Machine Intelligence*, pp. 1115–1138, 1991.

[7] B. Park, A. Vergara, O. Boric-Lubecke, V. Lubecke, and A. Høst-Madsen, "Quadrature demodulation with dc cancellation for a doppler radar motion detector," *submitted to IEEE MTT Transactions*.

[8] Ø. Aardal, S.-E. Hamran, T. Berger, J. Hammerstad, and T. S. Lande, "Radar Cross Section of the Human Heartbeat and Respiration," in *Biomedical Circuits and Systems Conference, 2010. BioCAS 2010.* IEEE, November 2010, pp. 53–57.

6.5 V Physical Working Principles of Medical Radar [5]

Abstract

There has been research interest in using radar for contact-less measurements of the human heartbeat for several years. While many systems have been demonstrated, not much attention have been given to the actual physical causes of why this work. The consensus seems to be that the radar senses small body movements correlated with heartbeats, but whether only the movements of the body surface or reflections from internal organs are also monitored have not been answered definitely. There has recently been proposed another theory that blood perfusion in the skin could be the main reason radars are able to detect heartbeats. In this paper an experimental approach is given to determine the physical causes. The measurement results show that it is the body surface reflections that dominate radar measurements of human heartbeats.

I. Introduction

Radar can be used to detect a person's heartbeats and respiration contact-less and from a distance, or by placing an antenna on the person's chest or back. Contact-less monitoring of heartbeats and respiration can be useful in long term vital signs monitoring, monitoring elderly people, sleep monitoring or as an early diagnostics tool supplementing already existing technologies. The vital signs are detected by the radar transmitting electromagnetic waves towards the person, and recording the received reflections. When the person is breathing and the heart is beating, modulations occur in the received radar reflections from the person.

Even though it has been a long time since the first radar heartbeat measurements were observed [1, 2], a complete understanding of what is measured has not yet been achieved. The dominating theory on the cause of the observed modulations, is that these are caused by small movements resulting in small phase changes in the received signal. For respiration measurements, the modulation can be seen as an arc in the complex plane compliant with a phase change caused by a moving target [3, 4]. Heartbeat measurements on the other hand, have a more complex shape in the complex plane not immediately recognized as coming from a single moving target.

In [5], the common acceptance that the radar detects heartbeats from small body movements was questioned. They provided a theoretical investigation into various physical mechanisms which could provide an explanation. For far field radar measurements, the following theories on what modulates the received radar signal were presented: Blood perfusion in the skin leading to skin impedance variation, internal body organ movements, skin/body surface movement and variations in black body radiation of the body because of temperature variations. It was concluded that the natural black body radiation cannot be the main cause of the heart signals observed in radar measurements, as the power contribution is too low. Reflections from internal body organs such as the heart walls was discarded as a theory. Simulations show that the reflections from the heart are too small to be of significance, at least when compared to the body surface reflections. This leaves the two theories of blood perfusion and body surface movements.

The calculations in [5] predict that while there could be some contribution in the received radar signals from the body surface movements, the blood perfusion is the main contributor. The beating of the heart leads to cyclic changes in the concentrations of oxygenated blood in human tissues. These changes are also present in the skin and body tissues close to the skin, leading directly to a change in the skin reflection coefficient.

Another issue is whether the heartbeat modulations are solely caused by body surface reflections or if there is a contribution from waves reflected from moving organs within the body such as the heart. It is known that electromagnetic waves can propagate inside the body [5, 6, 7] and a portion of this wave will be reflected at the boundaries of each tissue back towards the receiving antenna. However, the electric field attenuation in body tissues is high. This coupled with the fact that the air/skin interface provides a strong backscattering suggests that reflections from inside the body does not contribute significantly to the modulations, even though the heart itself has a larger motion than the chest surface. This has been assessed through simulations [6, 7, 8], but to the authors' knowledge has not yet been confirmed experimentally.

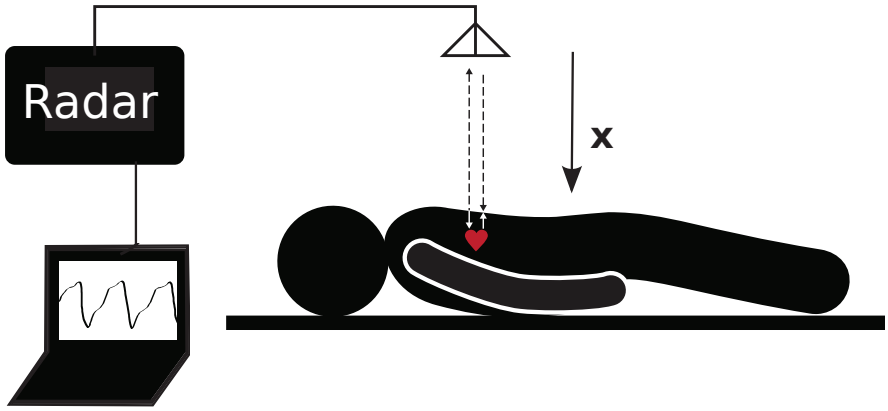

Figure 1: A typical non-contact radar heartbeat measurement. An antenna is aiming at a person's chest, and regular modulations correlated with the person's heartbeats are observed.

Fig. 1 shows a typical remote heartbeat monitoring setup. The main objective of this paper is to present an experimental approach to address the following questions:

- Are the observed radar modulations caused by body movements or blood perfusion in the skin?
- Is there sufficient penetration of electromagnetic (EM) waves inside the body so that the actual movement of the heart is seen in non-contact radar measurements?

The experimental approach to answering these questions was based on some simple principles: If the modulations are caused by the chest displacement of the person, reducing the movement will also reduce the observed modulations. If the modulations are caused by changes in skin properties, concealing the skin from the radar waves will reduce the observed modulations. Reversely, hindering the movement will not have an effect on the modulations if they are caused by skin property changes. Likewise, concealing the skin without hindering movement will not have an effect on the modulations if they are caused by chest movement.

Based on the mentioned principles, the following experiment was designed. Measurements of a person's heartbeat were conducted normally to be used as a reference. Then, the person's chest was pressed flat by a transparent plexiglass plate, hindering the movement of the chest. Third, the

person's chest was covered in a thin film of silver concealing the radar waves from being reflected from the skin while not hindering the movement.

Before the experiments are described, theoretical background on electromagnetic waves interacting with the human body is given in the next section. Here, two main theories of blood perfusion versus chest movement are also discussed. In Section III. the experimental setups and data analysis methods are described. Last, the results are presented in sections IV. and V..

II. Electromagnetic wave interaction with the human body

An electromagnetic wave travelling through a medium with permittivity ε', conductivity σ and magnetic permeability μ will at position x and time t have an electric field:

$$E(x,t) = \mathbf{Re}\{E_0 e^{-\alpha x - ikx + i\omega t}\} \quad (1)$$

$$\alpha = \omega\sqrt{\mu\varepsilon'}\left\{\frac{1}{2}\left[\sqrt{1+\left(\frac{\sigma}{\omega\varepsilon'}\right)^2}-1\right]\right\}^{1/2} \quad (2)$$

$$k = \frac{\omega}{v} = \omega\sqrt{\mu\varepsilon'}\left\{\frac{1}{2}\left[\sqrt{1+\left(\frac{\sigma}{\omega\varepsilon'}\right)^2}+1\right]\right\}^{1/2}, \quad (3)$$

where ω is the angular frequency, E_0 is the initial value of the electric field, v is the speed of propagation in the medium, α the attenuation constant of the medium and k the phase constant. For air and body tissues the magnetic permeability is equal to the free space permeability $\mu = \mu_0$.

An electromagnetic wave transmitted a sufficient distance from a human body will hit the body as a plane wave. Here, two factors determine the scattering of the wave: The shape of the body and the body dielectric properties. The shape of the body varies from person to person and with posture, while the dielectric properties are similar. For this reason, the shape of the body is disregarded in the following theory. Thus the theory is not accurate for a real world scenario, but sets the orders of magnitude for the reflection and attenuation of the EM waves. This illustrates the scattering from the body surface and the attenuation of the wave travelling inside the body.

When the wave hits an interface between two media with different dielectric properties, part of the wave is reflected while part of the wave is transmitted into the second medium. For normal incident waves on a planar surface, the reflected and transmitted electric fields are given by

$$E_r(x,t) = \mathbf{Re}\{\Gamma E_0 e^{\alpha_1 x + ik_1 x + i\omega t}\} \quad (4)$$

$$E_t(x,t) = \mathbf{Re}\{T E_0 e^{-\alpha_2 x - ik_2 x + i\omega t}\}. \quad (5)$$

Note that the scattered wave $E_r(x,t)$ is travelling in the negative x direction, while the transmitted wave $E_t(x,t)$ is travelling in the positive direction. The reflection coefficient Γ and transmission coefficient T between medium 1 and 2 are connected to the dielectric constants by

$$\Gamma_{1/2} = \frac{\eta_2 - \eta_1}{\eta_2 + \eta_1} \quad (6)$$

$$T_{1/2} = \frac{2\eta_2}{\eta_2 + \eta_1}, \quad (7)$$

where

$$\eta_n = \sqrt{\frac{i\omega\mu}{\sigma_n + i\omega\varepsilon'_n}}. \tag{8}$$

Using the Gabriel & Gabriel database for dielectric properties of human tissues [9, 10, 11] the air to skin reflection coefficient $\Gamma_{air/skin}$ can be found as a function of frequency, the results seen in Fig. 2. This agrees with the results by [12] where the reflection between air an skin was calculated to be 72.7% at 1.4 GHz.

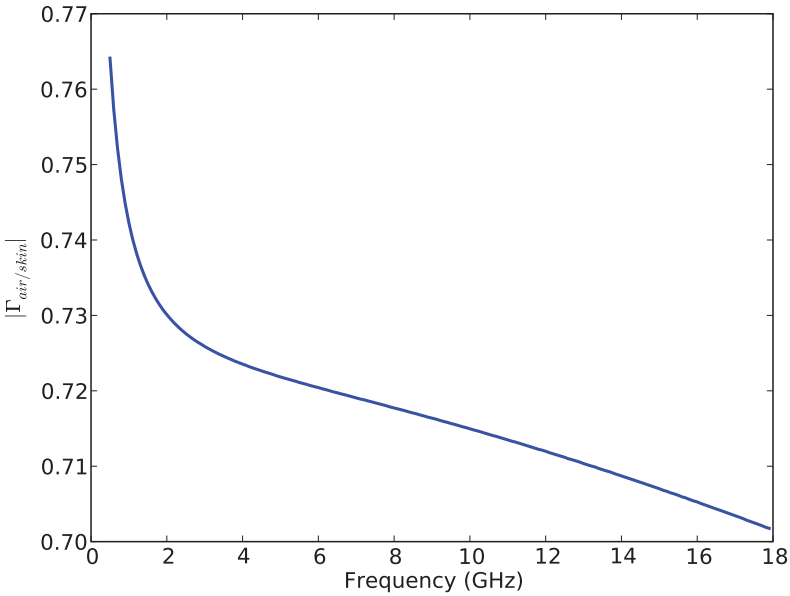

Figure 2: The magnitude of the reflection coefficient $|\Gamma_{air/skin}|$ between air and skin as a function of frequency.

The tissue parameters ε' and σ vary with frequency. For all tissues between the skin and the heart wall (skin, fat, muscle, bone, blood) the conductivity is increasing with frequency, which through (2) increases the attenuation with frequency. Several simulation studies have been performed on the attenuation of electromagnetic waves in the human body, confirming these results. Simulations by [6] show a two way attenuation of a 1.5 GHz wave between the chest and heart to be 40 dB. In [7] the total loss on the two way travel distance was reported to be about 60 dB at 3 GHz, rising to about 160 dB at 10 GHz with an average power loss of 80 dB in the band. A circuit model by [8] provides attenuation of about 25 dB at 100 MHz increasing to about 50-55 dB at 3 GHz.

A large part of the incoming wave at the air/skin interface is scattered, while there is great attenuation of the wave traveling inside the human body according to the results mentioned above. Even though the radar receiver may pick up some signal from inside the body, the body surface

scattering is much stronger and with a similar periodic movement, making it unrealistic to separate the in-body response from the strong surface response. This leads to the conclusion, from theory, that the body surface scattering dominate ranged measurements. This theory is further strengthened by the experimental results presented later in this paper.

Radar recordings using I & Q sampling can be displayed in the complex plane [3]. An actual radar recorded heartbeat is displayed in Fig. 3 and Fig. 4. The displayed data is a single frequency continuous wave (CW) recording of several heartbeats that have been high-pass filtered to remove stationary components and slow movements. The modulation follows a complex shape in the

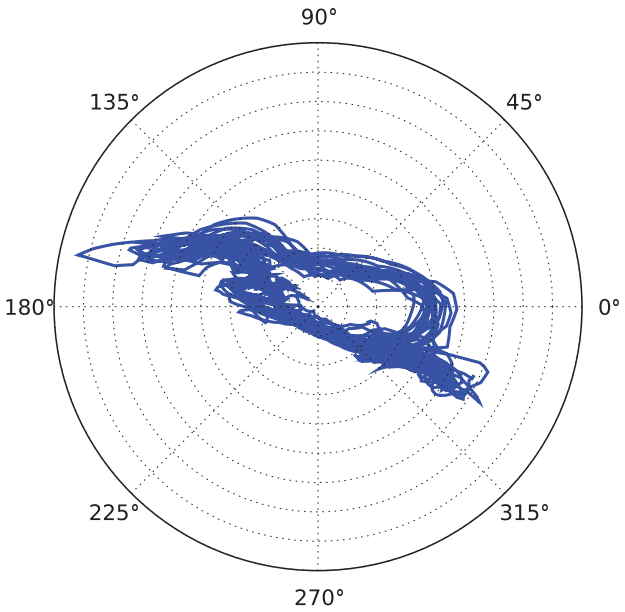

Figure 3: A 2 GHz CW recording of several heartbeats seen in the complex plane. The axes are linear scale with the real part of the voltage along the horizontal axis and the imaginary part of the voltage along the vertical axis. The mean has been subtracted from the data.

complex plane, and is not a pure phase or amplitude modulation.

There are, theoretically, more than one way the observed radar modulations can be created. The most common theory in the literature on the heartbeat modulation seen in radar recordings is that it stems from body movements caused by the heartbeat. The beating heart causes millimeter to sub-millimeter movements on the chest surface. Throbbing blood veins and changes in the body's gravitational center with the blood flow are also body movements closely connected to the heartbeat. Movements on this small scale are recorded as phase changes by the radar receiver.

As mentioned in the introduction, the other most plausible theory on what we see when observing heartbeats with radar is that we are seeing changes in the electromagnetic properties of the skin. This theory, called the blood perfusion theory, is explored in the following section. Attention is then turned to the body movement theory.

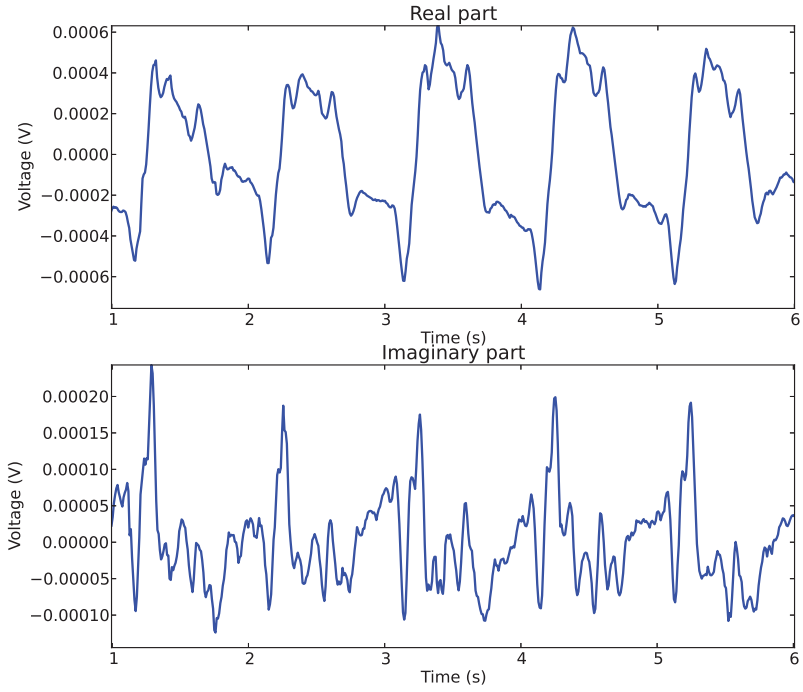

Figure 4: The real and imaginary part of an example non-contact recording of heartbeats using 2 GHz CW radar.

A Blood perfusion theory

During a heartbeat, the density of blood in the skin changes slightly [5]. The skin reflection coefficient changes accordingly; with no change in blood density in the skin, there will be no reflection coefficient changes. If on the other hand the blood density changes from 0 % to 100% , the reflection coefficient would change from the skin reflection coefficient $\Gamma_{air/skin}$ to the the blood reflection coefficient $\Gamma_{air/blood}$. During a heartbeat the blood density change will be much less than 100%, meaning that the change in reflection coefficient during a heartbeat will be much less than the difference between $\Gamma_{air/skin}$ and $\Gamma_{air/blood}$. For the sake of analysis though, one can look at the extreme cases of a pure air/skin interface and a pure air/blood interface. These reflection coefficients can be computed using Gabriel et. al.'s database [9, 10, 11] and equations (6) and (8). The difference in reflection coefficient between these two cases, $\Delta\Gamma = |\Gamma_{air/skin} - \Gamma_{air/blood}|$, is plotted in Fig. 5.

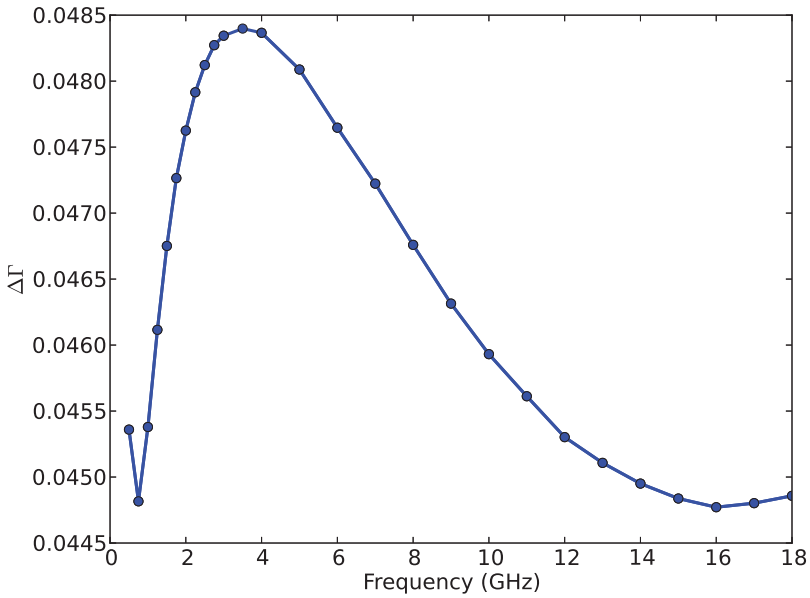

Figure 5: Difference in reflection coefficient $\Delta\Gamma$ between an air/skin interface ($\Gamma_{air/skin}$) and an air/blood interface ($\Gamma_{air/blood}$).

The reflection coefficient is connected to the radar cross section of a target through

$$RCS_P = W\Gamma^2, \tag{9}$$

where RCS_P is the radar cross section of the person and W is the radar cross section of the person if he had been perfectly conductive.

Assuming that what is seen in a radar heartbeat recording is the blood perfusion, this will be

seen as a change in the RCS through the relation

$$\Delta RCS_P = W\Delta\Gamma^2, \tag{10}$$

where $\Delta\Gamma$ is the actual change in skin reflection coefficient of the person. Any contribution to the observed modulation from the blood perfusion effect will manifest itself as amplitude modulations in the person echo. These are modulations that would be present regardless of any movements of the person. Since the chest of a person spans a small range of distances from the radar, the amplitude modulations may appear at slightly different ranges. Such a scenario is compliant with the modulation seen in Fig. 3

B Body movement theory

In the body movement theory, the observed radar modulation is explained as small chest movements causing phase variations in the received signal. A single point scatterer with a time varying distance from the antennas will be seen as a pure phase change directly proportional to the movement. In baseband, this can be written $Ae^{\phi(t)}$, where A is the amplitude of the signal and $\phi(t) = \frac{2\omega R(t)}{c}$ is the time varying phase. ω is the signal angular frequency, $R(t)$ is the time varying range and c is the speed of light. The amplitude of the signal is dependent on the object's RCS.

The human chest however, is not a point scatterer. Different parts of the chest are at slightly different distances R from the radar antenna. The total contribution from the moving parts of the chest is a sum of the reflections over all the ranges R:

$$A_m(t)e^{i\phi_m(t)} = \int_{R_0}^{R_1} A_m(R)e^{i\phi_m(R,t)}dR, \tag{11}$$

$$\phi_m(R,t) = \frac{2\omega R(t)}{c}, \tag{12}$$

with R_0 being the range to the closest part of the moving chest, and R_1 the range to the farthest part of the moving chest. From the equation, the resulting vector has modulations both in amplitude and phase because phase modulations from different ranges have been summed. Contributions from the static scatterers such as the non-moving parts of the body are also part of the received signal. The sum of these contributions will have non-varying amplitude and phase, $A_s e^{i\phi_s}$. The total received signal is the sum of the static and moving parts:

$$b(t) = A_s e^{i\phi_s} + A_m(t)e^{i\phi_m(t)}. \tag{13}$$

This theory is also compliant with the observed heartbeats plotted in Fig. 3. For more details on the complex modulation of heartbeat recordings and the movement theory, the reader is referred to [13] and [3].

III. Measurements and methodology

As explained, the recorded heartbeat modulations are complex in shape and fits both the blood perfusion model and the body movement model. In this section, our experimental approach to finding the correct explanation for the modulations is described. The experiment consists of three

measurement setups and post processing. The first setup, called the bare measurement, is of a person lying on his back with a bare chest and the radar antenna above the chest. The second setup, called the plexiglass measurement, is the same setup with the person's chest being pressed flat by a plexiglass plate. Last is the silver measurement, where the person's chest is covered in a layer of silver leaves.

A The experimental setup

All measurements were conducted on a male subject of age 26 in an anechoic chamber using a vector network analyzer [14]. A network analyzer transmits electromagnetic signals and measures the phase and amplitudes of the reflections. With antennas connected to the network analyzer, it can be used as a radar. The transmitted signals were single frequency continuous waves with an IF bandwidth of 100 Hz which were sampled at 113 Hz sampling frequency. Two different antennas were used, one for the 0.5-4 GHz range and one for the 4-18 GHz range. Fig. 6 shows

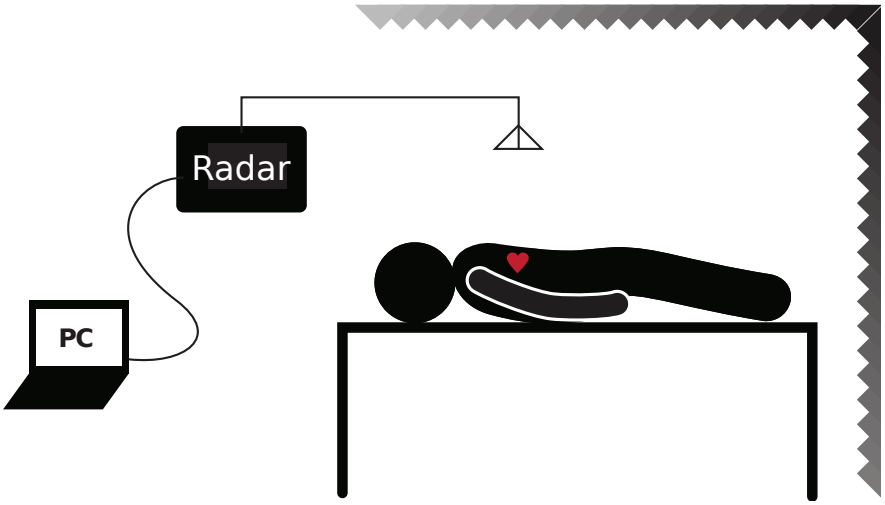

Figure 6: The measurement setup. The person was lying on a table placed inside an anechoic chamber. An antenna was placed over the person directed towards his chest, and connected with the network analyzer placed outside of the anechoic chamber.

the measurement setup.

A series of 155 measurements using three different setups has been performed. The measurements were performed using $0.6, 1, 2, 3, 4, 8, 12, 15$ and 18 GHz Tx frequencies. In the first setup, seen in Fig. 7, a person is lying on his back with an antenna directly above aimed down at the chest. In Fig. 8, the plexiglass setup where the test person's chest is pressed flat by a plexiglass plate is shown. This suppresses any modulation caused by movement in the radar recordings because the chest is hindered from moving by the plexiglass plate. Modulation caused by blood perfusion on the other hand should stay the same or be magnified because the gain of the chest is increased when pressed flat. In addition, any modulation caused by reflections from moving internal body parts such as the heart should not be much affected. Waves penetrating into the chest and being reflected

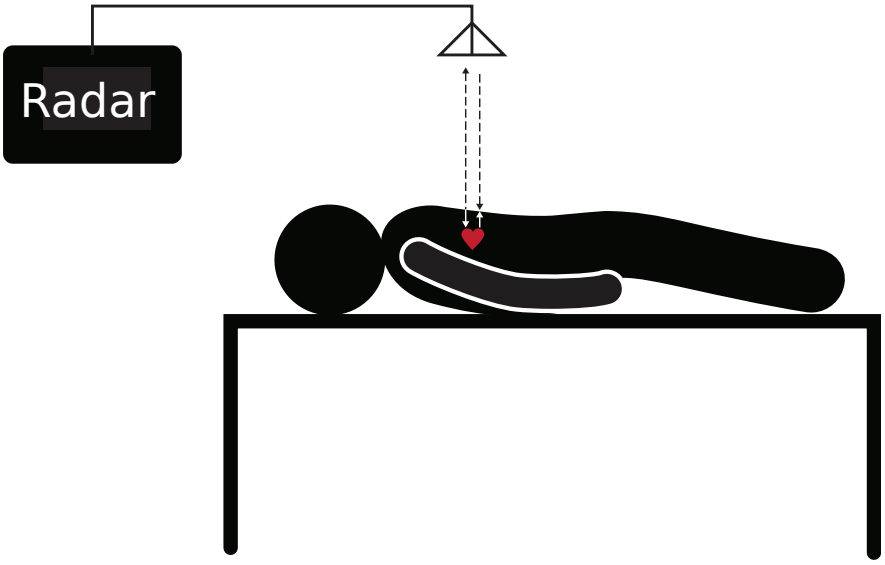

Figure 7: The test person with a bare chest.

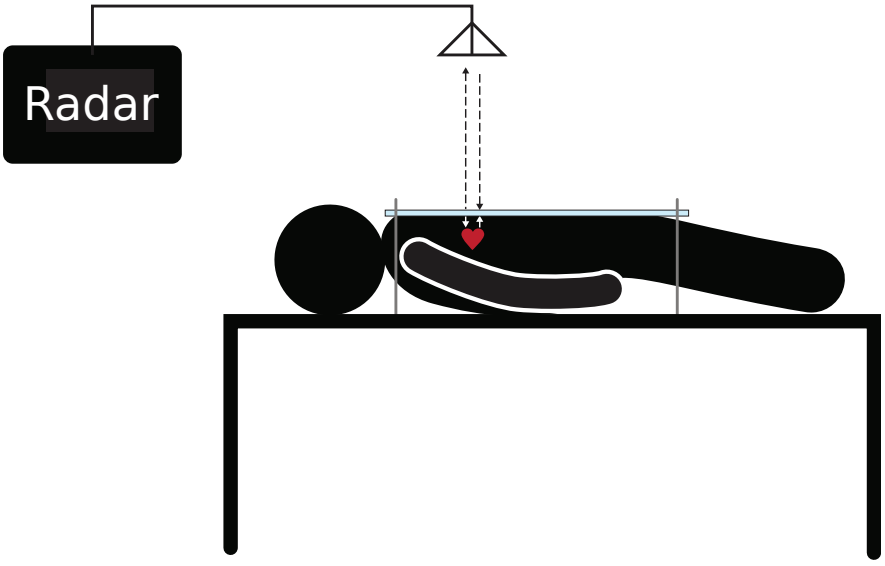

Figure 8: The test person with a plexiglass pressing tightly against his chest. Note that most of the person's chest directly under the antenna is now pressed flat and is prevented from moving by the stiff plexiglass plate. The sides of the torso, as well as the area by the neck though are still free to move.

from the moving heart should not be suppressed compared to the bare chest measurements. From modelling however, this is not expected to be noticeable as the attenuation is too large.

The third measurement setup, showed in Fig. 9, is of the test person with his chest covered in silver leaves. The silver leaves are squares of thin silver film, which stick to the skin and follow the contours of the body closely. Silver is a conducting material, which blocks electromagnetic waves from penetrating into the body tissues and will reflect any incoming fields back. In this scenario, the radar modulation caused by movement should stay the same or be magnified because of the increased reflection. The chest surface reflection coefficient is increased from $|\Gamma| \approx 0.7$ to $|\Gamma| \approx 1$ when the silver leaves are applied, increasing the reflected power because of the increased conductivity in (6). On the other hand, the modulation caused by blood perfusion should be greatly decreased, as the largest contributor to this modulation is covered in metal. Additionally, no pen-

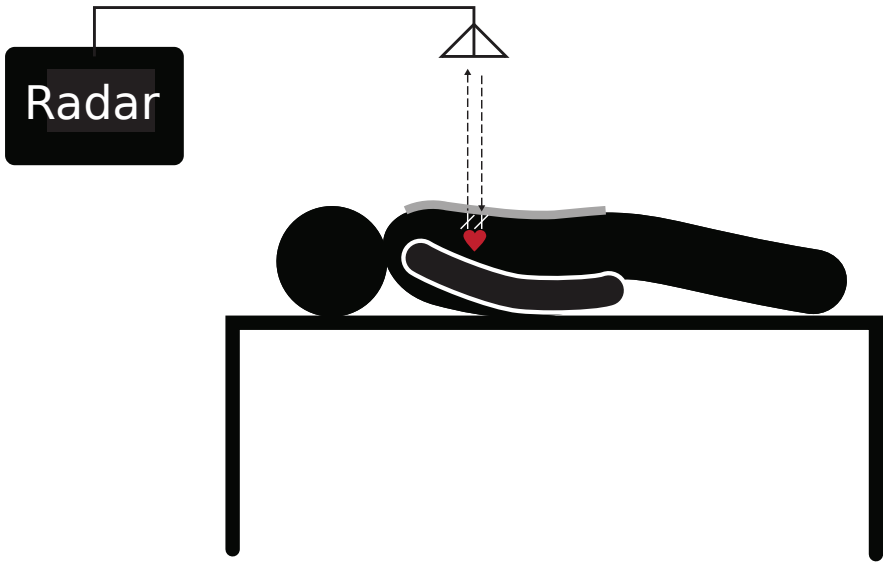

Figure 9: The test person's chest and stomach has been covered with a thin layer of silver leaves. Since the area of the person within the antenna main lobe is covered, the majority of the reflections from the person back to the antenna is from this region.

etration of the EM waves into the person's torso will occur. Thus only surface motion modulation from the chest and other body parts can occur in the radar recording. All these measurements were conducted with the person lying in the same spot, making the only change between the measurements being whether the chest was bare or covered with plexiglass or silver leaves.

B Processing

The bare, plexiglass and silver measurements need some processing of the data before results can be extracted. The aim of the experiments is to compare the sizes of the modulation using the three explained measurement setups. Therefore, it is important for the processing to provide a robust and simple measure of the modulation size without introducing any unnecessary error sources. With this in mind, the post processing of the data is explained here.

As Fig. 3 shows, the actual modulation follows a complex shape that varies between persons, aspect angle and frequency. However, the modulation occurs along one main direction. When considering the blood perfusion model, this main direction of modulation is the change in RCS. In the movement model this main direction is connected to the phase change from the changing range to the chest. In both cases though, it is the main direction of modulation that will be used in this investigation.

To compare the modulation in different measurements, we used a procedure to rotate the modulation to always lie along the real axis, similar to the linear regression method presented in [15]. First, the mean is subtracted from the data to center it around the origin. Then, a linear least squares fit of a straight line to the data set is made in the complex plane. The angle this straight line approximation has to the real axis is subtracted from the data vector, resulting in the data vector having its main direction of modulation along the real axis. Keeping the real part and discarding the imaginary part, leaves only the main modulation in the measurement vector.

The filtering and rotation of the measurement explained in the last paragraph leaves a vector $\tilde{b}$ of real values containing the modulation along the main modulation axis. A measure of the size of the heartbeat modulation through several heartbeats is to take the mean absolute value of this vector:

$$\hat{M} = \sum_{n=0}^{N-1} \frac{|\tilde{b}_n|}{N}, \tag{14}$$

where N is the length of the modulation vector $\tilde{b}$. Several measurements were conducted for each frequency and setup, and the mean value of the modulations $\hat{M}$ for each frequency is denoted $\tilde{M}$.

The goal of the experiments is to find out if the modulation is bigger or smaller when applying the plexiglass or silver leaves to the chest compared to the bare chest modulation. This goal is achieved by computing the ratios:

$$\text{plexi/bare ratio} = \frac{\tilde{M}_{plexi}}{\tilde{M}_{bare}} \tag{15}$$

$$\text{silver/bare ratio} = \frac{\tilde{M}_{silver}}{\tilde{M}_{bare}}. \tag{16}$$

A ratio of one means that the modulation is the same size as in the reference bare chest modulation. A ratio less than one means that the modulation is less, while a ratio greater than one means that the modulation has increased compared to the bare chest modulation.

In addition to comparing the magnitudes of the modulations, the heartbeat waveforms recorded using the three experimental setups were compared. From each measurement $\tilde{b}$, a series of ten heartbeats were picked out, each series starting at the same phase of the heartbeat. Each series were re-sampled to be of the same number of samples in total. For each experimental setup, several measurements were performed at each frequency. The mean measurement series were made, such that each of the bare chest, silver and plexiglass setups has one mean measurement $\bar{b}$ ten heartbeats long for each tested frequency. These mean measurements were used to compare the shape of the silver

and plexiglass waveforms to the bare chest waveforms through the normalized cross correlation:

$$\rho = \frac{\sum_{n=1}^{N} \bar{b}_{1,n}\bar{b}_{2,n}}{N\sigma_1\sigma_2}, \tag{17}$$

where ρ is the normalized cross correlation with zero delay, N is the number of samples in each time series, σ_1 is the standard deviation of $\bar{b}_1$ and σ_2 is the standard deviation of $\bar{b}_2$. The bare chest waveforms were used as $\bar{b}_2$, while either the silver or the plexiglass waveforms were used as $\bar{b}_1$.

IV. Results

A total of 155 measurements were conducted, distributed as plexiglass, silver leaf and bare chest measurements. The measurements were conducted at $0.6, 1, 2, 3, 4, 8, 12, 15$ and 18 GHz Tx frequency.

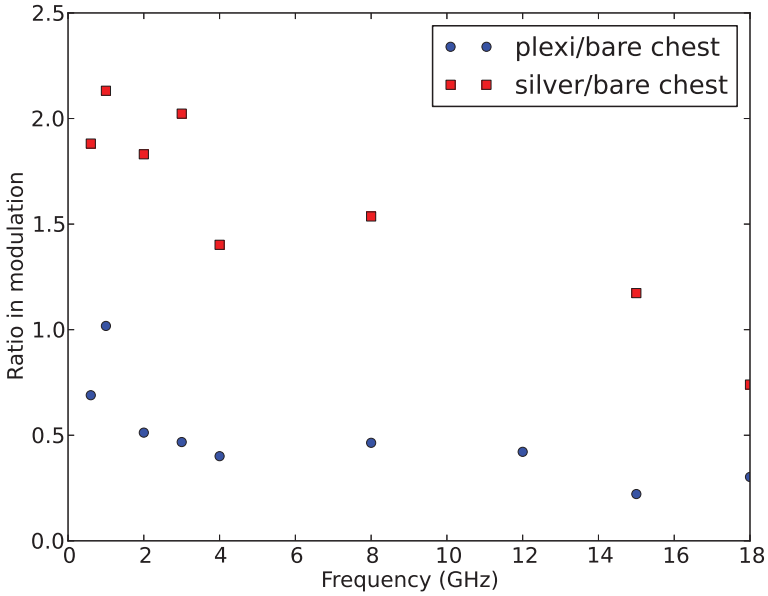

Figure 10: The ratio between the modulation in plexiglass covered chest and bare chest and between silver covered chest and bare chest. For most frequencies, the modulation is smaller with the plexiglass covered chest while it is larger for silver covered chest.

For all the tested frequencies, the data were processed as outlined in Section B. Using (14), a measure $\tilde{M}$ of the modulation was found for each of the three measurement setups for each frequency. The ratios (15) and (16) were computed for each frequency, and plotted in Fig. 10. It is seen that the modulation was reduced when the plexiglass plate was pressing the chest flat. Had the main contributor to the modulation been blood perfusion or reflections from internal organs, this reduction in modulation would not have been observed. The RCS of the chest remained ap-

proximately the same, but the phase modulation from movement was reduced. It is noted however that the modulation was not completely suppressed. For the lower frequencies this could in part be from waves penetrating the chest and reflecting of the heart wall, although this is unlikely. Parts of the body that were not hindered from moving by the plexiglass plate could be a contributor to the modulation. However, while the plexiglass plate suppressed chest movements, it did not completely remove them.

When the chest was covered in silver leaves, the modulation was larger than when the chest was bare. This dispels the blood perfusion theory, as the modulation increased when most of the skin in the antenna main beam was concealed. An example time series from each of the three setups recorded at 15 GHz has been plotted on top of each other in Fig. 11. For each frequency, the silver

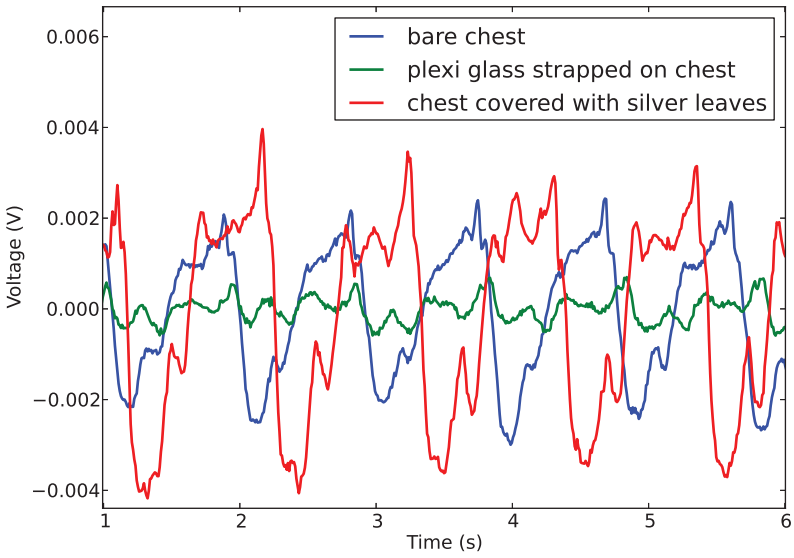

Figure 11: The heartbeats measured on a bare chest, a chest covered in silver leaves and the chest under pressure from a plexiglass plate. All measurements were conducted under the same conditions, with the only change being the chest covered in silver, plexiglass or being bare. Note that the plexiglass measurement modulation is decreased while the silver leaves measurement modulation is increased compared to the bare chest measurement.

and plexiglass waveforms were compared to the bare chest waveform through the normalized cross correlation. The results are plotted in Figure 12. With the exception of the 4 GHz measurements, the silver leaf recordings show good correlation with the bare chest recordings. The plexiglass measurements show good correlation at frequencies below 2 GHz but worse at higher frequencies. At the lower frequencies the changes in chest morphology are small compared to the wavelength, and the waveform is not expected to change much in shape from the plexiglass pressing down on the chest. The heartbeat waveform is similar in shape but increased in magnitude when the chest is covered in silver leaves, which supports the theory of the modulations being caused by body surface reflections. In this case, the phase modulations from the movements stayed similar, while the RCS

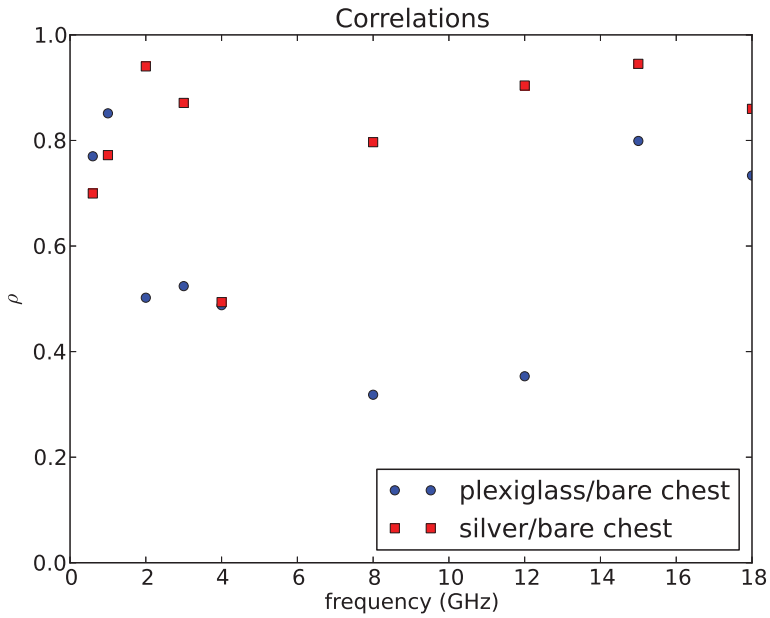

Figure 12: The normalized cross correlation ρ between plexiglass and bare chest measurements and between silver and bare chest measurements as a function of frequency.

was increased from the silver leaves.

To be sure that the plexiglass plate was actually suppressing the movement of the chest, an accelerometer was placed on the chest in some of the bare chest measurements, and on the same location on the plexiglass plate in some of the plexiglass measurements. On average the movement of the chest with the plexiglass tightened was one third that of the bare chest, confirming that the chest surface movement was indeed decreased during the plexiglass measurements.

V. Discussion

The bare, silver and plexiglass measurements dispels the theory that changes in blood density in the skin are the cause of modulations seen in radar recordings, while confirming the theory that the chest movement caused by the heartbeat is seen. For all tested frequencies except 18 GHz the modulation was larger with the chest covered in silver leaves than with a bare chest or the chest pressed flat with the plexiglass plate. While this indicates that the chest movement dominates the modulation, the modulation in the 1 GHz plexiglass measurements are on average about as large as the modulation in the bare chest measurements. Using an accelerometer it was established that the chest movement was reduced as much in the 1 GHz plexiglass measurements as for the other frequencies, so other explanations need to be sought for this particular result. One explanation is possible penetration of the EM wave into the chest, meaning the modulation is from reflections from the actual heart movement. However, there is significant attenuation in the body tissues at

this frequency, meaning that it is unlikely that the modulation would be as big as the modulation caused by surface movements. Another explanation is that it is movements from other parts of the body than the chest area under the plexiglass plate that is seen. The upper part and sides of the torso are unaffected by the plexiglass plate. At the lower frequencies, the used antenna is much less directional than at the higher frequencies. Thus, not only the chest is present in the antenna main beam, and the rest of the body will contribute more in the receiver. Indeed, in [16] it was found that respiration can be detected using radar by only looking at the arm of a person.

Movements of other parts of the body than the chest could have a significant effect on the modulation seen in the radar receiver. Penetration into the body at sub-GHz frequencies cannot be totally ruled out, and movements from other body parts stand as a plausible significant contributor to the total modulation. When looking at the results in total though, the bare, plexiglass, silver measurements show that the dominant cause of the heartbeat modulations is the chest surface movement.

A large portion of the research on remote heartbeat detection using radar have focused on Ultra wideband (UWB), with one of the reasons being the good penetration of the lower frequencies. From the results in this paper, the heartbeat modulations are dominated by chest surface movements. Higher frequencies are better suited for detection of small movements, as the movements will increase relative to the wavelength with higher frequencies. Narrow band radars operating at high microwave or even millimeter-wave frequencies will thus be better suited for remote heartbeat detection than low frequency or UWB systems. This is however, only valid for remote detection as antennas placed in contact with the chest are not dominated by the chest surface reflection and may receive reflections from the actual heart.

VI. Conclusion

An experimental approach was taken to answer the question of what is actually measured in a non-contact radar heartbeat measurement. The three tested theories were blood perfusion in the skin, body surface movements and internal body organ movements. To test the hypotheses, three measurement setups of a person under normal conditions, with chest movement constrained and with skin tissue properties concealed were performed over the $0.5 - 18$ GHz frequency range. The chest movement was constrained by pressing the chest of the person under test flat using a plexiglass plate. To conceal the skin tissue properties without affecting the movements the chest was covered in thin silver leaves. The results show that it is body surface movements that are dominating remote radar measurements of heartbeats.

References

[1] C. Johnson and A. Guy, "Nonionizing electromagnetic wave effects in biological materials and systems," *Proceedings of the IEEE*, vol. 60, no. 6, pp. 692–718, June 1972.

[2] J. Lin, J. Kiernicki, M. Kiernicki, and P. Wollschlaeger, "Microwave apexcardiography," *Microwave Theory and Techniques, IEEE Transactions on*, vol. 27, no. 6, pp. 618–620, Jun 1979.

[3] Ø. Aardal, S.-E. Hamran, T. Berger, Y. Paichard, and T. S. Lande, "Chest movement estimation from radar modulation caused by heartbeats," in *Biomedical circuits and systems conference (BIOCAS 2011), 2011 IEEE*. IEEE, November 2011, pp. 452–455.

[4] B.-K. Park, O. Boric-Lubecke, and V. M. Lubecke, "Arctangent Demodulation With DC Offset Compensation in Quadrature Doppler Radar Receiver Systems," *Microwave Theory and Techniques, IEEE Transactions on*, vol. 55, no. 5, pp. 1073–1079, May 2007.

[5] G. Varotto and E. Staderini, "On the UWB medical radars working principles," *International Journal of Ultra Wideband Communications and Systems*, vol. 2, no. 2, pp. 83–93, 2011.

[6] E. Staderini, "UWB radars in medicine," *Aerospace and Electronic Systems Magazine, IEEE*, vol. 17, no. 1, pp. 13–18, Jan 2002.

[7] D. Zito, D. Pepe, B. Neri, D. De Rossi, A. Lanata, A. Tognetti, and E. Scilingo, "Wearable System-on-a-Chip UWB Radar for Health Care and its Application to the Safety Improvement of Emergency Operators," in *Engineering in Medicine and Biology Society, 2007. EMBS 2007. 29th Annual International Conference of the IEEE*, Aug. 2007, pp. 2651 –2654.

[8] S. Pisa, P. Bernardi, M. Cavagnaro, E. Pittella, and E. Piuzzi, "Monitoring of cardiopulmonary activity with UWB radar: A circuital model," in *Electromagnetic Compatibility and 19th International Zurich Symposium on Electromagnetic Compatibility, 2008. APEMC 2008. Asia-Pacific Symposium on*, May 2008, pp. 224–227.

[9] C. Gabriel, S. Gabriel, and E. Corthout, "The dielectric properties of biological tissues: I. Literature survey," *Physics in medicine and biology*, vol. 41, p. 2231, november 1996.

[10] S. Gabriel, R. Lau, and C. Gabriel, "The dielectric properties of biological tissues: II. Measurements in the frequency range 10 Hz to 20 GHz," *Physics in medicine and biology*, vol. 41, p. 2251, november 1996.

[11] ——, "The dielectric properties of biological tissues: III. Parametric models for the dielectric spectrum of tissues," *Physics in medicine and biology*, vol. 41, p. 2271, november 1996.

[12] G. Ossberger, T. Buchegger, E. Schimback, A. Stelzer, and R. Weigel, "Non-invasive respiratory movement detection and monitoring of hidden humans using ultra wideband pulse radar," *Ultra Wideband Systems, 2004. Joint with Conference on Ultrawideband Systems and Technologies. Joint UWBST & IWUWBS. 2004 International Workshop on*, pp. 395–399, May 2004.

[13] C. Li and J. Lin, "Random Body Movement Cancellation in Doppler Radar Vital Sign Detection," *Microwave Theory and Techniques, IEEE Transactions on*, vol. 56, no. 12, pp. 3143 –3152, dec. 2008.

[14] "Agilent Network Analyzer N5245A PNA-X, http://www.home.agilent.com/agilent/product.jspx?nid=-536902643.898624.00&cc=NO&lc=eng."

[15] D. R. Morgan and M. G. Zierdt, "Novel signal processing techniques for doppler radar cardiopulmonary sensing," *Signal Process.*, vol. 89, no. 1, pp. 45–66, 2009.

[16] K. Mostov, E. Liptsen, and R. Boutchko, "Medical applications of shortwave FM radar: Remote monitoring of cardiac and respiratory motion," *Medical physics*, vol. 37, p. 1332, 2010.

6.6 VI Detecting changes in the human heartbeat with on-body radar [6]

Abstract

Radar can be used to detect human heartbeats. This makes radar a potential alternative to today's heartbeat monitoring techniques in medicine. In this paper, two antennas were located on the chest to monitor the heart activity. Simultaneous with the radar measurements, the Electrocardiogram (ECG) and blood pressure were measured. Details of the heart activity, such as opening and closing of heart valves and the filling and ejection of heart chambers, were catched by radar monitoring. Through physical activity, blood pressure as well as the pulse of the person were increased. Matching changes were observed in backscattered radar signal waveforms, thus showing that radar can be used to detect changes in the heartbeat in a reliable way.

I. Introduction

Radar transmits electromagnetic waves and receives echos from targets within the antenna beam. When one or more of these targets change either in position or shape, it can be seen as modulations in the received signal. With low power, sensitive radar systems, small heartbeat movements can be recorded. The use of radar for physiological measurements dates back to the early seventies [1], when radar was used to monitor breathing of infants. Among the proposed applications for this technology are monitoring of human vital signs, sleep monitoring, detection of humans through the wall or through the ground and as a medical diagnostic tool. This paper will focus on the topic of using radar heartbeat measurements as a diagnostic and monitoring tool.

The most widely used heartbeat monitoring tool of today is ECG, which monitors the electrical activity in the heart. Unlike ECG, radar can be used to directly monitor the actual movements of the heart, and does not require a number of patches like ECG monitoring. In this way, radar heartbeat measurements are comparable to echocardiograph measurements, disclosing mechanical activity as well. Since ultrasound uses sound waves propagating inside the body while radar uses electromagnetic waves, the contrasts between tissues are different between the two techniques. Thus, radar and ultrasound measurements may be able to detect different things. Advantages with radar recordings over ultrasound is that radar can be used through clothing, it does not require gel between the probe and the skin, and can be implemented in low-cost hardware.

A radar wave propagating inside the human body is attenuated because the body tissues are lossy media. In [2, 3, 4] it was simulated that an electromagnetic wave will be attenuated 25-160 dB in the 100MHz to 10 GHz range when travelling the two way distance between the chest and heart wall. Using a database on human tissues dielectric properties [5, 6, 7], it was computed in [8] that approximately 70% of the incoming energy will be reflected at the air to skin interface when doing non-contact radar measurements. Because of this the backscattering from a human is dominated by the surface reflections, and the observed heartbeat modulations are caused by small movements of the body surface [8]. To measure the movements of the heart directly, the antennas need to be located on the body. This way the body surface reflections are minimized due to coupling, and the smaller in-body movements can be captured.

Placing an antenna on the chest to look at the heart movement was reported several decades ago. In [9] modulations in the transmission loss of a 915 MHz wave passing through the thorax matching the heartbeat were observed. This was used to measure the ventricular volume changes. A 2.45 GHz radar placed on the chest area close to the bottom of the heart recorded heartbeats

simultaneously with ECG and PCG in [10]. The knowledge of parts of the heartbeat matching characteristic points in the ECG and PCG was used to label the radar measurement with these heartbeat instances. In [11] and [12], 2.45 GHz radar heartbeat recordings were further explored. Radar recordings were matched with the heartbeat through Impedance Cardiography (ICG) and ECG. In addition to using the receiver voltage directly, its derivative was also plotted. In these papers, the same position on the chest was used. In [13], four different antenna positions on the chest were used to perform the same analysis. It was found that the radar waveforms recorded from the different chest positions were significantly different from each other.

If radar observations of the human heart is to become a viable diagnostic tool in the future, medical information in addition to heart rate is required. This paper presents diagnostic information extractable from radar observation using a body-contact antenna. To make sure that the observed radar modulation is indeed coming from the heart itself, Ultra Wide-band (UWB) measurements with good range resolution were performed. Further, narrowband Continuous Wave (CW) measurements were performed in conjunction with both ECG and blood pressure measurements both before and after physical activity. When the person was exercising, both his pulse and blood pressure increased, before slowly going back toward normal. The measurements were analyzed to see changes in the radar waveforms with changing pulse and blood pressures. These experiments were repeated with a few days between to ensure that the characteristic changes are the same over time.

A description of the measurement setup and methodology is given in the next section, before the results are presented and discussed in Section III. and IV..

II. Methodology

A Equipment and measurement setups

As a radar we used a vector network analyzer [14] connected to a pair of bow-tie antennas. For the depth measurements described in Section B, a single antenna was used for both the transmitter and the receiver. For the narrowband CW measurements described in Section C, two antennas with 8 cm spacing were used. In both these setups, the antennas were strapped to the chest with only a T-shirt between the antennas and the skin. A 4.5 cm thick 14.5 x 17.5 cm cuboid of electromagnetic absorbing material was placed on top of the antennas. Most of the energy was transmitted either into the chest or absorbed in the absorbers, thus limiting the disturbance from other movements in the room. In free space, dipoles of these dimensions transmit at several GHz. The permittivity of the body means that the electromagnetic propagation speed is lower than in free space, thus shortening the wavelength of the transmitted waves. The S11 scattering parameter indicate absorptions in the body better than 10 dB for frequencies above 640 MHz.

Blood pressure and ECG measurements were performed simultaneously with the radar measurements. ECG electrodes at the right arm (RA), left arm (LA), right leg (RL) and left leg (LL) were used. Blood pressure measurements were started at the same times, and measured automatically with an electronic Sphygmomanometer. A draft of the measurement setup is seen in Figure 1.

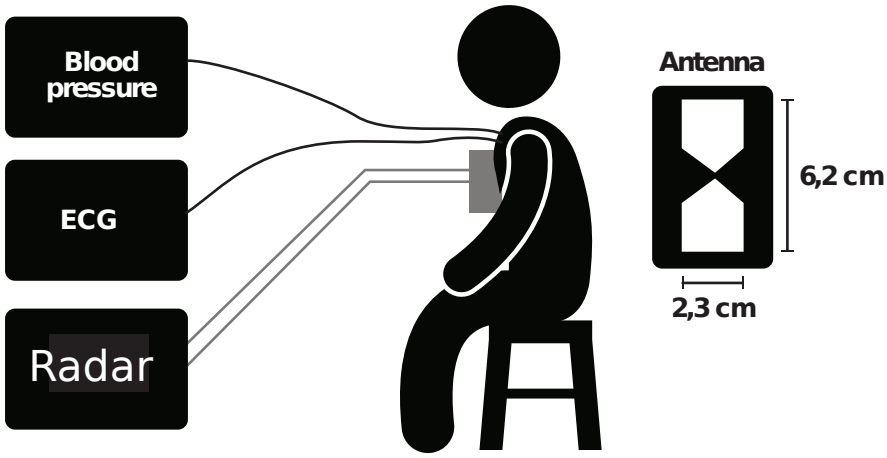

Figure 1: The measurement setup. A network analyzer connected to a pair of dipole antennas was used as a radar. The antennas were placed at the chest with a cuboid of electromagnetic absorbing material placed tightly behind. Simultaneously with the radar measurements, ECG and blood pressure were also recorded. During the measurements the person was holding his breath. The antenna with dimensions is drawn to the right.

B Measuring the depth of the heartbeat modulation

An antenna located on the body surface could possibly pick up modulations from other sources than the heart, such as the cables vibrating, antennas moving on the chest etc. By doing UWB measurements, we used the range resolution to determine the depth inside the body from which the periodic heartbeat modulations were coming. This was used to determine if the source of the modulations is the beating heart or other external factors. Linear sweeps from 500 MHz to 1.75 GHz sampled at 51 points in the frequency range, and with a pulse repetition frequency (PRF) of 92 Hz were used for this. For these measurements, a single antenna was used. A measurement of heartbeats with the antenna placed on the body sampled in the frequency domain is in baseband

$$b_H(\omega, t) = A_H(\omega, t)e^{i\phi_H(\omega,t)}. \tag{1}$$

$b_H(\omega, t)$ is the total sampled signal, ω is the angular frequency, t the slow time, and $A_H(\omega, t)$ and $\phi_H(\omega, t)$ the total amplitude and phase. To calibrate these recordings, a similar measurement of the antenna cables connected together was performed:

$$b_C(\omega) = A_C e^{i\omega\tau_0}, \tag{2}$$

with τ_0 the total travel time of the signal in the cables. Dividing (1) by (2), the result is

$$\tilde{b}_H(\omega, t) = \frac{A_H(\omega, t)}{A_C} e^{i(\phi_H(\omega,t)-\omega\tau_0)}. \tag{3}$$

Thus, the travel time of the cables have been removed from the phase of the heartbeat recordings, making the zero phase point at the antenna connections. The phase of $\tilde{b}_H(\omega, t)$ can then be used

to compute the travel time from the body surface to the modulating target.

In this paper, two different time variables are used: The fast time τ in the order of nanoseconds is used for the propagation time of the radar waves. The slow time t in the order of seconds is used for the time development of the measurement, influenced by the beating heart. After a Hamming window was applied to the data, an inverse Fast Fourier Transform (IFFT) transformed each frequency sweep $\tilde{b}_H(\omega)$ to the fast time domain representation $\tilde{b}_H(\tau)$. In the fast time domain, the range R from the antenna is connected to the two way travel time τ through the relation $R = v\tau/2$, with v being the electromagnetic propagation speed in the medium. The speed of light in a medium is $v \approx c/\sqrt{\varepsilon_r'}$, where ε_r' is the relative permittivity of the material and c the speed of light. Functions for computing the body dielectric properties can be found in [5, 6, 7].

A high pass filter along slow time with cut-off frequency 0.5 Hz was applied to filter the heartbeats from the stationary reflections. The filter was a 5 point two way chebyshev type 2 IIR filter. The signal matrix after filtering is denoted $\hat{b}_H(\tau, t)$. The two way travel time between antenna and point of max modulation was found by searching for the range cell with the largest fluctuations. This was achieved taking the mean absolute value through slow time, resulting in a vector containing the mean modulation at each fast time sample:

$$m(\tau) = \sum_n |\hat{b}_H(\tau, t_n)|. \tag{4}$$

The range cell with the largest modulation was found by searching for the maximum of $m(\tau)$. The depth in meters from the chest wall to the point of max modulation is

$$d = \frac{v\tau_{max}}{2} \tag{5}$$

with τ_{max} being the two way travel time to the max modulations. From [5, 6, 7] the relative permittivity of muscle at 1 GHz is $\varepsilon_r' = 54.8$, which was used to approximate the in-body electromagnetic propagation speed v.

C CW measurements and waveform analysis

We chose single frequency 1 GHz CW measurements for analyzing the heartbeat waveform. The available equipment have a higher duty cycle for single frequency measurements and a good antenna match is possible. On day one, an IF bandwidth of 200 Hz and sampling frequency $f_s = 223$ Hz was used. Day two we used an IF bandwidth of 300 Hz, and the CW data were sampled at $f_s = 333$ Hz.

For the narrow-band CW measurements an I & Q receiver was used, sampling the received signal in the complex plane. The heartbeats are seen mainly as a phase modulation offset by static scatterers and system DC[15]. While most of the modulation appear in the phase, there is some in the amplitude as well. Under the assumption that the heartbeats are detected mainly as phase variations, the heartbeat movement can be estimated using phase estimation and DC offset cancellation techniques [16]. Such a method was used here to produce the time varying phase $\phi(t)$ of the heartbeat recording. The estimation of the phase uses the approach from [15]. $\phi(t)$ is directly related to the movements of the heart.

In addition to the phase, the instantaneous frequency can reveal important information about

the heartbeat not easily seen by looking at the phase itself. The instantaneous frequency is defined as

$$\frac{d\phi(t)}{dt}. \tag{6}$$

Phase changes in radar recordings are directly connected to the movements of the targets in the scene. Large movements will be more visible than small movements as they create larger phase variations. Ventricular volume changes and heart rotation are examples of large movements which contribute to the total phase modulation. The recorded phase changes are the sum of the combined movement inside the antenna beam.

By definition, the instantaneous phase is connected to the velocities of the heart movements. Movements which are fast but small in extent will have large excursions in the instantaneous phase, while they may be hard to see in the phase.

The same series of measurements were performed over both of the two days. The person under test was seated on a chair, and simultaneous radar, ECG and blood pressure measurements were performed while holding his breath. The blood pressure measurements need about a minute to complete, setting the observation interval to approximately one minute. Slight variations in the time of a blood pressure measurement led to slight variations in the interval between measurements. Four measurements were done before physical activity initiated increased blood pressure as well as heart rate, followed by another series of observations. All conditions were the same before and after the physical activity.

III. Results

A The depth of the heartbeat in the chest

A series of UWB measurements with the antenna placed on the sternum were performed. The measurements were spread over several days, so a slight variation on the actual antenna position between the measurements may have occurred. The two way travel times between the antenna and the point of maximum modulation was measured 34 times on the same person, with a mean two way travel time $\tau_{max} = 1.4$ ns and a standard deviation of $\sigma = 0.15$ ns. Using (5), the mean depth inside the chest with maximum modulation is $d = 2.8$ cm. This fits well with the distance from the chest wall to the heart inside the body, strengthening the explanations that the observed modulations are directly related to the beating heart. The slow time development of a heartbeat measurement versus the depth inside the body is seen in Figure 2. In addition to these measurements, a series with the antenna attached to the thigh was performed. No modulations in phase with the heartbeats were observed. From this, we can conclude that the observed modulations are originating from the moving heart excluding other physiological phenomena or external factors.

B Analysis of CW heartbeat waveforms

Since the radar records the mechanical activity of the heart, various heart movements such as filling and ejecting of the ventricles should be recognizable. A radar recording displaying both the phase and the instantaneous frequency of two heartbeats is seen in the lower part of Figure 3. Together

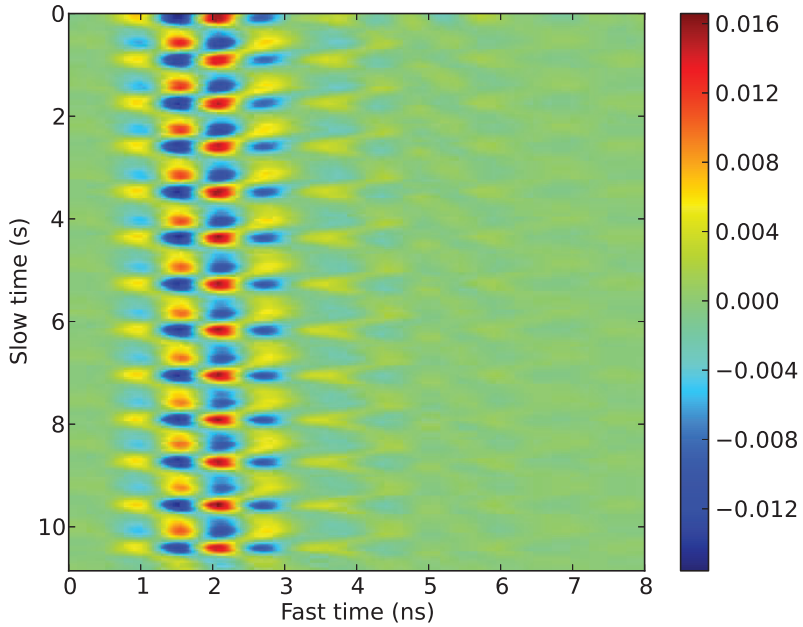

Figure 2: The real part of a heartbeat measurement seen as a function of fast time (ns) and slow time (s). In muscle tissue, 1 ns of two way travel time corresponds to a distance of approximately 2 cm. The data have been high-pass filtered along slow time, removing stationary reflectors while leaving the heartbeat modulation.

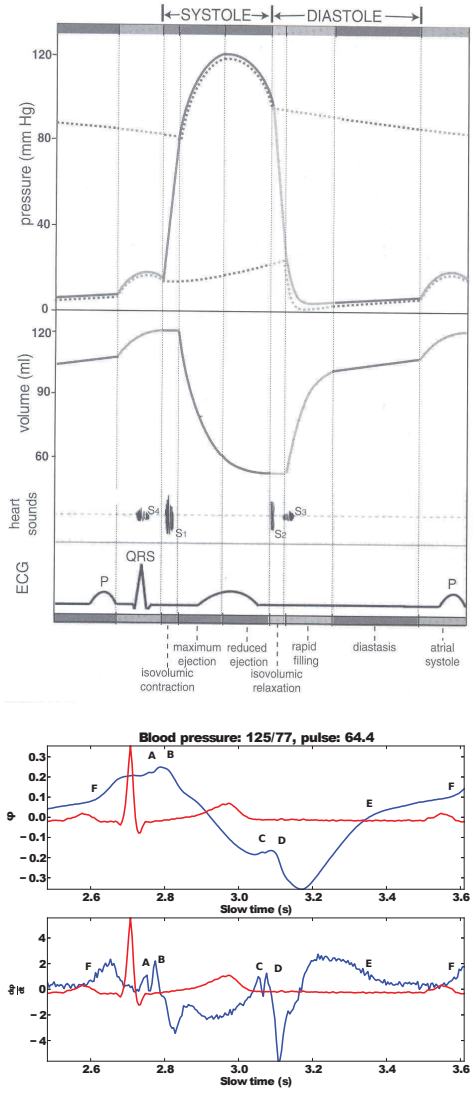

Figure 3: The top figure is the Wigger's diagram taken from a textbook in heart physiology [17], the bottom figure is the phase and instantaneous frequency of a heartbeat recorded in resting condition using radar. The radar recordings are drawn in a blue line, with the ECG normalized and plotted in red. Some characteristic points and periods of the heartbeats are marked on the two radar waveforms. They are as follows: The A-C period is the Systole, while the C-A period is the Diastole. Point A: Closing of the AV valves. The A-B interval is the isovolumic contraction of the ventricles. Point B: Opening of semilunar valves. The B-C interval consists of ventricular ejection. Point C: Closing of the semilunar valves. C-D interval: isovolumic relaxation. Point D: Opening of the AV valves. The D-E interval is the period of rapid filling of the ventricles, while the E-F interval is the period of reduced filling (diastasis). Point F: Onset of atrial contraction. The F-A interval consists of the atrial contraction.

with the radar recording, ECG recorded simultaneously is shown. In the upper part of Figure 3, the textbook Wigger's diagram from [17] is displayed. The Wigger's diagram shows the ventricular, atrial and aortic pressures and the ventricular volume together with the ECG and heart sounds. The phase of the radar recording follows the ventricular volume, while the heart sounds connected to the opening and closing of the heart valves are co-located in time with peaks in the instantaneous frequency waveform. Features in the radar recording can be labeled with their corresponding heartbeat events. The opening and closing of the heart valves, marked A, B, C, D in the figure, are visible as spikes in the instantaneous frequency waveform. The ejection and filling of the ventricles as well as atrial contraction are more easily seen in the phase waveform as outlined in the figure.

Before physical activity, four observations were taken followed by 30 observations afterwards. Day two used the same setup, but with an additional period of physical activity performed after the initial 34 measurements, and a following set of 15 measurements. In Figure 4, plots of the phase and instantaneous frequency in the heartbeat measurements before and after activity are shown. In all the figures, two consecutive heartbeats are plotted. There is not only an increased frequency of heartbeats after exercise, but also a change in the waveform of both the phase and instantaneous frequency. In both the high pulse/high blood pressure recordings, the reduced filling period marked EF in Figure 3 disappeared. The spikes A, B, C, D in the instantaneous phase connected with the opening and closing of the heart valves are still present. However, they change slightly in shape with changing pulse and blood pressure.

Measurements from the two different days can be compared, showing that the waveforms stay the same. Additionally, the experienced change in the waveforms after exercise are reproducible. This shows that the observed change is indeed connected to the changed behavior of the heart with changed pulse and blood pressure.

The post activity waveforms of Figure 4 are gradually converging towards the rest waveforms as the pulse and blood pressure decreases. In Figure 5, the instantaneous frequency waveform of two heartbeats from each measurement are plotted along the horizontal lines in parallel with the corresponding pulse and blood pressures. The red parts in the figure are parts where the instantaneous frequency is large while in the blue parts it is low. Before exercising, the instantaneous frequency is stable from measurement to measurement. Recognizable changes in the waveforms are observed the first few minutes after exercising, especially around the A and B spikes which are seen as blue areas in Figure 5. Additionally, where the rest waveforms have close to zero instantaneous frequency in the reduced ejection period, the complete period is elevated after activity.

IV. Discussion

Using phase calibrated UWB measurements we found that the radar modulations in phase with the heartbeats are originating from approximately 2.8 cm inside the body when measured from the center of the chest. While we believe that these modulations are caused by the heart movement, other phenomena may influence the measurement as well. During a heartbeat the density of blood changes, leading to a slight change in the dielectric properties of the tissues. The flow of blood through the path of the radar waves may also modulate the backscattered echo.

During a heartbeat, the heart does not simply expand and contract with the filling and ejection of blood. It rotates and stretches, and the opening and closing of heart valves produce shock waves that spread over the heart surface and into surrounding tissues. A radar measurement is a

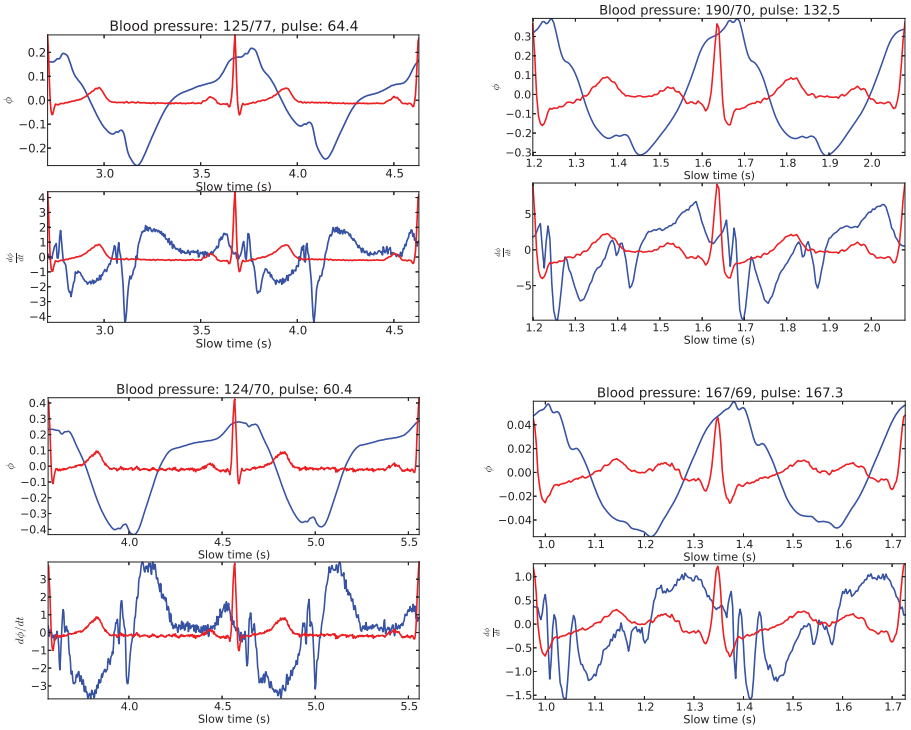

Figure 4: The phase and instantaneous frequency waveforms before and after exercise. The two rest and exercise pairs were recorded three days apart on the same person. The top left figure displays before exercise day one, the top right figure displays after exercise day one, the bottom left figure displays before exercise day two and the bottom right figure displays after exercise day two. One can see from the figures that both the waveforms and the waveform changes with increased pulse and blood pressure are preserved.

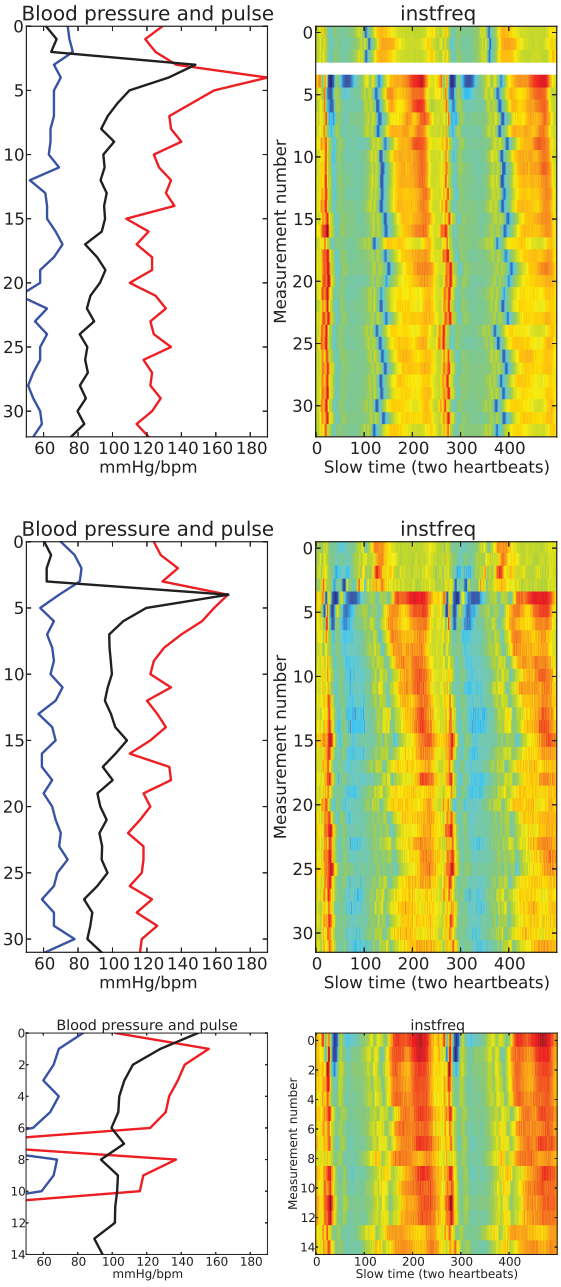

Figure 5: To the left are the systolic (red) and diastolic (blue) blood pressures together with the pulse (black) for each of the measurements in a series. To the right are the normalized instantaneous frequencies. Each horizontal line contains two heartbeats, and the next line is the next measurement taken approximately one minute after the last. The top plot is from day one, while the two bottom plots are from day two.

measurement of all these effects combined.

We recognized some features of the heartbeat waveform that are changing with pulse and blood pressure. Radar observations remain stable over time and in agreement with changes in heart rate and blood pressure. Most likely additional diagnostic information may be extracted from the radar recordings. Many heart diseases change the beating of the heart. Following the results in this paper that physiological changes of heart behavior can be detected using radar, there is great potential for using radar to detect heart diseases as well. Such a radar system can be implemented as an easily accessible monitoring tool, for example integrated in a bed, chair or clothing.

An issue not addressed in this paper is the choice of frequency and aspect angle. The optimal frequency is a compromise between the attenuation of the wave inside the body and the radar sensitivity to heart movements, both believed to increase with frequency. With aspect angles, it is not clear whether there exist an optimal point on the chest for observing the heartbeat. Most likely, different dynamics can be observed from different angles. Multi channel recording or imaging using an antenna array on the body is a good candidate for fully realizing this potential.

V. Conclusion

Human heartbeats were monitored with radar, using antennas located on the chest only separated by a T-shirt. Using the presented signal processing algorithm, several details of the heart movements were reliably detected. These include the opening and closing of the heart valves and ventricular ejection and filling, which were validated by simultaneous ECG measurements. The blood pressure and pulse of the person were increased through physical activity. These changes in the state of the heart were detectable by radar in a stable and reliable way. The ability to detect changes in the heart confirms medical radar as a viable diagnostic tool.

Acknowledgment

This work is part of the MELODY project funded by the Research Council of Norway under contract number 187857/S10. Thanks to Asbjørn Kleivstul for the antennas used.

References

[1] C. G. Caro and J. A. Bloice, “Contactless apnoea detector based on radar,” *The Lancet*, vol. 2, pp. 959–961, October 1971.

[2] E. Staderini, “UWB radars in medicine,” *Aerospace and Electronic Systems Magazine, IEEE*, vol. 17, no. 1, pp. 13–18, Jan 2002.

[3] D. Zito, D. Pepe, B. Neri, D. De Rossi, A. Lanata, A. Tognetti, and E. Scilingo, “Wearable System-on-a-Chip UWB Radar for Health Care and its Application to the Safety Improvement of Emergency Operators,” in *Engineering in Medicine and Biology Society, 2007. EMBS 2007. 29th Annual International Conference of the IEEE*, Aug. 2007, pp. 2651 –2654.

[4] S. Pisa, P. Bernardi, M. Cavagnaro, E. Pittella, and E. Piuzzi, “Monitoring of cardiopulmonary activity with UWB radar: A circuital model,” in *Electromagnetic Compatibility and*

19th International Zurich Symposium on Electromagnetic Compatibility, 2008. APEMC 2008. Asia-Pacific Symposium on, May 2008, pp. 224–227.

[5] C. Gabriel, S. Gabriel, and E. Corthout, "The dielectric properties of biological tissues: I. Literature survey," *Physics in medicine and biology*, vol. 41, p. 2231, november 1996.

[6] S. Gabriel, R. Lau, and C. Gabriel, "The dielectric properties of biological tissues: II. Measurements in the frequency range 10 Hz to 20 GHz," *Physics in medicine and biology*, vol. 41, p. 2251, november 1996.

[7] ——, "The dielectric properties of biological tissues: III. Parametric models for the dielectric spectrum of tissues," *Physics in medicine and biology*, vol. 41, p. 2271, november 1996.

[8] Ø. Aardal, Y. Paichard, S. Brovoll, T. Berger, T. S. Lande, and S.-E. Hamran, "Physical Working Principles of Medical Radar," *Biomedical Engineering, IEEE Transactions on*, vol. 60, no. 4, pp. 1142–1149, 2013.

[9] C. Johnson and A. Guy, "Nonionizing electromagnetic wave effects in biological materials and systems," *Proceedings of the IEEE*, vol. 60, no. 6, pp. 692–718, June 1972.

[10] J. Lin, J. Kiernicki, M. Kiernicki, and P. Wollschlaeger, "Microwave apexcardiography," *Microwave Theory and Techniques, IEEE Transactions on*, vol. 27, no. 6, pp. 618–620, Jun 1979.

[11] J. Thijs, J. Muehlsteff, O. Such, R. Pinter, R. Elfring, and C. Igney, "Comparison of continuous wave doppler radar to impedance cardiography for analysis of mechanical heart activity," *Proceedings of the 2005 IEEE Engineering in Medicine and Biology 27th Annual Conference*, pp. 3482–3485, 2005.

[12] J. Muehlsteff, J. Thijs, and R. Pinter, "The use of a two channel Doppler radar sensor for the characterization of heart motion phases," *Engineering in Medicine and Biology Society, 2006. EMBS '06. 28th Annual International Conference of the IEEE*, pp. 547–550, 30 2006-Sept. 3 2006.

[13] J. Muehlsteff, T. Pinter, G. Morren, and G. Muesch, "A handheld device for simultaneous detection of electrical and mechanical cardio-vascular activities with synchronized ECG and CW-Doppler Radar," *Proceedings of the 29th Annual International Conference of the IEEE EMBS*, pp. 5758–5761, August 2007.

[14] "Agilent Network Analyzer N5245A PNA-X, http://www.home.agilent.com/agilent/product.jspx?nid=-536902643.898624.00&cc=NO&lc=eng."

[15] Ø. Aardal, S.-E. Hamran, T. Berger, Y. Paichard, and T. S. Lande, "Chest movement estimation from radar modulation caused by heartbeats," in *Biomedical circuits and systems conference (BIOCAS 2011), 2011 IEEE*. IEEE, November 2011, pp. 452–455.

[16] B.-K. Park, O. Boric-Lubecke, and V. M. Lubecke, "Arctangent Demodulation With DC Offset Compensation in Quadrature Doppler Radar Receiver Systems," *Microwave Theory and Techniques, IEEE Transactions on*, vol. 55, no. 5, pp. 1073–1079, May 2007.

[17] A. Katz, *Physiology of the Heart*, 4th ed. Lippincott Williams & Wilkins, 2006.